University of Palermo, DIEETCAM, TTI Lab.

Ph.D. Course on Electronic and Telecommunication Engineering
(ING-INF 03)

XXIII Course - Final Thesis:

Resource allocations in heterogeneous 4G wireless networks

Ph.D. Candidate

Francesco Ivan Di Piazza

Ph.D. Advisor

Prof. Ilenia Tinnirello

Ph.D. Co-Advisor

Prof. Stefano Mangione

Ph.D. Course Advisor

Prof. Giovanni Garbo

February 2012

Contents

List of Figures

List of Tables

1 Introduction

In addition to well-established standard for local area networks, such as IEEE 802.11, in recent years there has been an increasing proliferation of broadband networks, capable of providing applications and services, characterized by high data rate and stringent requirements of QoS. More specifically we refer to next-generation technologies, in particular 3GPP Long Term Evolution (LTE) and, to a lesser exent, IEEE 802.16 (WiMAX). Along with a technological evolution of networks, there is a gradual development of these ones also from an architectural point of view, migrating from traditional cellular networks (with macro Base Stations located on the territory to provide connectivity to users) to heterogeneous network scenarios where different devices coexist in the same layout. In particular the inclusion within a network of so-called femto Base Stations (femto-BSs), i.e. devices with the same functionalities of macro-BSs but at low power (and therefore low coverage) and low cost, gives rise to a performance improvement from a global point of view. In fact these BSs can ensure coverage and service to users experiencing bad channel conditions, such as users on cell-edge or users in indoor environments. However many integration problems for placing the femtocells into existing homogeneous network layouts must be faced, especially if the femto-BSs adopt a policy of restricted access to only authorized users.

This thesis provides an overview of these emerging network scenarios, highlighting the main aspects and problems and the current solutions proposed in the literature. The considered scenarios (new generation broadband homogeneous network environments and mixed macro-femto ones) are modeled in terms of optimization problems and analyzed through simulations carried out using a custom-made network simulator (developed in C++ and Matlab). This simulator implements a mixed macro-femto layout, with macro-hexagonal cells arranged on a toroidal surface and a channel model consistent with the specifications contained in the document 3GPP TR 25996 (release 8) [3].

With regards to a typical OFDMA network with a reuse factor equal to 1 and characterized by only macro-BSs (possibly with different transmit power levels), the effects of different allocation schemes on the aggregated network-level performance are analyzed. In particular greedy allocation schemes, i.e. schemes utilizing all the carriers available in each cell, and non-

greedy schemes, i.e. schemes leaving some resources empty, in order to reduce interference with other cells, are compared. Different policies of power allocation on the subchannels (uniform and according to a water filling approach) are investigated too. Simulations are repeated by varying the propagation models, the topology of the network and under different operation conditions. Simulation results are devoted to investigate the network scenarios in which network planning and mobile station feedbacks are (or are not) advantageous from a network point of view.

As far as concerns mixed macro-femto scenarios, simulations have been run with the aim to evaluate the effects on the network peformance deriving from the introduction of femtocells in a homogeneous layout. Total and per-user statistics are considered, analyzing the benefits and/or disadvantages encountered by users respectively associated to macro- and femto-BSs, under different network configurations. Different scenarios are simulated, by varying the density of femtocells, the scheme of distribution of power on the subchannels, the maximum transmit power levels for macro- and femto-BSs and the percentage of resource usage (forcing only the macro-BSs or all the BSs in the network to make a partial use of the available per-cell resources).

Finally a study devoted to consider energy implications in these heterogeneous contexts is presented. Energy considerations are carried out both on Base Station-side (macro and femto) and on user-side. Simulations, devoted to compare the energy efficiency of macro- and femto-BSs, confirm that femto-BSs provide a consistent improvement in the system capacity, while maintaining a very low energy consumption compared to the macro-BSs. For this reason the use of femtocells represents a suitable solution for the deployment of green networks. With reference to the user-side implications, we referred to the 802.11 technology for evaluating experimental measurements, and specifically to a common USB dongle. The rationale of this study was to understand the impact of transmit power tunings on the overall card consumption, under the assumption that 3G USB cards (over which we do not have full configuration control) will exhibit a similar behavior. The accurate measurements have enabled to evaluate the energy consumption of these cards under different operation conditions (different PHY transmit rates and transmit powers), isolate the consumption quota of different card sub-systems, including

the power amplifier, the RF-front end, the baseband and the host interface, and study the effects of power control on their energy saving (which has led to support the low efficiency of this technique aimed at saving energy).

2 OFDMA-based technologies

Orthogonal Frequency Division Multiple Access (OFDMA) is the multi-user version of the *Orthogonal Frequency Division Multiplexing* (OFDM) digital modulation scheme. Its scalability, its MIMO-friendliness and its ability to take advantage of channel frequency selectivity make it one of the most promising multiple access technologies for the emergent broadband wireless communication systems. Not by chance in fact standards as IEEE 802.16 (WiMax) [4] and 3GPP Long Term Evolution (LTE) [5] just implement it as physical layer multiple access scheme. This chapter describes in detail the OFDMA modulation and its implication in the main wireless communication systems which implement it, WiMax and LTE precisely.

2.1 Generalities

OFDMA can be considered as an evolution of previous access schemes, in particular *Frequency Division Multiplexing* (FDM) and *Orthogonal Frequency Division Multiplexing* (OFDM). They are spread spectrum techniques in which signals are transmitted over multiple frequencies simultaneously, at the same time slot. The initial high rate data stream is divided into multiple parallel lower rate data streams: each sub-stream is then modulated using schemes such as PSK (*Phase Shift Keying*) or generically QAM (*Quadrature Amplitude Modulation*) at different cardinality (i.e. BPSK, QPSK, 16-QAM, 64-QAM).

In the FDM case, each subcarrier is separately modulated and a guard band is placed between two adjacent subcarriers in order to avoid signal overlap, as shown in Fig. 1 on the following page. In OFDM the subcarriers are closely spaced to each other (absence of guard bands between adjacent frequencies, Fig. 2 on the next page), without causing interference. This is possible because the subcarriers are orthogonal, i.e. the peak of a subcarrier coincides with the null of an adjacent one. So OFDM needs less bandwidth than FDM to carry the same amount of information, that means higher spectral efficiency. In addition to this, OFDM is efficiently able to face interference and frequency-selective fading caused by multipath because equalizing is done on a subset of subcarriers instead of a single broader carrier and frequencies with high bit-rate errors can selectively be ignored. ISI (*Inter Symbol Interference*) effect is suppressed thanks to a longer symbol period of the parallel OFDM subcarriers compared to a single carrier system

Figure 1: Placement of subcarriers in FDM.

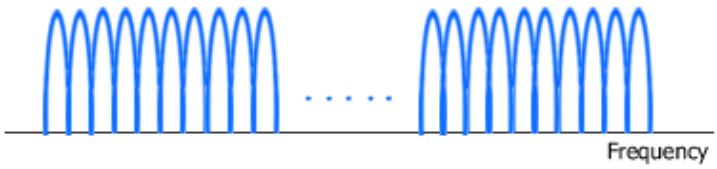

Figure 2: Placement of subcarriers in OFDM.

and thanks to the use of a *cyclic prefix* (CP). These aspects make OFDM particularly suitable for *Non-Line-Of-Sight* (NLOS) environments. Nowadays OFDM is implemented in many broadband applications, including digital TV broadcasting, digital audio broadcasting, *Asynchronous Digital Subscriber Line* (ADSL) modems and WiFi technologies (IEEE 802.11a/g).

Like OFDM, OFDMA employs multiple closely spaced subcarriers, but they are grouped into units named subchannels (Fig. 3). Different grouping policies for the subcarriers are possible: as specified for example in the IEEE 802.16e standard [6], PUSC (*Partial Usage of Sub Channels*) and AMC (*Adaptive Modulation and Coding*) are permutation schemes that define non-adjacent and adjacent subcarrier groupings for a subchannel, respectively. The reason to consider appropriate grouping schemes is that the multipath channel responses are frequency selective. Consequently exploiting the frequency diversity is a key aspect in these contexts and this can be achieved by suitable mapping of subcarriers to subchannels and by coding and in-

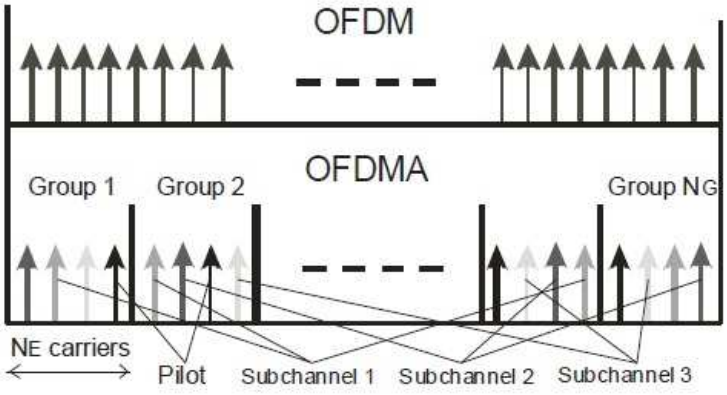

Figure 3: Subcarrier management in OFDM and OFDMA.

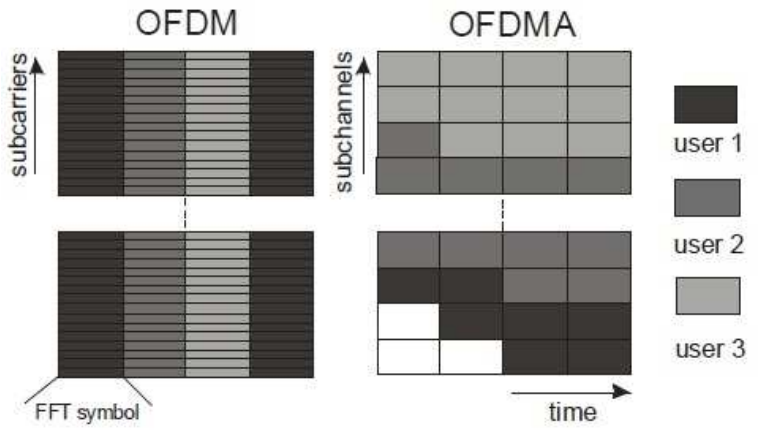

Figure 4: Resource allocations in OFDM and OFDMA.

terleaving. In [7] the author shows that by leveraging frequency diversity, the performance of OFDMA can be much better than that of Single Carrier FDMA (SC-FDMA) schemes, used for example in the UL of LTE for power efficiency reasons.

Fig. 4 shows the allocation of the subchannels in a time-frequency plan, respectively in OFDM and OFDMA schemes. While in the OFDM case, for a fixed time slot, all the subcarriers are allocated to an unique user, in the OFDMA scheme different subchannels can be assigned to different users (each colour is related to a specific user). So OFDMA can be seen as a combination of frequency domain and time domain multiple access, where the resources are partitioned in the time-frequency domain, being slots assigned along the OFDM symbol index as well as the OFDM subcarrier index.

Subchannelization guarantees a high flexibility in the assignment of the subchannels within the same time slot, but it causes a computational overhead compared to other more static techniques: in fact how many and what resources are assigned to the different users of the network is an information which must be periodically signaled. Based on feedback information, subchannels can be allocated to users in an adaptive way, depending on their channel conditions, data requirements and required *Quality of Service* (QoS). If the assignment is done sufficiently fast, this further improves the OFDM robustness to fast fading and interference, and even better system spectral efficiency can be achieved. So, while OFDM is very suitable for fixed and low mobility scenarios where the channel conditions are constant or slowly changing, OFDMA works well in high mobility scenarios too. Exploiting the subchannelization of OFDMA, within a same time slot, heterogeneous levels of transmit power can be allocated on the resources

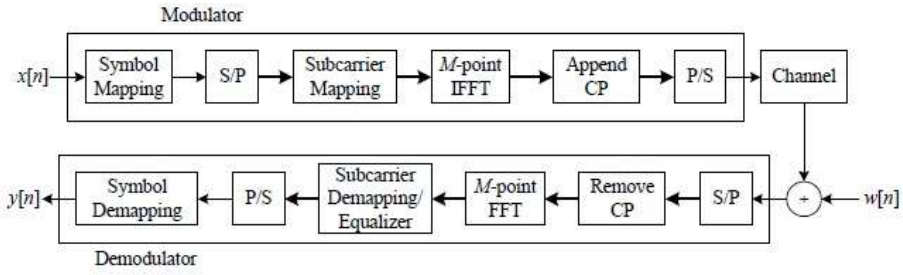

Figure 5: Discrete-time system model of OFDMA [1].

assigned to the various user devices, depending on the different SINR (*Signal-to-Interference and Noise Ratio*) values perceived. Moreover in uplink, the subchannelization can guarantee energy saving especially to battery-powered user devices (in mobile contexts for example), because they can concentrate power selectively on the subset of carriers assigned to them, rather than on all the carriers.

Nowadays OFDMA is mainly used in the mobility mode of the *IEEE 802.16 Wireless MAN* standard (commonly known as WiMax), in the downlink of the *3GPP Long Term Evolution* (LTE) fourth generation mobile broadband standard (also referred to as *Evolved UMTS Terrestrial Radio Access - E-UTRA*) and it is a candidate access method for the *IEEE 802.22 Wireless Regional Area Networks* (WRAN) [8] too, thought to design the first cognitive radio based standard, operating in the VHF-low UHF spectrum (TV spectrum).

2.2 Signal model of OFDMA

In this section an uplink signal model of OFDMA is described [1]. Fig. 5 shows a block diagram for the whole chain, from an OFDMA transmitter to the receiver. As for the OFDM, from the uplink receiver perspective, an OFDMA block can be seen as the aggregation of signals coming from multiple user devices, the generic one being generated by an *Inverse Fast Fourier Transform* (IFFT) operation including the *cyclic prefix* (CP). Let N be the number of subcarriers (including the virtual subcarriers in the guard band) and K the number of users. Among the N subcarriers, only a subset of them is assigned to the generic k_{th} user device: let $[c_0^k, c_1^k, ..., c_{P_k-1}^k]$ be the set of P_k resources assigned to it. Let $[X_{g,0}^k, X_{g,1}^k, ..., X_{g,P_k-1}^k]$ be the correspondent modulation symbols in the g_{th} OFDMA block. Precisely, for data subcarriers the correspondent modulation symbols are data symbols, for virtual subcarriers they are padded zeros, for pilot

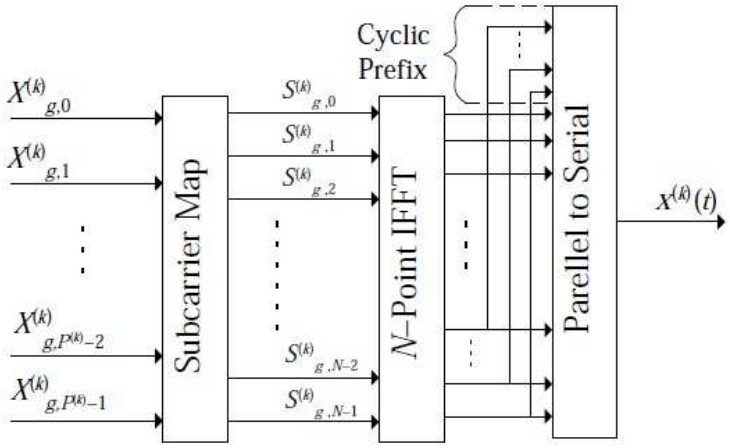

Figure 6: Uplink OFDMA transmitter scheme [1].

subcarriers the modulation symbols are pilot symbols or training symbols useful for estimating the channels. In Fig. 6 the generation of the signal in a generic OFDMA transmitter is depicted. The P_k symbols are mapped into a set of N symbols, $S^k_{g,i}$, ($i = 0, 1, ..., N-1$), according to the following rule:

$$S^k_{g,i} = \begin{cases} X^k_{g,p} & \text{if } i = c^k_p \\ 0 & \text{otherwise} \end{cases} \tag{1}$$

for $p = 0, 1, ..., P_k - 1$. The N symbols $S^k_{g,i}$ are modulated onto the N subcarriers via an N-point IFFT. A *cyclic prefix* (CP) is added to avoid *Inter Block Interference* (IBI) due to the multipath fading. So the baseband signal transmitted by the k_{th} user, in output from the parallel to serial converter, can be written as:

$$x^k(t) = \sum_{g=-\infty}^{\infty} \sum_{i=0}^{N-1} S^k_{g,i} F_{g,i}(t) = \sum_{g=-\infty}^{\infty} \sum_{p=0}^{P_k-1} X^k_{g,p} F_{g,c^k_p}(t) \tag{2}$$

where:

$$F_{g,i}(t) = \begin{cases} e^{j2\pi(i\Delta f)(t-T_{cp}-gT_b)} & \text{if } gT_b \le t < (g+1)T_b, \\ 0 & \text{otherwise} \end{cases} \tag{3}$$

Δf being the subcarrier spacing, T_{cp} the length of CP and $T_b = T + T_{cp}$ (with $T = 1/\Delta f$) the duration of a single OFDMA block. The signals are assumed to travel through slowly time-variant multipath fading channels, so fading coefficients can be considered constant during an OFDMA block. The channel between the k_{th} user and the uplink receiver is characterized by

the following response:

$$h^k(\tau, t) = \sum_{l=1}^{L^k} \alpha_l^k(t)\delta(t - \tau_l^k) \tag{4}$$

where L^k is the total number of paths, α_l^k and τ_l^k are respectively the complex gain and the time delay of the l_{th} path.

At the uplink receiver, the signal of an OFDMA block is the superposition of contributions from all the K users, assumed to be synchronized in time. So the received sampled signal, in the absence of noise, is:

$$\gamma(nT_s) = \sum_{k=1}^{K} \sum_{l=1}^{L^k} \alpha_l^k(nT_s)x^k(nT_s - \tau_l^k) \tag{5}$$

where $T_s = T/N$ is the sampling interval. Let H_p^k be the channel frequency response on the c_p^k subcarrier of the k_{th} user, during one OFDMA block (the index g is now neglected, because we focus on a generic OFDMA block):

$$H_p^k = \sum_{l=1}^{L^k} \alpha_l^k e^{-j2\pi c_p^k \Delta f \tau_l^k} \tag{6}$$

Using equations (2-6), the N signal samples of the OFDMA block (after the removal of CP) at the uplink receiver are given by:

$$\gamma(n) = \sum_{k=0}^{K-1} \sum_{p=0}^{P_k-1} H_p^k X_p^k e^{j2\pi(c_p^k \Delta f)nT_s} = \sum_{k=0}^{K-1} \sum_{p=0}^{P_k-1} H_p^k X_p^k e^{j(2\pi/N)nc_p^k} \tag{7}$$

where $n = 0, 1, ..., N-1$, under the assumption that Δf^k, the *carrier frequency offset* (CFO) between the k_{th} user and the uplink receiver, is, in its absolute value, less than the half of OFDMA subcarrier spacing. Indeed, compared to OFDM, the main problem of an OFDMA scheme is its high sensitivity to frequency offset. In OFDM in fact, since all the frequencies are used by one transmitter, maintaining orthogonality of the subcarriers is relatively easy. On the other hand, in OFDMA, since many users transmit simultaneously, each one with its own estimate of the subcarrier frequencies, a frequency offset occurs. This offset between the transmitters and the receiver destroys the orthogonality and introduces inter-carrier interference resulting in

multiple access interference. CFO estimation for OFDM has been extensively studied in recent years ([9],[10]). The problem is easier to deal with in the downlink, where different signals are multiplexed by the same transmitter, the Base Station, and the orthogonality among the subcarriers is maintained. Each user can perform the frequency synchronization by estimating a single CFO, between itself and the transmitter. Many CFO estimation algorithms proposed for OFDM can also be used for the OFDMA downlink. On the other hand, the problem is evident in the uplink of OFDMA, because many users share all the subcarriers and each one has its own CFO. CFO estimation in this case becomes a multiple parameter estimation problem. The problem has been investigated in ([11],[12]), however it is beyond the present thesis.

2.3 WiMax and LTE

In this section, the two main standards (WiMax and LTE) that exploit OFDMA are taken into account: it should be noted that they will be treated with regard to aspects relevant to the discussion of the resource allocation problem in OFDMA-based systems, main topic of the thesis. For a more detailed description of the individual standards specifically refer to [4] [5].

2.3.1 Evolution of WiMax and LTE standards

WiMax comes from IEEE family of protocols and extends the wireless access from the *Local Area Networks* (typically based on the IEEE 802.11 standard) to the *Metropolitan Area Networks (MAN)* and *Wide Area Networks (WAN)*. The earliest versions of WiMax were approved with the TDMA TDD and FDD with *Line of Sight* (LOS) propagation across the 10 to 66 GHz frequency range. Later the technology was expanded to include operation in the 2 to 11 GHz range with *Non Line of Sight* (NLOS) capability using the robust OFDMA PHY layer, with subchannelization allowing dynamic allocation of time and frequency resources to multiple users. A summary of the main standards/amendements that have occurred over time is listed below:

- *802.16*: it was the basic *802.16* standard, released in 2001. It provided high data rate links at frequencies between 11 and 60 GHz. It was withdrawn;
- *802.16a*: this amendment addressed certain spectrum issues and enabled the standard to

be used at frequencies below the 11 GHz, that was the minimum threshold of the original standard. It was withdrawn;

- *802.16b*: it increased the spectrum in order to include frequencies between 5 and 6 GHz while also providing support for *Quality of Service* aspects. It was withdrawn;

- *802.16c*: this amendment to *802.16* provided a system profile for operating between 10 and 66 GHz and more details for operations within this range, in order to achieve greater levels of interoperability. It was withdrawn;

- ***802.16d (802.16-2004)***: this version was released in 2004 and designed only for fixed scenarios. It was the major revision of the initial *802.16* standard, all previous documents were withdrawn. The standard provided improvements to *802.16a* and it was aligned with the *ETSI HiperMAN* standard to allow for global deployment;

- *802.16e (802.16-2005)*: this version was designed for nomadic and mobile use, including handover aspects. Compared to the previous versions in fact, it included many new features and functionalities needed to support enhanced QoS and high mobility broadband services at speeds greater than 120 Km/h. Depending on the antenna configuration and modulation, mobile WiMax was thought to reach uplink and downlink peak data rate capabilities of upto 75 Mbps, downto 10 Mbps within a 6 miles (10 Km) radius;

- *802.16f*: its purpose was to provide a *Management Information Base (MIB)* to *802.16-2004*. Generically a *Management Information Base* is a virtual database used for managing the various entities in a communication network;

- *802.16g*: it was designed to offer management plane procedures and services;

- ***802.16h***: it was designed to improve coexistence mechanisms for license-exempt operation;

- ***802.16j***: its purpose is to guarantee a support for multi-hop relay specification;

- ***802.16k***: it was thougth to ensure support for bridging in *802.16* networks;

- ***802.16-2009***: it consolidates IEEE Standards *802.16-2004*, *802.16e-2005*, *802.16f* and *802.16g*;

- ***802.16m***: it aims to improve interworking and coexistence with other access technologies such as 3G cellular systems, WiFi and Bluetooth and enhance the peak rates to 4G standards, set by the ITU under IMT-advanced umbrella, which calls for data rates of 100 Mbps for high mobility and 1 Gbps for fixed/nomadic wireless access. It was designed to allow cellular, macro and micro cell coverage, without restrictions on the RF bandwidth although it is expected to be 20 MHz or more;

- *P802.16n*: it was thought for higher reliability networks;

- *P802.16p*: it was designed to provide enhancements to support machine-to-machine applications.

The current versions of WiMax are highlighted in bold in the previous list, the other versions were totally withdrawn (where specified) or are in progress (the last two entries on the list).

As far as concerns LTE, it evolves from the third-generation technology which is based on WCDMA (*Wideband Code Division Multiple Access*) technique and defines the long term evolution of the 3GPP UMTS/HSPA cellular technology. The first version of LTE is documented in the Release 8 of 3GPP specifications: it defines a physical layer radio access technology based on OFDMA for the downlink (similar to the PHY layer of mobile WiMax) and a SC-FDMA (*Single Carrier Frequency Division Multiple Access*) scheme for the uplink. Nominally LTE supports high mobility broadband services at speeds upto 350 km/h with 500 km/h under consideration, peak data rates from 100 to 326.4 Mbps on the downlink and from 50 to 86.4 Mbps on the uplink, depending on the antenna configuration and modulation. LTE also targets to achieve the data rates set by the 4G IMT-Advanced standard: it aims to provide an all IP backbone with reduction in cost per bit, flexibility in the use of new and existing frequency bands, a simple network architecture with open interfaces and a lower power consumption. LTE inherits all the frequency bands defined for UMTS, spectrum which typically consists of the 800 MHz, 900 MHz, 1800 MHz and 1900 MHz. However, depending on regional and local variables, LTE deployments can be undertaken in the any of the band range from 800 MHz to 2.62

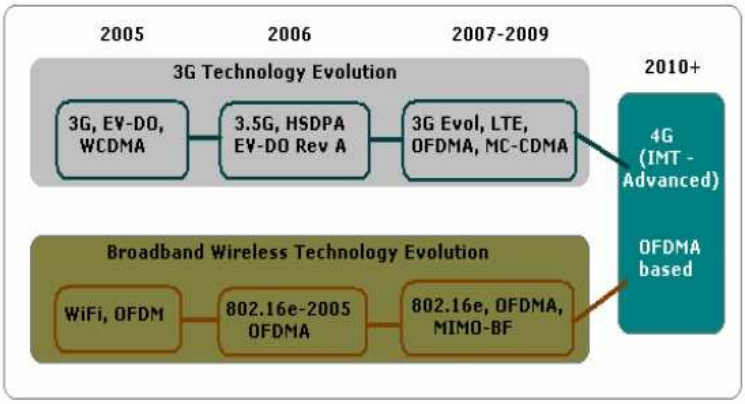

Figure 7: Evolution path of mobile wireless technologies towards 4G.

GHz. Fig. 7 shows the wireless technology evolution path for WiMax and LTE towards the ITU defined IMT-Advanced 4G standard.

2.3.2 Main aspects and parameters in WiMax and LTE

WiMax and LTE have several aspects in common, the main one is the use of OFDMA. Table 1 shows the main parameters of two stable versions of the technologies under consideration. In WiMax, OFDMA is used both on the downlink (DL) and the uplink (UL), whereas in LTE it is used only on the DL. Certain disadvantages like *Peak-to-Average Power Ratio* (PAPR) have been the reason for not using OFDMA on the UL in LTE.

Both LTE and WiMax support FDD (*Frequency Division Duplexing*) and TDD (*Time Division Duplexing*) as duplexing modes. Remember that duplexing defines as downlink and uplink data are arranged in a two-way wireless transmission. FDD requires two distinct channels for transmitting downlink sub-frames and uplink sub-frames at the same time slot. There are two versions of FDD, respectively the full-duplex FDD and the half-duplex FDD, both supported by WiMax. In the full-duplex version a user device can transmit and receive simultaneously, while in half-duplex FDD a user device can only transmit or receive at any given moment. Half duplex FDD mode is functional to support lower complexity terminals in which the hardware resources are shared in time between the uplink and the downlink. On the other hand TDD requires only one channel for transmitting downlink and uplink sub-frames at two distinct time slots. FDD is quite inefficient for handling asymmetric data services since data traffic may only occupy a small portion of a channel bandwidth at any given time, while TDD

Aspect	Mobile WiMAX (IEEE802.16e-2005)	3GPP-LTE (E-UTRAN)
Core network	WiMAX Forum™ All-IP network	UTRAN moving towards All-IP Evolved UTRA CN with IMS
Access technology: Downlink (DL) Uplink (UL)	 OFDMA OFDMA	 OFDMA SC-FDMA
Frequency band	2.3-2.4GHz, 2.496-2.69GHz, 3.3-3.8GHz	Existing and new frequency bands (~2GHz)
Bit-rate/Site: DL UL	 75Mbps (MIMO 2TX 2RX) 25Mbps	 100Mbps (MIMO 2TX 2RX) 50Mbps
Channel bandwidth	5, 8.75, 10MHz	1.25-20MHz
Cell radius	2-7Km	5Km
Cell capacity	100-200 users	>200 users @ 5MHz >400 users for larger BW
Spectral efficiency	3.75[bits/sec/Hz]	5[bits/sec/Hz]
Mobility: Speed Handovers	 Up to 120Km/H Optimized hard handovers supported	 Up to 250Km/H Inter-cell soft handovers supported
Legacy	IEEE802.16a through 16d	GSM/GPRS/EGPRS/UMTS/HSPA
MIMO: DL UL No. of code words	 2Tx X 2Rx 1Tx X NRx (Collaborative SM) 1	 2Tx X 2Rx 2Tx X 2Rx 2
Standardization coverage	IEEE 802.16e-2005 PHY and MAC CN standardization in WiMAX forum™	RAN (PHY+MAC) + CN
Roaming framework	New (work in process in WiMAX Forum™)	Auto through existing GSM/UMTS
Schedule forecast: Standard completed Initial Deployment Mass market	 2005 2007 through 2008 2009	 2007 2010 2012

Table 1: WiMax and LTE technologies in comparison.

can flexibly handle both symmetric and asymmetric broadband traffic. Compared to FDD, TDD saves the bandwidth because it uses half of FDD spectrum, it is less complex and cheaper: these are the main reasons for which the first release of fixed WiMax supported both TDD and FDD, while the subsequent mobile WiMax profiles only include TDD.

As far as concerns the adopted modulation schemes, the choice of which obviously depends on the channel conditions, LTE uses QPSK, 16QAM or 64QAM, while WiMax exploits BPSK, QPSK, 16QAM or 64 QAM. For both technologies, possible values of channel bandwidth are 1.25, 2.5, 5, 10 and 20 MHz (corresponding to FFT sizes of 128, 256, 512, 1024 and 2048).

In WiMax (TDD version) a frame duration of 5 ms is used. The frame is divided into symbols, some of them allocated for DL and the rest for UL transmissions. Fig. 8 shows the structure of the frame in WiMax. The BS schedules every frame period to convey the DL and the UL allocations. Remember that scheduling is a periodic process run from the BSs and finalized to decide how to commit resources among the different users. To avoid interference between

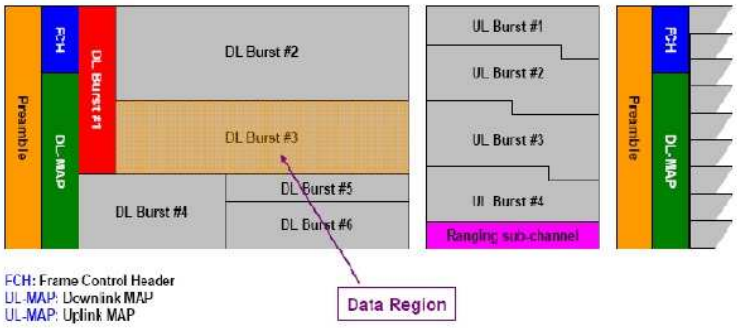

Figure 8: WiMax frame structure.

downlink and uplink signals, time gaps called *Transmit Time Gap* (TTG) and *Receive Time Gap* (RTG) are used respectively for the transition from downlink sub-frame to uplink sub-frame and for the reverse transition. The first symbol in the frame is used for preamble transmission and it is exploited by the MS for the BS identification, the timing synchronization and the channel estimation. A *Frame Control Header* (FCH) follows the preamble and provides information about the frame configuration, such as MAP message length, coding scheme and usable sub-channels. DL-MAP and UL-MAP are MAC layer messages that provide resource allocation and other control information, respectively for DL and UL sub-frames. Each MAP message consists of a fixed part and a variable one. The size of the variable part is proportional to the number of downlink and uplink users scheduled in that frame. Typical information contained in the MAP messages are the frame number, the number of zones and the location and content of all bursts. Each burst is uniquely determined by its symbol offset, its subchannel offset, the number of symbols, the number of subchannels, the power level and the repetition coding.

A mobile device has to search for a valid preamble to acquire frame synchronization. Once it acquires the synchronization, the mobile reads the FCH message which points to the length of the DL-MAP message which contains the various allocations in the frame. The location of the FCH and the DL-MAP is fixed once the segment is identified in the preamble processing.

In all the subchannelization methods used in WiMax, 48 data subcarriers are available in a slot. In the PUSC mode 24 subcarriers, scattered across the spectrum, are spread out over 2 consecutive OFDM symbols: the pseudorandom selection of the positions of the subcarriers is dependent on the CELL-ID and is clearly specified in the standard. In the AMC version, 16

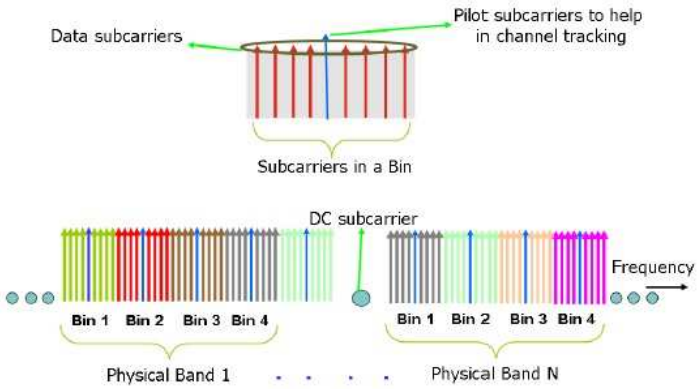

Figure 9: Subchannels in 802.16e - AMC configuration.

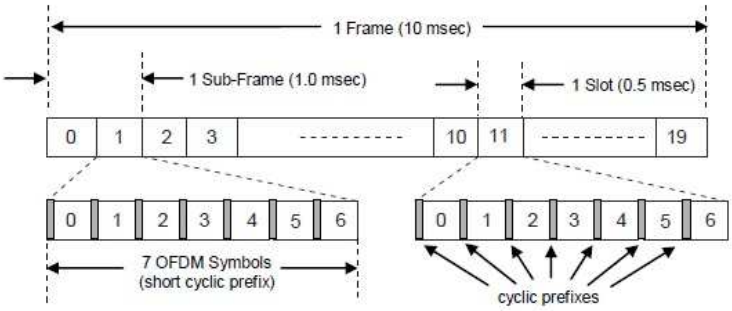

Figure 10: LTE frame structure.

subcarriers are distributed over 3 OFDM symbols. The subcarriers are organized into groups of 9 contiguous subcarriers which are called bins, as shown in Fig. 9. Each bin has 8 data and 1 pilot subcarrier and four such bins form a band. The generic user feeds back the best 4 bands perceived and periodically updates this information using certain messages defined in the standard. Based on this feedback, the Base Station chooses 2 bins in one of these bands and allocates the same bins over 3 consecutive OFDM symbols resulting in 48 data subcarriers in a slot. The information used as feedback from the users to determine the best bands are tipically the *Received Signal Strength Indicator* (RSSI) and the *Signal to Interference plus Noise Ratio* (SINR). These information are periodically reported through medium access control (MAC) messages. In addition, there can be on-demand messages which can report changes in conditions as responses to requests from the BSs.

In LTE, the frame duration is 10 ms: the frame is divided into subframes of 1 ms duration and the BS schedules transmissions every subframe time. Fig. 10 shows the typical structure of a LTE frame. Each subframe is made up of two slots of 0.5 ms. Twelve adjacent subcarriers are grouped in the frequency domain and 7 OFDM symbols (or 6 OFDM symbols in case of

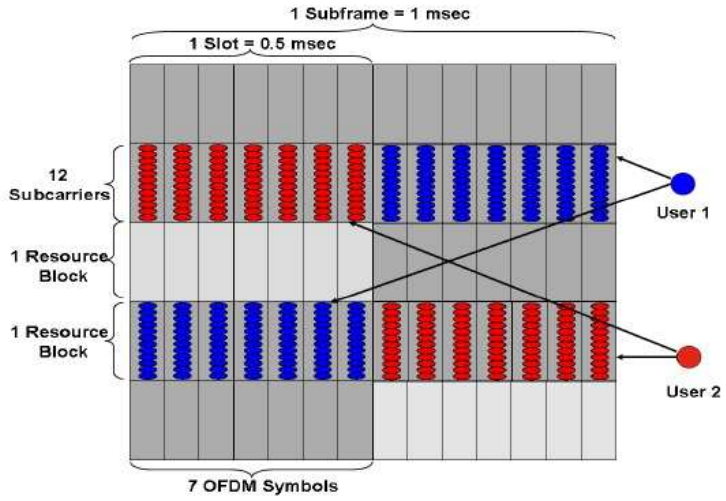

Figure 11: Frequency distributed data mapping in LTE downlink.

extended CP) in the time. The 84 (72) subcarriers thus obtained form an unit called *Resource Block* (RB); 2 RBs are the minimum unit allowed in a frame. However, in order to achieve frequency diversity, instead of using the same RB in the second part of the subframe, another RB can be used in the second slot of the subframe as illustrated in Fig. 11. The RBs to be used for sending data to MSs are chosen by the BSs based on feedback information.

Two types of feedback, periodic and aperiodic, are possible in LTE. In the first case user device sends feedback information in a separate control channel at predefined regular time intervals, ranging from a minimum of 2 ms to a maxinum of 160 ms. In the aperiodic case instead, the BS requests the user to send a channel status report. The channel feedback can be one value for the entire operating bandwidth or a sequence of values for a sequence of sub-bands covering the entire bandwidth. The sub-bands are basically groups of RBs. The minimal bandwidth resolution of the feedback that is possible in LTE is 2 RBs.

Irrespective from the configuration (seven different configurations are possible in LTE), sub-frames 0 and 5 are always used for downlink transmissions, while sub-frame 1 is always a special sub-frame. The composition of other sub-frames instead varies, based on the particular configuration.

Synchronization is performed in two steps, exploiting two different synchronization sequences, a primary sequence and a second one. The *Primary Synchronization Sequence* (PSS) is sent twice in a frame and the number of subcarriers used for it, unlike the preamble in WiMax, is fixed. The identification of PSS in the received signal gives two potential starting points in

the frame as there are two PSS transmissions in the frame. The ambiguity is resolved by the *Secondary Synchronization Sequence* (SSS) which is sent 1 OFDM symbol ahead in the same set of subcarriers as the PSS. The detection of the SSS allows the frame synchronization and the discovery of CP duration and cell identifier. So in LTE, irrespective of bandwidth and number of subcarriers, the first step is the same for all the devices, i.e. locating PSS and SSS and obtaining the CELL-ID.

3 Resource allocations and performance analysis in homogeneous cellular systems

A typical cellular system consists of a certain number of Base Stations opportunely located in the territory, with users randomly distributed within it. We use the term homogeneous to refer to a context with a single layer of similar equipments, the Base Stations, which provide coverage to the users. They exhibit similar transmit power levels, antenna patterns and backhaul connectivity to the data network. Moreover, they offer unrestricted access to users in the network, and serve roughly the same number of terminals, all of which carry similar data flows with similar QoS requirements. The location of macro BSs are carefully chosen by network planning and their setting is properly configured to maximize the coverage and control the interference. As the traffic demands grow and the RF environment changes, the network relies on cell splitting or additional carriers to overcome capacity and link budget limitations and maintain uniform the service level of users. However this deployment process is complex. Moreover, site acquisition for macro-BSs with towers is difficult in dense urban areas. So a more flexible deployment model is needed for operators to improve broadband user experience in a ubiquitous and cost effective way. In the next chapter we will look at more complex heterogeneous scenarios in which femto-BSs are added to the traditional Base Stations with the aim to increase the service level, especially of cell edge users. Additional problems occur in these contexts, scenarios which on the other hand are more and more frequent.

OFDMA is based on the independence of fading statistics, i.e. a subchannel which appears to a user to be in deep fade at any given time, can result a good channel for other users at the same time. So there are two different decisional levels in an allocation mechanism: the choice of the radio resources to assign to each user on one hand and the modulation, coding and power level to adopt on the other one. Many algorithms and proposals on resource allocation in OFDMA systems exist, especially with reference to single-cell scenarios, but the problem is not banal when the size of the network and the number of users increase.

The chapter begins with the description of a semplified system/signal model of a homogeneous cellular context. Then the *water filling* approach ([13],[14]), that represents the optimal

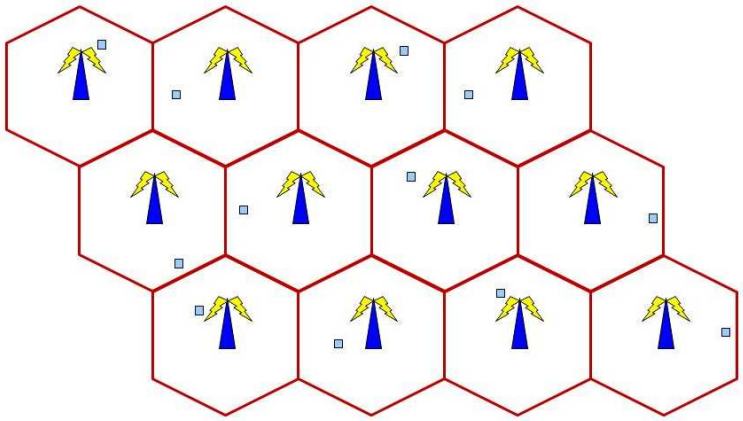

Figure 12: Example of layout with 12 cells.

solution in scenarios with a single cell and a single user, is presented and a description of the main basic scheduling principles is made, together with an analysis of some approaches existing in literature. A section devoted to simulation results closes the chapter.

3.1 System and capacity model

In this section a semplified model of a system with a single-user per cell is deliberately described [15]. The reason to consider a such semplification is functional to the introduction of the *water filling* approach that is the optimal solution when a single BS serves a single user. Moreover it is the basic model used for simulations that we run with the aim to compare different channel reuse policies without considering scheduling implications. However, a complete multi-user model, which also takes into account a more generic heterogeneous network context, will be described in detail in the next chapter.

Fig. 12 shows an example of network topology with 12 cells. In our semplified model each BS serves a unique Mobile Station (MS), associated to the BS from which it senses the best channel. Therefore, being N the number of BSs, the network includes N cells and N users. The same band is available at each BS and can be allocated according to an OFDMA access scheme. Let K_{FFT} be the total number of carriers and let K be the number of carriers actually used for transporting data. In each symbol interval, each carrier can be in principle modulated with an adaptive scheme according to the channel quality perceived by the receiver. In order to limit the signaling overhead required for informing the transmitter about the receiver channel quality and for communicating the allocation map to the MSs, the common solution

(typical of the OFDMA systems) to group multiple subcarriers into a single allocation unit is adopted. Hereafter, these units will be called *Physical Base Units* (PBUs) or *Resource Blocks* (that is the notation, typical of LTE, already adopted in the previous chapter) regardless. So K_{PBU} carriers are grouped together according a predefined permutation scheme. Consequently, the total number of allocation units results $U = \lfloor K/K_{\mathrm{PBU}} \rfloor$.

Let i be the cell index (also corresponding to a BS and a MS index) in the range $[1, N]$ and let k be the carrier index in the range $[1, K]$. The downlink channel gain between the i-th BS and the j-th MS is denoted as $\gamma_{i,j}$ and the fading coefficient for the k-th carrier as a complex number $h^k_{i,j}$. The received signal $y_{i,k}$ at the user i in the k-th carrier is generally given by:

$$y_{i,k} = \gamma_{i,i} h^k_{i,i} x^k_i + \sum_{j \neq i}^{N} \gamma_{j,i} h^k_{j,i} x^k_j + n^k_i, \tag{8}$$

where x^k_i is the signal transmitted by BS i on carrier k, and n^k_i is an additive thermal noise on the same carrier.

Let $p^k_i = E\{|x^k_i|^2\}$ the power allocated in cell i on the k-th carrier and let $\boldsymbol{p_i} = (p^1_i, p^2_i, \cdots p^K_i)$ the power allocation vector in cell i. Since each cell i has a maximum transmit power constraint P_i, in each symbol time $\sum_k p^k_i \leq P_i$. The *Signal to Noise and Interference Ratio* (SINR) in each carrier is given by:

$$\mathrm{SINR}^k_i = \frac{\gamma^2_{i,i} |h^k_{i,i}|^2 p^k_i}{\sigma^2 + \sum_{j \neq i}^{N} \gamma^2_{j,i} |h^k_{j,i}|^2 p^k_j} \tag{9}$$

Assuming that adaptive coding and modulation allows to reach the channel capacity of each subcarrier, by using a single transmission format for a whole PBU, a conservative estimate of the capacity (in bits/channel usage) available in a generic l-th PBU ($l \in [1, U]$) is given by:

$$C^l_i = K_{\mathrm{PBU}} \min_{k \in \mathrm{PBU}_l} \log(1 + \mathrm{SINR}^k_i) \tag{10}$$

where PBU_l represents the set of carriers included in the l-th PBU (for example the set $\{K_{\mathrm{PBU}} \cdot (l-1), K_{\mathrm{PBU}} \cdot (l-1)+1, \ldots, K_{\mathrm{PBU}} \cdot l-1\}$ if the AMC permutation scheme is used). Obviously, the capacity depends not only on the power allocated within the cell, but also on the power

allocated in all the other cells.

An approach largely studied in literature is based on the maximization of the aggregated capacity of the cell. The vector $\boldsymbol{p_i}$ has K components that vary in the space $\Pi = \mathbb{R}_+^K$, being $\mathbb{R}_+$ the set of non-negative real numbers. Therefore, the power vector can be determined as:

$$\boldsymbol{p_i} = \arg\max_{\boldsymbol{p_i}\in\Pi} \sum_{l=1}^{U} C_i^l(\boldsymbol{p_1}, \boldsymbol{p_2}, \cdots \boldsymbol{p_N}) \tag{11}$$

under the constraint $\sum_{k=1}^{K} p_i^k \leq P_i$, and can be easily found with the *water filling* algorithm. Since this optimization requires the knowledge of the SINR values experienced in each carrier, it also requires a feedback from the receiver to the BS, which can be sampled in time and quantized in order to limit the signaling overhead.

The extension of the allocation problem to the multi-cell scenario, although formally immediate, presents several challenges and leads to a significant increment of the dimensionality of the optimization space. In particular the capacity-maximizing approach can be extended to the whole network, by considering an allocation problem involving a vector $\boldsymbol{p}$ of vectors $\boldsymbol{p_1}, \boldsymbol{p_2}, \cdots \boldsymbol{p_N}$, varying in Π^N:

$$\boldsymbol{p} = \arg\max_{\boldsymbol{p}\in\Pi^N} \sum_{i=1}^{N} \sum_{l=1}^{U} C_i^l(\boldsymbol{p}) \tag{12}$$

This optimization problem is non-convex [16] and standard optimization techniques do not apply directly. Moreover, even neglecting the computational issues, the solution requires a centralized allocator knowing instantaneous inter-cell channel gains (and thus creating acute signaling overheads).

So the problem from the network perspective is already difficult to face at this level, even though aspects concerning scheduling (until now just a user per-cell was considered), coexistence of heterogeneous Base Stations and different traffic demands from users, were not yet included.

In real contexts, BSs have to serve multiple users simultaneously, each one with its own service request. Compared to the previous networks, designed to support a single type of service, next generation networks are increasingly looking to provide multiple services to

QoS	Pros	Cons
UGS	No overhead. Meet guaranteed latency for real-time service	Bandwidth may not be utilized fully since allocations are granted regardless of current need.
ertPS	Optimal latency and data overhead efficiency	Need to use the polling mechanism (to meet the delay guarantee) and a mechanism to let the BS know when the traffic starts during the silent period.
rtPS	Optimal data transport efficiency	Require the overhead of bandwidth request and the polling latency (to meet the delay guarantee)
nrtPS	Provide efficient service for non-real-time traffic with minimum reserved rate	N/A
BE	Provide efficient service for BE traffic	No service guarantee; some connections may starve for long period of time.

Table 2: WiMax QoS service classes in comparison.

Classes	Applications	Bandwidth Guideline		Latency Guideline		Jitter Guideline		QoS Classes
1	Multiplayer Interactive Gaming	Low	50 kbps	Low	< 25 ms	N/A		rtPS and UGS
2	VoIP and Video Conference	Low	32-64 kbps	Low	< 160 ms	Low	< 50 ms	UGS and ertPS
3	Streaming Media	Low to high	5 kbps to 2 Mbps	N/A		Low	< 100 ms	rtPS
4	Web Browsing and Instant Messaging	Moderate	10 kbps to 2 Mbps	N/A		N/A		nrtPS and BE
5	Media Content Downloads	High	> 2 Mbps	N/A		N/A		nrtPS and BE

Table 3: WiMax application classes and correspondent requirements.

the users. For instance WiMax standard supports five service classes, listed in Table 2, and applications are classified into five categories (as shown in Table 3), each one characterized by specific constraints on bandwidth, latency and jitter.

Scheduler designers need to consider the allocations logically and physically. Logically the scheduler should calculate the number of slots necessary to satisfy a request, based on QoS service classes. Physically, the scheduler needs to select which subchannels and time intervals are suitable for each user. The goal usually is to minimize the power consumption or the bit error rate or to maximize the total throughput.

The problem of scheduling resources in its generality involves three distinct scheduling processes: two at the Base Station (BS), one for the downlink and the other one for the uplink, and one at the Mobile Station (MS) for the uplink. At the BS, packets from the upper layer are put into different queues, depending on the traffic type. Based on the QoS parameters and some extra information such as the channel state condition, the DL-BS scheduler decides which queue to serve and how many data units should be transmitted to the MSs. Similarly the UL-BS scheduler decides how many resources must be granted to each MS in the subsequent uplink subframes, based on the bandwidth requests from the MSs and the associated QoS parameters. Finally the third scheduler at the generic MS decides, once the UL-BS grants the bandwidth for

the MS, which queues should use the reserved resources: consequently its goal is to manage the MS queue in order to establish possible priorities if heterogeneous traffic is handled by the user.

In this thesis, focus is on the DL-BS scheduling; however the discussed scheduling principles are also valid for the other cases.

3.2 The water filling approach

Consider a single-user OFDMA system in which there are only one transmitter (the BS) and one receiver (the mobile device). With regard to this scenario, OFDMA coincides with OFDM, because within a slot all the resources can be allocated to a single user. So for simplicity we can refer to the OFDM case, thinking in terms of subcarriers rather than in terms of subchannels. So the signal $y(k)$ received on the k_{th} ($k = 0, 1, ..., K-1$) resource, in output from the FFT block, is:

$$y(k) = \sqrt{P(k)}a_k H(k) + n(k) \tag{13}$$

where $P(k)$, a_k, $H(k)$ and $n(k)$ respectively are the allocated power, the transmitted symbol, the channel response and the thermal noise on the k_{th} subcarrier. Exploiting the knowledge of the channel matrix *H*, the transmitter adapts the transmit power and the format to be used on each subcarrier, according to a predetermined criterion of optimality. The problem is then to choose the parameters determining the transmit power $P(k)$ and the modulation format $c(k)$ to be used on each subcarrier. In other terms, as mentioned in the previous section, assigned an objective function that characterizes the performance of the system, the goal is to find the vectors ***c*** and ***P*** which maximize it, in accordance with certain constraints on the maximum power, the permissible minimum rate or the maximum probability of error.

One of the most well-known problems of resource allocation is to distribute the power on the different subcarriers to maximize the capacity of the system, respecting the constraint on the transmit power. The capacity of a given channel is defined as the maximum information rate that can be transmitted on that channel with arbitrarily low probability of error for a given *Signal to Noise Ratio*. Despite the channel capacity is a theoretical value, it is of fundamental importance to determine a theoretical limit to the performance of any transmission system.

The K subcarriers of an OFDM system can be considered as parallel AWGN channels,

consequently the total capacity can be evaluated as the sum of the capacities associated to these individual subcarriers:

$$C(\mathbf{P}) = \sum_{k=0}^{K-1} log(1 + \frac{|H(k)|^2 P(k)}{\sigma^2}) \tag{14}$$

The goal pursued by the *water filling* approach is to determine the vector ***P*** that maximizes the capacity:

$$\mathbf{P_{opt}} = \arg\max_{\mathbf{P}} C(\mathbf{P}) \tag{15}$$

with the following constraint on the total transmit power:

$$\sum_{k=0}^{K-1} P(k) = P_{tot} \tag{16}$$

If the transmitter did not have any information about the state of the channel, the optimal resource allocation would be an uniform power allocation, consisting in transmitting the same power on all the subcarriers. When the receiver knows the channel status, the problem can be solved in closed form using the technique of Lagrange multipliers and the solution (carrier by carrier) is:

$$P(k) = (\mu - \frac{\sigma^2}{|H(k)|^2})^+ \tag{17}$$

where:

$$(x)^+ = max(0, x) \tag{18}$$

and

$$\mu = \frac{P_{tot} + \sigma^2 \sum_{k=0}^{K-1} \frac{1}{|H(i_k)|^2}}{K} \tag{19}$$

being K the number of the subcarriers and $i_0, i_1, ..., i_{K-1}$ the indices of the subcarriers for which $P(k) > 0$. The solution is called *water filling* because the power is distributed like water in a basin whose depth depends on the SNR on the different subcarriers (Fig. 13 on the following page). The total power determines the water level while the channel gains determine the amount of power to be allocated on the different subcarriers. According to this approach, most of the power is allocated on the best channels, and, if a subcarrier is too attenuated, it can not be used at all. When the water level is low, i.e. the available power is low, it is transmitted only on the

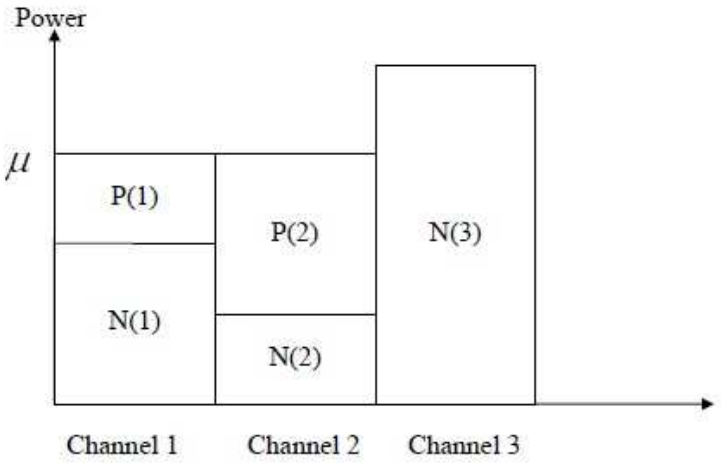

Figure 13: *Water filling* for parallel channels.

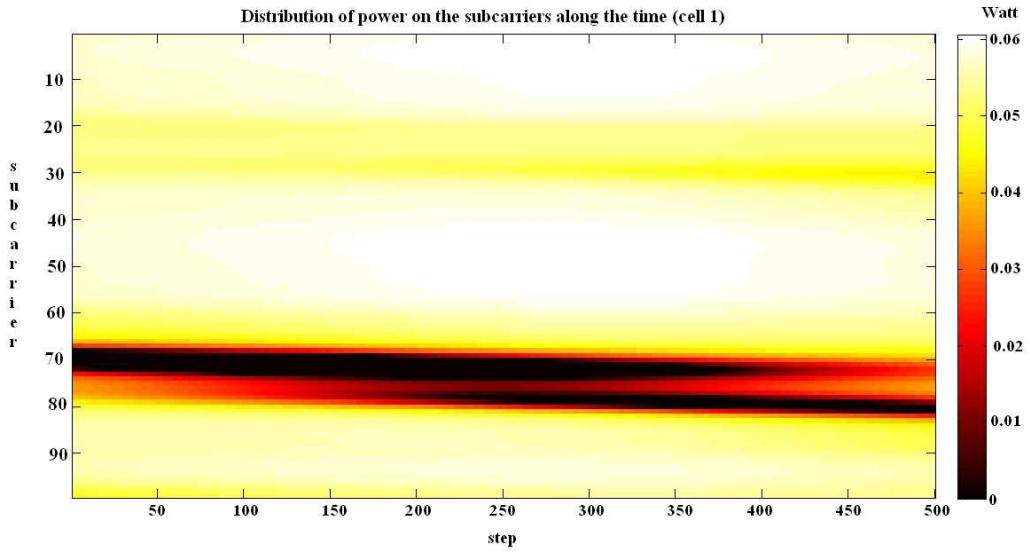

Figure 14: Distribution of power on the subcarriers over time (cell one), according to a *water filling* approach.

best channels. On the other hand, when all the SNR values are on average similar, the *water filling* solution tends asymptotically to distribute the power in a uniform way.

Figures 14 and 15 on the following page show a graphic trend of the distribution of the powers on the single subcarriers over the time in a particular simulated context, when the *water filling* algorithm is applied. The figures were obtained exploiting a self-made simulator, whose details are described in the Appendix of the thesis. In the specific case they refer to a context with two cells and two users (one user per cell, according to the semplified model considered until now): the BSs allocate all the available resources to their associated users and the power is distributed according to the *water filling* criterion (with a total transmit power available at

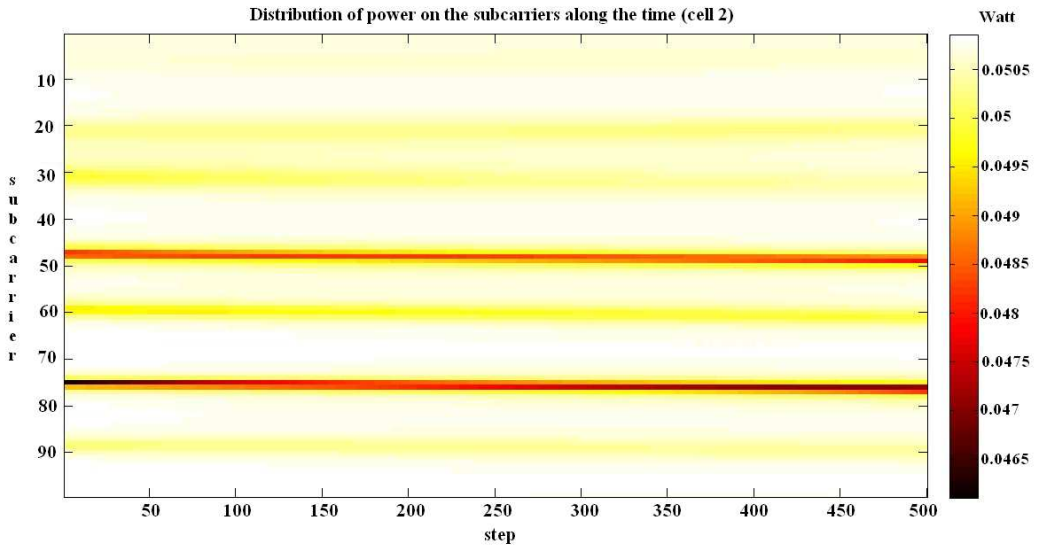

Figure 15: Distribution of power on the subcarriers over time (cell two), according to a *water filling* approach.

each BS set to 5 Watt). Each temporal step (sample) corresponds to a frame time of 10 ms and the resources consist of 96 subcarriers (grouped in 12 PBU of 8 subcarriers each one). The users are quasi-static (a mobility of 3 km/h is set), consequently the channels vary slowly over time. This is the reason for which the figures present a stripe pattern, being the best (and the worst) channels estimated by a user as such for all the simulation duration. As reported in the legend (values in Watt), lighter shades of color correspond to higher values of power assigned to a subcarrier and vice versa.

The *water filling* approach gives an optimal solution to the problem of resource allocation in single-user scenarios, consequently it can not be used in actual contexts where multiple users compete for the resources. Approaches for multi-cellular and multi-user environments will be considered in the next paragraph.

3.3 Scheduling problems and proposals

The goal of this section is to focus on scheduling in OFDMA multi-cellular and multi-user contexts, in order to highlight the problems that a careful scheduler designer has to face in designing a good scheduling algorithm. The main aspects and trends existing in literature are now taken into account; in the next chapter the treatment will be generalized to heterogeneous contexts.

Next generation wireless networks have the need to cope with the scarcity of the spectral resource in areas with heavy user demand. Therefore, they have to simultaneously pursue the maximization of spectral reuse and per-link capacity. These two needs have been traditionally faced by decoupling the multi-cell resource allocation problem from the single cell capacity optimization. In other words, in current approaches, resource allocation is performed in two different levels, in terms of a priori frequency planning at the network level and run-time scheduling, power control and link adaptation at the cell level. Indeed, each resource allocation level strongly affects the performance of the other one. For example, the interference suffered in each cell depends on the reuse pattern, while advanced scheduling techniques (based on channel or user location information) can allow shorter reuse distances.

Recent literature however is considering joint optimization solutions for the multi-cell ([17],[18],[19],[20]) and single-cell ([21],[22]) resource allocation problem. While the degrees of freedom of such an optimization offer a significant space for improving the overall network performance, the actual feasibility of these solutions is limited because of the computational complexity of the optimization and the significant overhead due to the required signaling.

In order to reduce the signaling, some allocation solutions introduce artificial *structures* devised to make interference more predictable. For example grouping contiguous multi-carriers, shaping power according to a pre-defined profile ([23],[24]), switching periodically transmission beams, and so on, can help in reducing the optimization space and the required interference information.

Another way to reduce (even avoid) the signaling is to use approaches that do not use information of the channel state condition in making the scheduling decisions. They are normally referred to as *channel-unaware* schedulers and generally assume error-free channel since it makes easier to prove assurance of QoS. So there is no signaling overhead due to the feedback from MSs. However, in wireless environments where there is a high variability of radio link such as signal attenuation, fading interference and noise, the channel-awareness is important. In fact, if the radio channel conditions are taken into account, the improvements in throughput can be considerable and the resources can be scheduled efficiently.

As far as concerns another aspect, i.e. the optimization criteria that can be followed

in making scheduling decisions, the literature is generally oriented in two directions: *Margin Adaptive* (MA) approaches ([25],[26]) that aim to minimize the total transmission power while satisfying QoS requirements (minimum data rate, maximum Bit Error Rate (BER), maximum delay, etc) of users, and *Rate Adaptive* (RA) ([22],[27],[28]) strategies devoted to maximize the system throughput subject to constraints on maximum total transmission power and QoS requirements. It is easy to understand that the *water filling* approach falls into the latter trend. In every case allocation techniques really focus on the optimization of power or throughput under the common hypothesis that a radio resource can be used by a single MS at a time, in order to avoid intra-cell interference. From the point of view of classical RA approaches, the capacity is maximized when each subcarrier (or subchannel in the OFDMA case) is assigned to the user with the best subchannel gain and power is distributed by the *water filling* algorithm. Nevertheless, as already mentioned in the previous section, this could not be the optimal solution in multi-user contexts because the system becomes unfair. In fact users who have good channel gains can be well-served while users who perceive bad channel gains can not be assigned any subchannel. This is the reason for which, for RA approaches, the introduction of fairness criteria has been considered by searches.

In wired communications a scheduler is recognized to be fair if the resources are shared equally among the users, since a fair share in resources results in equalized user data rates. In wireless communications instead, a fair share in resources usually does not result in equalized user data rates since users have different geometries, which result in different achievable data rates. So two different fairness criteria should be considered in wireless contexts, precisely:

- *Allocation Fairness* which refers to the amount of allocated resources within a given time interval, defined in [29]:

$$F_A(\Delta T) = \frac{(\sum_{m=1}^{M} A_m(\Delta T))^2}{M \sum_{m=1}^{M} A_m(\Delta T)^2} \tag{20}$$

- *Data Rate Fairness* which refers to the achieved data rate within a given time interval,

which is equivalent to the fairness criterion defined in [30]:

$$F_{DR}(\Delta T) = \frac{(\sum_{m=1}^{M} R_m(\Delta T))^2}{M \sum_{m=1}^{M} R_m(\Delta T)^2} \tag{21}$$

where M denotes the number of users, $A_m(\Delta T)$ is the number of allocation units scheduled to user m in time interval ΔT and $R_m(\Delta T)$ is the data rate that user m achieved in the same time interval ΔT. In both cases, a fairness value of one corresponds to optimal fairness within a given time interval ΔT with respect to the defined criterion, i.e. $F_A(\Delta T) = 1$ and $F_{DR}(\Delta T) = 1$ respectively indicate that all users received identical resources/data rates within the interval ΔT.

The time to converge to fairness is important since the fairness can be defined as short term or long term. The short-term fairness implies long-term fairness but not vice versa.

Some basic strategies, such as *Round Robin* or *Max-Min* approaches, aim to obtain fairness, as opposed to other ones which aim to maximize the throughput (*Max Rate* approaches).

In particular *Round Robin* (RR) approach fairly assigns the allocation one by one to all users/connections. It provides fairness among the users but it may not meet the QoS requirements and it can be inefficient since the allocation is made for connections that may have nothing to transmit. *Max-Min* approaches instead are designed to maximize the worst case, i.e. they aim to give priority in terms of scheduling to users which experience bad SINR values. These schemes, which provide quasi-perfect system fairness, penalize users with better condition, so reducing the system efficiency.

On the other hand, *Max Rate* approaches aim to serve, step by step, users with the highest achievable instantaneous data rate. This solution benefits the users closer to the Base Stations or with a higher power capability. So users who have constantly good channels will be provided more chance, while others who have constantly bad channels will have less chance to be served.

Consequently a tradeoff between maximal throughput and fairness becomes the most important issue in OFDMA systems. It can be obtained by adopting a *Proportional Fairness* (PF) criterion, so called because it aims to reach fairness in proportion to the user conditions. For a fixed step, a PF scheduler allocates the user m^* who maximizes the ratio of achievable

instantaneous data rate over average received data rate:

$$m^* = \arg\max_m \frac{R_m(t)}{R_m^{avg}(t)} \tag{22}$$

where $R_m(t)$ and $R_m^{avg}(t)$ respectively denote the achievable instantaneous data rate for user m at time t and the average data rate that user m received up to time t. A law for the update of the second term can be formulated as:

$$R_m^{avg}(t) = (1 - \frac{1}{T_c})R_m^{avg}(t-1) + \frac{1}{T_c}R_m(t-1) \tag{23}$$

where $R_m^{avg}(t-1)$ and $R_m(t-1)$ are respectively the average and the instantaneous data rate of user m at the previous time instant and T_c is the average window size which is an adjustable parameter, which choice affects the temporal depth of the fairness (short term or long term fairness) that the scheduler designer wants to achieve.

Introducing appropriate weighting factors in the expression (22), a more flexible scheduling strategy can be obtained. In other words, considering $\alpha \in [0; \infty[$ and $\beta \in [0; \infty[$, the choice of the user to be scheduled falls in that one which maximizes the following expression:

$$m^* = \arg\max_m \frac{[R_m(t)]^\alpha}{[R_m^{avg}(t)]^\beta} \tag{24}$$

For a parameter setting of α=β=1, conventional PF scheduling is achieved, which is known to provide a good tradeoff between allocation fairness and system throughput by utilizing the multiuser diversity. Tuning opportunely parameters α and β, the tradeoff between allocation fairness and system throughput can be modified slightly. An increase of α will increase the influence of the achievable instantaneous data rate which enhances the possibility that an user in currently good condition can be scheduled. This results in higher system throughput, but less allocation and data rate fairness. On the other hand, higher values of β will increase the influence of the average data rate, then the probability of a user with a low average data rate to be scheduled. This results in higher data rate fairness, but lower system throughput. In particular, the two extreme cases are achieved by setting the values of α and β in the following way:

- $\alpha = 1$ and $\beta = 0$ corresponds to the *Max Rate* (MR) scheduler, where the user with the highest achievable instantaneous data rate at time t is scheduled, since the denominator in equation (24) is equal for all users. The maximum system throughput is obtained at low fairness.

- $\alpha = 0$ and $\beta = 1$ schedules the user with the lowest average data rate up to at time t, i.e. equalizes the average data rates of users, since the numerator in equation (24) is equal for all of them. This results in maximum data rate fairness, but in low system throughput.

The parameters can be changed over time, depending on factors such as the system load or the distribution of users on the network, so adaptively giving more weight to a factor over the other one. In this way a *Dynamic Resource Allocation* (DRA) technique is obtained.

Existing optimized single-cell based algorithms are not practical for use in multi-cell environment since the co-channel interference among the cells, due to the reuse of the same spectrum in adjacent cells, affect the performance significantly. According to the reuse factor in fact, only the cells belonging to the same cluster use orthogonal resources.

Multi-cell resource allocation with *Inter-Cell Interference* (ICI) consideration can be basically classified into two categories. The first one extends the single-cell allocation context to the multi-cell scenario, mainly by considering the *Signal to Interference and Noise Ratio* (SINR) instead of the *Signal to Noise Ratio* (SNR), i.e. considering the interfering quota from other cells as additional noise. Li and Liu [17] proposed a two-level resource allocation scheme, in which a radio network controller coordinates multiple cells in the first level and performs per-cell optimization in the second level. The first level is based on perfect and predetermined knowledge of SINR for all MSs on all subchannels. Pietrzyk and Janssen ([31],[32]) proposed heuristic algorithms based on SINR with some QoS consideration. These approaches presuppose a perfect knowledge of SINR values, information difficult to obtain a-priori since the interference depends on the distance, location and occupied channel status of interferers, which are unknown before the resource allocation.

The second class of works aims to exploit *Radio Resource Management* (RRM) techniques and policies as *Inter-Cell Interference Coordination* (ICIC) ([20],[33]) and *Base Station Cooperation* (BSC) ([34],[35]) to mitigate ICI and improve the overall system performance.

These solutions have the defect of a high overhead due to the signaling.

Finally there are studies that aim to address the allocation problem as a game theory problem, for instance refer to [36] and [37]. Goodman et al. studied a game theoretic framework for the resource allocation problem. Their approach aim to solve the problem in a distributed way, so belonging to the domain of *non-cooperative* games where each user is only interested in achieving its own goal. This approach does not ensure fairness and it can be inefficient from the point of view of the overall system throughput. On the other hand in [37] it has been proposed a model of resource allocation problem using another branch of game theory, the *cooperative* game [38], which emphasizes collective rationality and fairness.

3.4 Simulation results

In this section the problem of multi-cellular resource allocation in OFDMA environments is analyzed from a simulation point of view. The simulated contexts are scenarios with reuse factor equal to 1, where macro-BSs with different power constraints coexist and different propagation environments (macro-cellular and micro-cellular ones) are considered. Details on the used simulator and the considered propagation models can be found in Appendix.

The simulations here reported aim at comparing the effects of different allocation schemes, independently performed in each cell, on the aggregated network-level performance, in order to enlighten the network scenarios in which network planning and mobile station feedbacks are (or are not) advantageous. In particular, greedy allocation schemes, i.e. schemes utilizing all the carriers available in each cell, and non-greedy schemes, i.e. schemes leaving some resources empty in order to reduce interference with other cells, are compared.

Given the complexity of the joint allocation, scheduling and power control problem, the network load scenario is semplified by considering a single user per cell in this set of simulations. Although this assumption hides the multi-user diversity gain, it allows to compare the different channel reuse policies without considering any user scheduling scheme (whose effect could complicate the interpretation of the results).

3.4.1 Resource allocation schemes in comparison

The resource allocation schemes implemented for comparison are:

- *Uniform:* According to this scheme, no signaling is required and the BS just transmits in each carrier with a constant power given by:

$$p_i^k = P_i/K, \forall k \in [1, K] \tag{25}$$

- *Water Filling:* In this case, the power allocation vector is determined by the *water filling* algorithm. The SINR values experienced at time $t-1$ are used as the estimates of the expected SINR values at time t. Therefore, the SINR values are supposed to be signaled at each symbol time by means of an error-free dedicated control channel.

- *Fractional Water Filling:* This scheme is similar to the previous one, but it is applied to a pre-defined sub-set of the available carriers. Specifically, at each time t, the BS selects a number $r \cdot K$ of transport carriers over which it applies the *water filling* algorithm. The ratio r is a scheme tunable parameter, while the carrier selection is based on the best SINR values experienced at time $t-1$.

The rational of considering both *water filling* and *fractional water filling* is that utilizing or non utilizing all the resources available in each cell can lead to different interference levels among the cells. Since *water filling* intrinsically discards the carriers experiencing the worst channel and interfering conditions, we consider the *fractional water filling* as a kind of dynamic and distributed scheme for resource repartition among the cells.

After that all the cells run the allocation scheme (whose convergence time is assumed to be negligible), the new SINR values are computed and the actual capacity available at time t is evaluated by using these SINR values. Unless otherwise specified, Table 4 summarizes the numerical settings adopted in simulation, where T_{sym} is the symbol duration, B is the available band, d_{site} is the distance between two BSs and v_{MS} is the speed of MSs. As far as concerns the modeling of the signaling overhead, required by the *water filling* schemes, each MS feeds back

Parameter	Value
Carrier Frequency	2100 MHz
K_{FFT}	128
K	84
N	12
K_{PBU}	7
T_{sym}	16 μs
B	6.6 MHz
d_{site}	250 m
v_{MS}	3 km/h

Table 4: Main system parameters.

to its serving BS the m-bit quantized *Channel State Information* (CSI):

$$\mathrm{CSI}_i^k = \frac{\mathrm{SINR}_i^k}{p_i^k} = \frac{\gamma_{i,i}^2 |h_{i,i}^k|^2}{\sigma^2 + \sum_{j \neq i}^{N} \gamma_{j,i}^2 |h_{j,i}^k|^2 p_j^k}. \tag{26}$$

The CSI values corresponding to carriers belonging to the same PBU are summed, thus obtaining an average information per-PBU. These informations, m-bit quantized, are fed back by each MS to its serving BS. Since the *fractional water filling* works only on a sub-set of PBUs, a possible signaling compression scheme is using a U-element bitmap, identifying the used PBUs U_{used}, and signaling only the U_{used} quantized ratios (26). With this assumption, it results a per-MS overhead O_i rate estimate of:

$$O_i = \frac{U + mU_{\mathrm{used}}}{q \cdot T_{\mathrm{sym}}}, \tag{27}$$

where q is the number of OFDMA symbols between two consecutive signaling updates.

3.4.2 Performance evaluation with heterogeneous power

A first set of simulations was run using heterogeneous P_i values among the cells. Specifically, two different power classes, called high-power and low-power BSs, were considered, employing respectively a peak power equal to 1 W and 0.1 W. The lower power level of 0.1 W has been chosen in order to guarantee an outage probability lower than 1%. Twenty different seeds were considered for generating the mobile station positions, the channel transfer functions and path losses, and the assignment of high-power BSs; then the aggregated capacities resulting in each

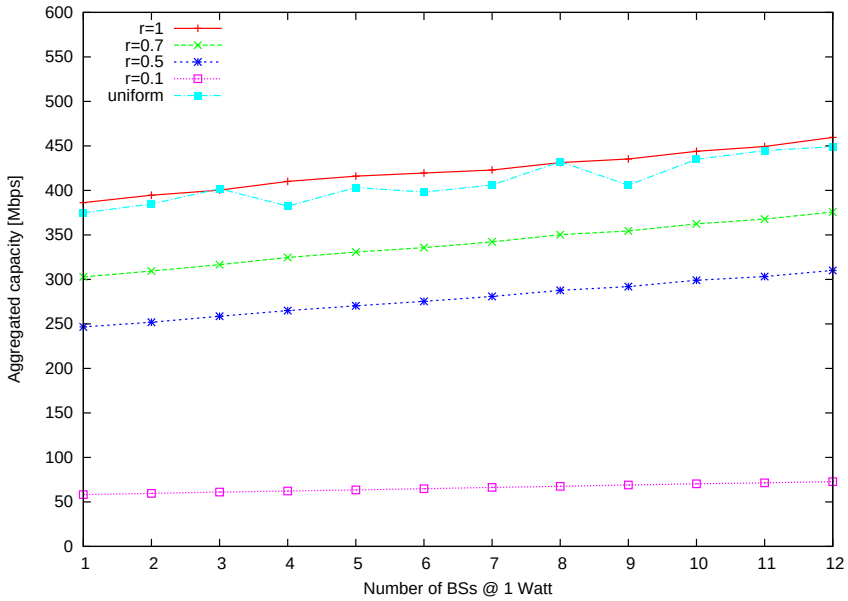

Figure 16: Aggregated network capacity as a function of the number of high-power BSs, in a micro-cellular propagation environment.

scenario were averaged.

Figures 16 and 17 on the following page show the aggregated network capacity as the number of high-power BSs varies, in two different propagation environments. The figures plot the network *gross* capacity, without considering the resource consumption due to the signaling overhead. Different allocation policies are compared. From the figures, it is possible to note that the simple uniform allocation scheme, requiring no feedback from the MSs, provides results comparable with the *water filling* scheme in case of micro-propagation model, while it under-performs *water filling* (with $r \geq 0.5$) in case of macro-propagation model. This phenomenon is due to the fact that in the micro-cellular propagation model it is included a LOS component, with probability $\max(1 - d/300, 0)$, being d the distance in meters between the BS and the MS [3]. Since the simulated inter-site distance is equal to 250m, it is very likely that the MSs have a LOS channel in the micro environment. The LOS component leads to high channel gains (which are also comparable from a PBU to another) and to a limited inter-cell interference. Therefore, selective power allocations and frequency planning are useless or even harmful. These higher channel gains are also responsible of the different aggregated capacity values plotted in Figures 16 and 17 on the following page, where the network capacity in the micro-cellular environment is about three times the one experienced in the macro-cellular one.

Whenever the LOS component is not present and the channel gains vary significantly

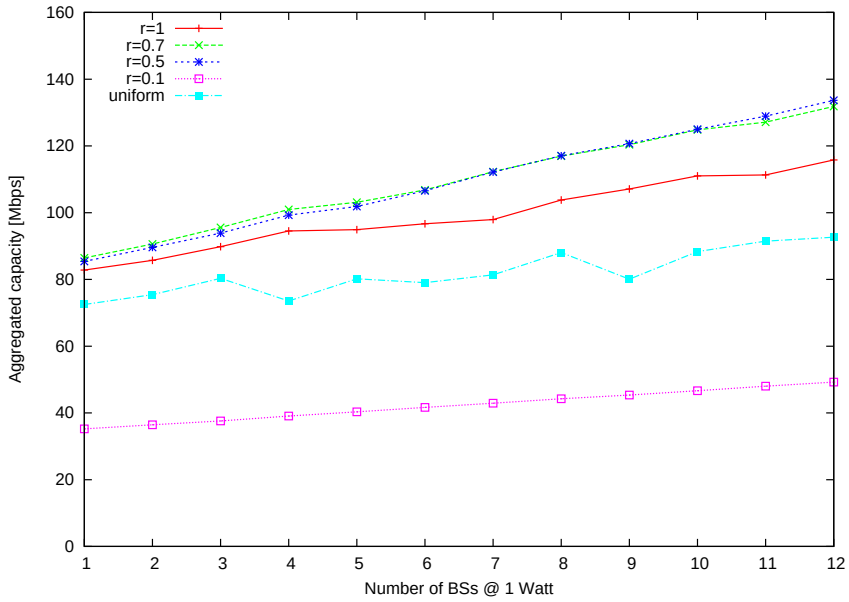

Figure 17: Aggregated network capacity as a function of the number of high-power BSs, in a macro-cellular propagation environment.

from a PBU to another, power allocations based on *water filling* provide better performance than uniform power allocations. For example, in Fig.17 the *water filling* scheme outperforms the uniform power scheme of more than 20 Mbps. Most interesting, the *fractional water filling* with $r = 0.5$ and $r = 0.7$ provides an aggregated capacity higher than the *water filling* one. When the number of high-power BSs is equal to 12, such a difference is about 20 Mbps. Such a difference can be even higher considering that the *fractional water filling* requires a signaling overhead lower that *water filling*. The higher capacity perceived under a *fractional water filling* scheme can be interpreted as the evidence that a resource repartition among the cells (i.e. a control on the inter-cell interference) is advantageous for this propagation scenario.

3.4.3 Impact of PBU and signaling overhead

In order to enlighten the effects of the network heterogeneity and the capacity quantization due to the per-PBU allocations, simulations with K_{PBU} set to 1 were run. Fig.18 compares the Cumulative Distribution Functions (CDF) of the per-cell capacity perceived under different allocation schemes in the macro-cellular environment. For improving the readability of the figure, being the *water filling* with $r = 1$ the best scheme, the case referring to the *fractional water filling* with $r < 1$ is not plotted. From the figure it is possible to see that the network heterogeneity does not affect significantly the CDF for the uniform allocation case, while it

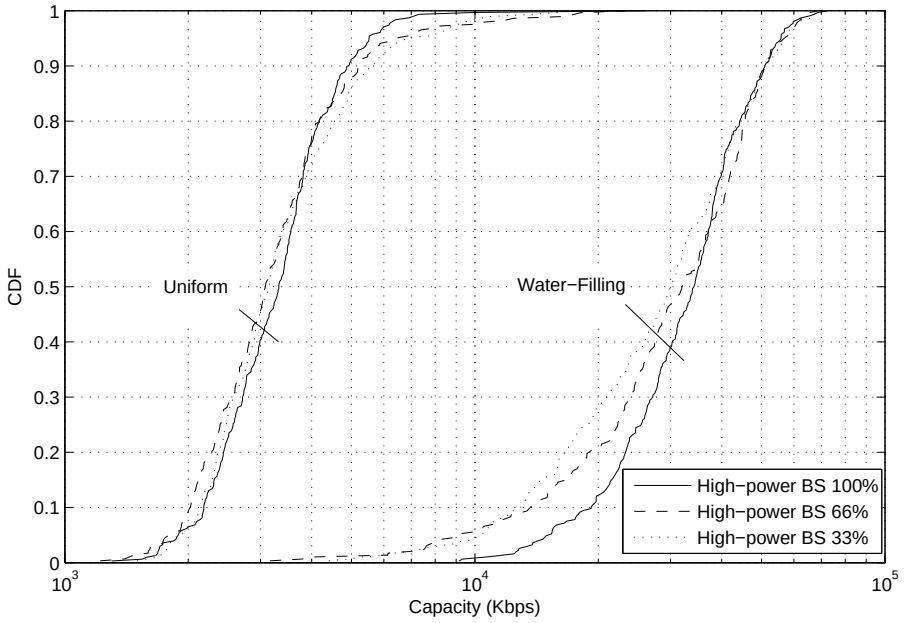

Figure 18: Cumulative Distribution Function of the per-cell capacity under different allocation schemes, in the macro propagation environment.

increases the probability that the cell capacity is low in case of *water filling*. Moreover, the average values of these distributions are higher than $1/12$ of the value obtained in the previous simulations, because the capacity of each carrier is fully exploited (i.e. $K_{\mathrm{PBU}} \min_{k \in \mathrm{PBU}_l} \log(1+ \mathrm{SINR}_i^k) \leq \sum_{k \in \mathrm{PBU}_l} \log(1 + \mathrm{SINR}_i^k)$).

Fig.19 shows again the aggregated network capacity for different K_{PBU} values corresponding to a variable number of PBUs $U = \lfloor K/K_{\mathrm{PBU}} \rfloor$. For improving the figure readability, only the *water filling* allocation approach ($r = 1$) and the *fractional water filling* with $r = 0.5$ are plotted. The increase of capacity with decreasing PBU size can be readily explained by recalling that the capacity estimate (10) is (very) conservative. Except the case $U = 84$, which corresponds to PBUs with one carrier only, from the figure it is evident that a dynamic network repartition among the cells is always advantageous, especially when the number of BSs employing a transmission power equal to 1 W is high.

Note that also this figure refers to a *gross* network capacity. A simple estimation of the *net* network capacity is given in Table 5, where the resource consumption due to the signaling overhead for $m = 4$ and $q = 12$ is computed. Although $q = 12$ could seem a too frequent ($12 \cdot 16\mu s$) feedback update in the considered mobility scenario, the signaling overhead for a more general mobility scenario was evaluated. The table proves that the *fractional water filling*

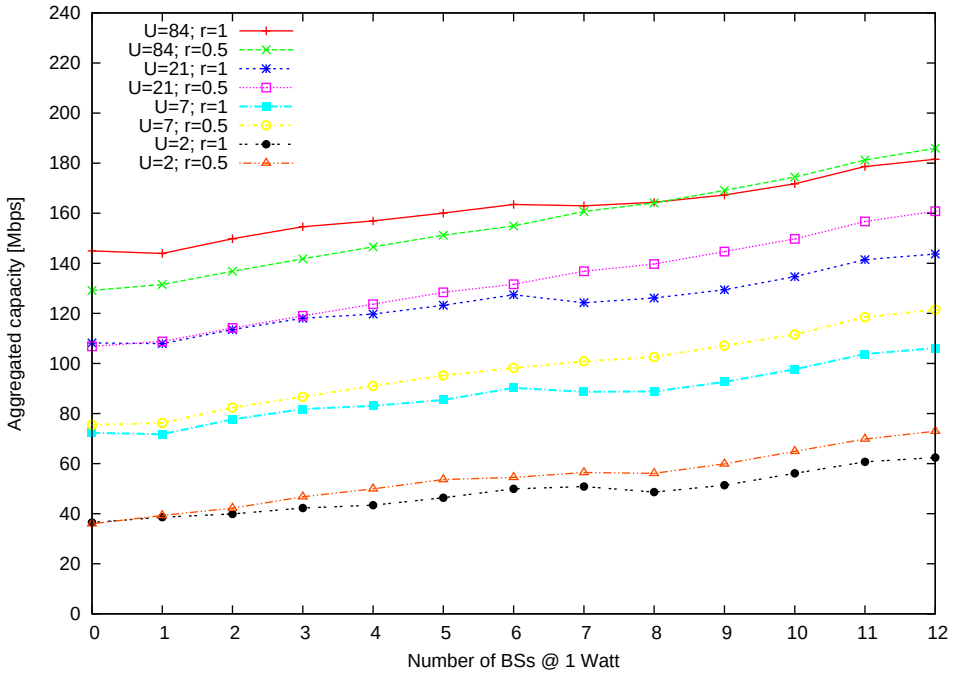

Figure 19: Aggregated network capacity as a function of the number of high-power BSs and PBU size, in a macro-cellular propagation environment.

BSs@1W	r	*No Signaling*			*With Signaling*		
		7	21	84	7	21	84
0	1	72.3	108.2	144.9	70.1	101.6	118.7
0	0.5	75.4	106.8	129.1	74.1	102.9	113.4
6	1	90.2	127.5	163.5	88.0	120.9	137.3
6	0.5	98.2	131.6	154.9	96.9	127.7	139.2
12	1	106.1	143.7	181.5	103.9	137.1	155.3
12	0.5	121.4	160.8	185.9	120.1	156.9	170.2

Table 5: Average network capacity values with and without signaling [Mbps], for zero, half and all high-power BSs, m=4, q=12.

can be even more beneficial than expected, thanks to the chosen signaling format.

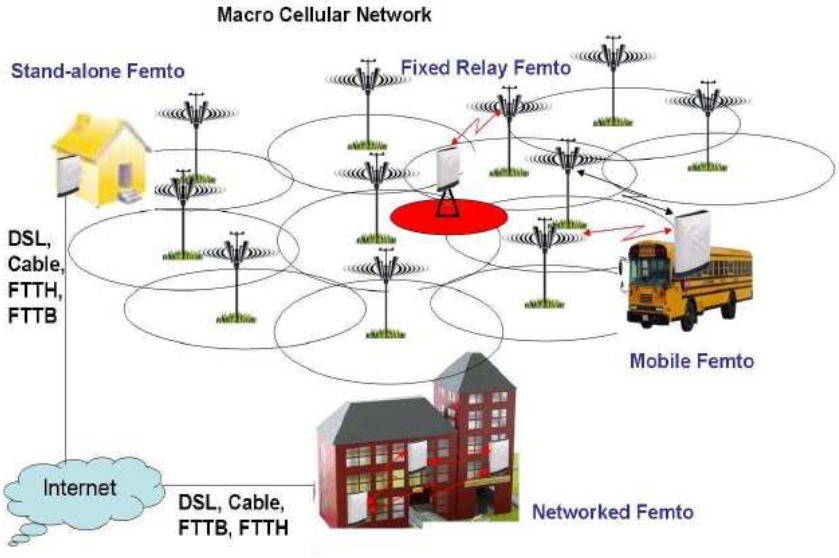

Figure 20: Example of heterogeneous network.

4 Approaches for resource allocations in hierarchical networks

Macro-cellular systems have the disadvantage that the users far from macro-BSs and the users in indoor environments are subject to poor service compared to others. Placing more macrocells can solve this drawback, but this would be a very expensive solution.

The alternative is to overlay the existing macro-cellular systems with low-power and low-cost base station devices, femto-BSs, able to provide high-speed wireless connections to subscribers within a small range, eliminate coverage holes in the macro-only systems and facilitate the capacity requirements of new applications and services, providing high-data-rate services in a cost-effective manner. For their limited power consumption, they additionally represent good candidates for the emerging green networks. The presence of femtocells leads to the development of so-called heterogeneous networks (Fig. 20) utilizing two different sets of BSs: regular (planned) macro-BSs that typically transmit at high power levels (typically in the range 5W-40W), overlaied with several femto BSs (deployed to provide services to fixed or mobile end users) which transmit at substantially lower power levels (100mW-2W) and are typically placed in a relatively unplanned manner, just based on a rough knowledge of coverage issues and traffic density (i.e. hot spots) in the network.

Femtocells are considered a promising solution by mobile operators. Commercial services that exploit femtocells are already operative in many countries and standardization activi-

ties are actively ongoing. However many technical challenges need to be addressed in order to achieve the coexistence of femtocells in a macro context without problems [39].

4.1 Towards self-organizing network configurations

The proliferation of increasingly heterogeneous networks leads to self-organizing network configurations. The functionality of femto-BSs is almost the same of typical macro-BSs, with the advantage that their price is significantly lower: in fact a femto-BS is expected to serve a small number of users and a relatively low transmit power is enough to cover the service area. Such low cost of the hardware is expected to make the femtocell technology widely accepted since femto-BSs could be directly bought by users and easily installed in a plug-and-play manner. This can lead to a huge and unpredictable deployment of femto-BSs in a given area and, unless the femtocell network is properly optimized, high levels of co-channel interference could be reached and the overall network capacity might be significantly compromised, especially if the existing macrocell networks and the femto-BSs share the same set of operating frequency channels (the channel assignment policies will be discussed later in the chapter).

The main problem is that it is almost impossible to keep such a network optimized by a centralized operator planning as done in conventional cellular networks. Indeed femtocells are under the ultimate control of users, which can switch them on and off. Therefore, the femtocell network is desired to be self-organizing such that the network configuration automatically keeps updated by being aware of the network environmental changes (in terms of addition/deletion of neighboring femto-BSs).

The ideal case would be a network architecture consisting of heterogeneous nodes that can automatically configure (specifically in terms of transmit power and frequency channels to use for the transmission), manage themselves and, in case, turn off if this possibility involves benefits in terms of interference reduction and consequent improvement of the system performance. The use of sophisticated self-organization techniques can just be useful to minimize the interference in femtocell deployments, maintaining a low level of network signaling. Such an approach would allow femtocells to integrate themselves into the network, monitor the surrounding environment (neighboring cells, interference levels) and consequently update the

power levels and the used resources to mitigate the interference from the neighboring cells.

Self Organizing Networks (SON) were analyzed within the project Socrates [40] which emphasizes the use of self-organization methods as a promising opportunity to automate wireless access network planning and optimization in future mobile communication networks. In the existing literature, some self-organization strategies for femtocells have been introduced. In [41] two self-organizing approaches for frequency assignment in OFDMA femtocells, respectively based on femto-level broadcast messages and measurement reports coming from the users, are presented. Authors show that using a self-organization approach leads to better system performance than using random assignments [42]. In [43] self-optimization in LTE systems is considered. Other existing proposals are mainly based on *Wideband Code Division Multiple Access* (WCDMA) networks and they exploit approaches such as power control, rather than appropriate resource allocation strategies, in order to mitigate the interference ([44],[45],[46]).

4.2 Modeling solutions for the hybrid scenario

As already mentioned in the previous chapter, a complete model of a generic hybrid macro-femto scenario is now provided. Let be:

- M: the total number of users in the network;
- N: the total number of Base Stations (macro plus femto) in the network;
- U: the number of Resource Blocks (RBs) available for transporting data in each cell;
- *i*: the index of a generic cell of the network ($i = 1, ..., N$);
- M_i: the total number of users in cell i;
- *t*: the temporal step, multiple of the symbol time T (for example equal to a frame time). The channel gains and the allocation decisions are supposed constant within this time *t*;
- H_t: the matrix of the channel gains (between the mobile devices and the BSs, macro or femto ones) at time t. Users are associated to the BSs from which they sense the best channel, however for each user it is important to keep in memory the gains towards the

other Base Stations too, in order to quantify the interference. Depending on the channel gains, some links (e.g. under a fixed threshold) could be neglected in order to semplify the model. Matrix H_t has a block structure, with a block for each BS (macro- and femto-one) of the network - for sake of presentation, each block is separated from the next one by a vertical bar. The matrix has M rows (a row for each user) and (U * N) columns:

$$\left(\begin{array}{ccc|ccc|c|ccc} h^1_{1,1} & .. & h^1_{1,U} & h^1_{2,1} & .. & h^1_{2,U} & .. & h^1_{N,1} & .. & h^1_{N,U} \\ h^2_{1,1} & .. & h^2_{1,U} & h^2_{2,1} & .. & h^2_{2,U} & .. & h^2_{N,1} & .. & h^2_{N,U} \\ .. & .. & .. & .. & .. & .. & .. & .. & .. & .. \\ h^M_{1,1} & .. & h^M_{1,U} & h^M_{2,1} & .. & h^M_{2,U} & .. & h^M_{N,1} & .. & h^M_{N,U} \end{array}\right)$$

- A_t: the allocation matrix at time t, i.e. a matrix having the same size and the same structure of matrix H_t and containing binary elements (1 if a resource is assigned, 0 otherwise). So the positions of the elements 1 indicate what BS has assigned a specific resource to a particular user;

- $\boldsymbol{p}_t$: the (U * N)-vector of the powers potentially associated at the different resources on the different sites (macro- and femto- ones) at time t. Vector $\mathbf{p}_t$ presents a block structure too: each block refers to a different Base Station and it is visually separated from the next one by a vertical bar.

$$[p^1_1 ... p^1_U | p^2_1 ... p^2_U | p^N_1 ... p^N_U]^T$$

  In order to semplify the notation, we omit the subscript *t* below, so assuming a generic temporal step.

The product $A\boldsymbol{p}$ gives a M-vector which indicates, MS by MS (row by row), how much power is assigned to each one. Not all the configurations for A and $\boldsymbol{p}$ are eligible. Introducing appropriate constraints on the structure of matrix A and on the possible values for the powers, it is possible to obtain acceptable solutions, i.e. physically realizable.

As far as concerns A, the presence of non-zero elements in a row is possible only in a single block: for example, if the first MS is associated to the BS 1, only BS 1 can allocate resources to it. Consequently, non-zero elements can be found only in the portion of the first

row of the matrix corresponding to BS 1 (i.e. the positions from 1 to U). Moreover A can have at most one non-zero element in each column: this condition prevents that the same resource can simultaneously be assigned to several users within a cell (macro- or femto-one).

As far as concerns the ***p***-vector, we must consider that a limit for the maximum power available on each cell exists, i.e.:

$$\sum_{r=1}^{U} p_r^n = \begin{cases} P_{max}^M, & \text{if the cell } n \text{ is a macrocell} \\ P_{max}^F, & \text{if the cell } n \text{ is a femtocell} \end{cases} \tag{28}$$

where P_{max}^M and P_{max}^F are the maximum values of power which, respectively, a macro-cell and a femto-one can erogate and n=1,...N. Revised in terms of constraint on ***p***, it means that the sum of the values of individual U-blocks in which the vector can be ideally partitioned (remember that each block refers to a particular Base Station) must not exceed the fixed bound.

Among all the eligible couples (A,***p***), the purpose of a hypothetical centralized optimum allocator is to find that one which maximizes the objective function, defined below. If this couple exists, the corresponding allocation will be optimal.

The capacity of a generic user m, associated to the Base Station n, can be expressed as:

$$C_m = \sum_{r \in U_m} \frac{BW}{U} \log_2(1 + SINR_{m,r}), \tag{29}$$

being U_m the set of resources allocated to the user m, U the number of resources per cell and BW the bandwidth. The single contribute $SINR_{m,r}$ is so defined:

$$SINR_{m,r}(h,p) = \frac{p_r^n |h_{n,r}^m|^2}{\sum_{i=1, i \neq n}^{N} p_r^i |h_{i,r}^m|^2 + n_{m,r}} \tag{30}$$

where $n_{m,r}$ is the thermal noise experienced by user m on resource r. Each user can claim the guarantee of certain QoS parameters: for simplicity the model takes into account just the data rate. So an additional constraint for each user, in terms of guaranteeing a minimum data rate, must be considered. Each user in the network generates a particular type of traffic. Considering for example the WiMax technology, it was seen in section 3.1 that five QoS service classes are

supported; consequently, user by user, one of the following five constraints on data rate should be respected:

$$\begin{aligned}
&\sum_{r\in U_m} \frac{BW}{U}\log_2(1+SINR_{m,r}) > r_{min}^{UGS} \\
&\sum_{r\in U_m} \frac{BW}{U}\log_2(1+SINR_{m,r}) > r_{min}^{ertPS} \\
&\sum_{r\in U_m} \frac{BW}{U}\log_2(1+SINR_{m,r}) > r_{min}^{rtPS} \\
&\sum_{r\in U_m} \frac{BW}{U}\log_2(1+SINR_{m,r}) > r_{min}^{nrtPS} \\
&\sum_{r\in U_m} \frac{BW}{U}\log_2(1+SINR_{m,r}) > r_{min}^{BE}
\end{aligned} \tag{31}$$

A possible objective function for the considered scenario is given by the sum of the capacities experienced by the single users, i.e.:

$$C = \sum_{m=1}^{M} C_m = \sum_{m=1}^{M}\sum_{r\in U_m} \frac{BW}{U}\log_2(1+SINR_{m,r}) \tag{32}$$

The maximization of a so-defined function allows to optimize the aggregated network capacity. Additional constraints could be inserted to guarantee fairness among the users.

The resolution of such a centralized theoretical approach would lead directly to the choice of the resources to assign to the different users in the network. However it is a not banal optimization problem, the global maximum of which is very difficult to find. For this reason, in practical implementations the problem is usually decomposed into two subproblems: the first one consists in establishing what frequencies to assign to macro- and femto-BSs, the second one is devoted to define what resources, among the available ones, must be assigned to end users by each-BS, in an independent way.

As far as concerns the first aspect, section 4.4 defines the main proposals existing in literature for the management of the spectrum between macro- and femto-BSs. With reference to the second aspect, the considerations about the OFDMA contexts discussed in section 3.3 can be applied, while typical approaches valid for the classical cellular networks could not be directly applied to OFDMA heterogeneous contexts, mainly due to the following reasons:

- instead of scheduling each individual subcarrier and time slot to users, user scheduling in LTE or WiMax networks is decided in the unit of Resource Blocks (RBs), which contain a group of subcarriers and time slots. The difference in granularity may cause large capacity loss when applying existing resource allocation algorithms to OFDMA networks;

- unlike DSL applications where all subcarrier interfere with each other, LTE and WiMax networks use orthogonal transmission within each cell and universal frequency reuse at different cells.

4.3 Femto access policies

Inter-cell interference in a hybrid macro/femto network depends largely on the femtocell access policy used, which defines how a femtocell allows or restricts its usage to users. From the femto- point of view, usual approaches are: *Closed Subscriber Group* (CSG), according to which only certain users are allowed to connect to the femtocell, and *Open Access* where all users are considered equal and allowed to connect to the femtocell. A *Hybrid Access* could also be possible: in this case a limited amount of the femtocell resources are available to all users, while the rest are operated in a CSG manner.

Overall, such a heterogeneous network can offer three services to the users: in Fig. 21 they are referred to as *mobile-only*, *mobile+open femto* and *mobile+closed femto*. As the names imply, *mobile-only* corresponds to the service of users subscribing to only 3G services with macro-BSs. Users of *mobile+open femto* and *mobile+closed femto* instead subscribe to the service allowing access to macro-BSs as well as femtocells. Users of *mobile+closed femto* can use femto BSs to which they are registered, while users of *mobile+open femto* can join only open femtocells.

Femtocell CSG approach is more suitable for home or enterprise environments, while the typical scenario for the *Open Access* is to guarantee free access to users everywhere, such as in a coffe shop or in an airport. The impact on the downlink capacity of CSG and *Open Access* OFDMA femtocells is analyzed in [47]: CSG leads to higher throughputs in downlink for femtocell subscribers but at the same time it generates high levels of interference to unsubscribed users in the proximity of femtocells. In fact when an uncertified user moves into the femtocell

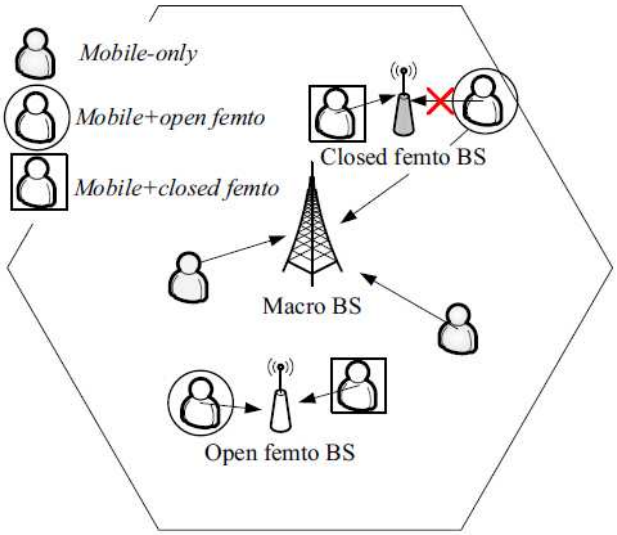

Figure 21: Service configurations for users in a typical two-layer hierarchical network.

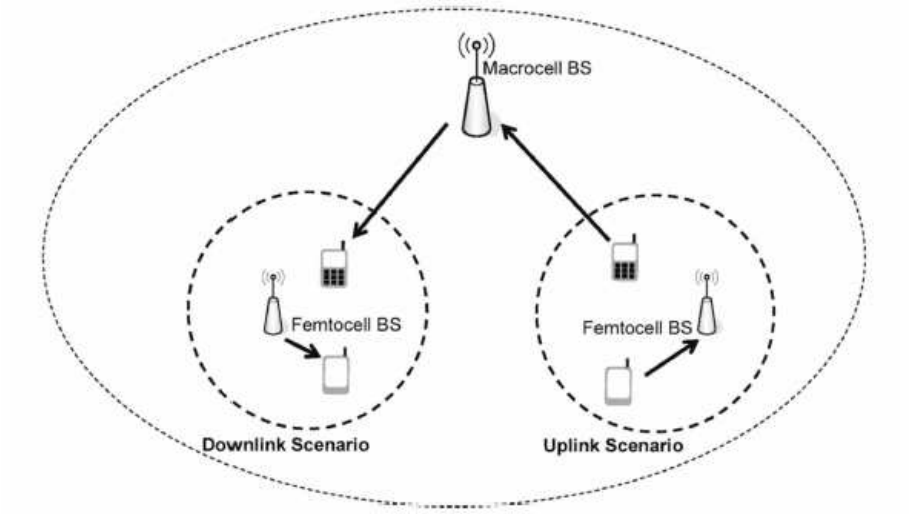

Figure 22: Interference suffered/caused by unsubscribed users in the proximity of CSG femtocells.

service coverage, the user can be served not by the femtocell but also by the macrocell. In this situation the downlink transmission of the femto-BS generates critical interference for the macrocell user. Moreover the uplink transmission of the macrocell user causes interference to the femtocell BS. The situation is showed in Fig. 22.

On the other hand, *Open Access* limits the interference and provides a better overall network performance in terms of QoS and throughput [48], being all the available resources shared among users. However, if the choice falls on the adoption of an *Open Access* approach, appropriate admission control strategies must be taken into account. There are many works on admission control in the literature, the main ones will be discussed in section 4.5.

Closed access Femtocells	Open Access Femtocells
Higher interference	More handovers
Lower network throughput	Higher network throughput
Serves only indoor users	Increased outdoor capacity
Home market	SMEs, hotspots
Easier billing	Security needs

Table 6: Closed vs *Open Access*.

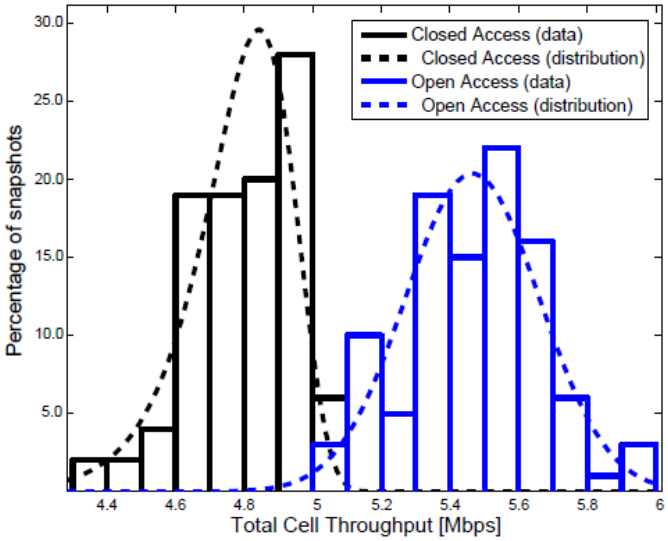

Figure 23: Total downlink network throughput in presence of CSG and *Open Access* femtocells [2].

Table 6 summarizes the main features of both CSG and *Open Access* policies. In [2], in order to analyze and compare the overall performance of these access methods, authors performed experimental system-level simulations, based on a deterministic radio coverage prediction tool calibrated with measurements and a Montecarlo snapshot based WiMax system-level simulator ([47],[49]). The simulations demonstrate that the network throughput of *Open Access* outperforms that of *Closed Access*, as shown in Fig. 23. In it the total downlink network throughput in a residential (200 x 100 m) area covered by 22 OFDMA femtocells and 1 macrocell (10 MHz bandwidth) is plotted. Each house hosting a femtocell contains 2 indoor users demanding 128 kbps each one and 10 macro users are located outdoors demanding 64 kbps each one.

Finally, in Table 7, authors compare the performance of CSG and *Open Access* in terms of user outages and handover signaling, using a dynamic system-level simulator [41]. The table refers to simulations run for a residential area (300 x 300 m) covered by several femtocells and 1 macrocell (10 MHz bandwidth). Each house hosting a femtocell contains 4 indoor users

Number of femtocells	25		36		49		64	
Access method	Closed	Open	Closed	Open	Closed	Open	Closed	Open
HO attempts in the network over 1 hour	-	342	-	480	-	680	-	887
Average Hand IN attempts per femtocell over 1 hour	-	6.84	-	6.67	-	6.94	-	6.92
Average Hand IN attempts per macrocell over 1 hour	-	171	-	240	-	340	-	444
Outages in the network over 1 hour	69	0	81	8	120	15	164	22
Average non-subscribers tier throughput [Mbps] over 1 hour	5.339	5.604	5.409	5.740	5.340	5.604	5.002	5.720
Average subscribers tier throughput [Mbps] over 1 hour	51.228	52.081	69.545	71.342	51.228	52.081	124.230	130.445

Table 7: Performance comparison of CSG and *Open Access* configurations [2].

demanding one OFDMA subchannel each one, while 8 macro users are located outdoors demanding one OFDMA subchannel each one too. It can be noted that in CSG femtocells the number of outages is large due to the high level of interferences. A user is considered in outage (dropped call) when it is not able to transmit for a given period of time (set to 200 ms as it is recommended for VoIP services). On the other hand, in *Open Access* there are several handover attempts, which causes outages due to handover failure. A handover attempt occurs when the received signal strength of the pilot signal of a neighboring cell is larger the one received from the serving cell.

4.4 Resource allocation in hybrid OFDMA networks: state of art

Two types of channel assignment can be thought for a femtocell which must operate in a macrocell network: *dedicated* channel assignment and *co-channel* assignment. In the first case different frequency channels are assigned to the femtocell and the macrocell, thus avoiding to interfere each other. Authors in [42] just propose a spectrum allocation policy which aims to avoid cross-tier interference by assigning orthogonal spectrum resources to the macro tier and the femto tier. Additionally femto-to-femto interference is reduced by allowing each femtocell to access only a random subset of the frequency channels that are assigned to the femto tier.

However, due to limited spectrum availability (which does not always allow to assign a dedicated spectrum for femtocell deployments), femtocells can be obliged to operate in the same

spectrum as macrocells [50]. This leads to the second channel assignment policy, the co-channel method, which assigns the same frequency channels to the femtocells and the macrocells. The co-channel assignment implies a more efficient use of the frequency resource and an efficient hand-off, but the interferences between the femtocells and the macrocells may generate great problems. To alleviate these interferences, practical solutions provide that, for each transmission time interval, a macrocell can use all the available RBs, while each femtocell randomly selects a subset of the available RBs for transmissions. As a result, the average number of interfering femtocells in each RBs is reduced. The size of each RB subset per transmission interval is determined based on optimizing the throughput per cell. However optimizing such a resource allocation leads to a nonconvex optimization problem, consequently heuristic algorithms are often considered. Among them, a recommended one is the *Least Interference Power* (LIP) algorithm [51], according to which a powered-up femtocell BS chooses a frequency segment that minimizes the interference level. In turn-on ordered algorithm, frequency allocation is conducted according to the order of the femtocell turned on. In [52] authors study an utility-based subchannel allocation problem for the OFDMA-based femtocell networks. They first define the optimization problem that aims at maximizing the sum of utilities of femtocells. Since the original problem is a nonlinear integer optimization problem, which is an NP-hard problem, they develop a two-step suboptimal subchannel allocation algorithm. Using the graph theory, at first they calculate the number of subchannels that should be granted to each femtocell to maximize the sum utility; then they find the actual subchannel allocation that achieves the granted number of subchannels for each femtocell. Another hybrid frequency assignment for femtocells in co-channel operation system was proposed in [53]. Co-channel operation is allowed only in the edge zone, while femtocells in the center zone use a dedicated frequency band which is not used by macrocell users. Even though this method can reduce interference between the macrocell and femtocells in the center zone, macrocell users in the edge zone suffer severe interference from the femtocells due to complete co-channel operation and low received signal power from macrocell BS. In [54] a hybrid resource allocation technique based on measurements reports both from macro users and femto users is proposed.

However, apart from the particular adopted solution, limiting femtocells to use a fraction

of the available resources corresponds to a sort of application of *Fractional Frequency Reuse* (FFR) principle. *Fractional Frequency Reuse* (FFR) is discussed in the OFDMA based networks ([39],[55],[56]) and it is one of the key solutions to reduce inter-cell interference and to enable a reuse factor equal to one, typical of OFDMA based networks, such as LTE and WiMax. The reason for which OFDMA networks use a reuse factor of one is that large reuse factor systems tend to lose more spectral efficiency. In classical FFR approaches for homogeneous cellular layouts, whole frequency band is typically divided into several sub-bands, and each sub-band is differently assigned to center zone and edge zone of the cell. As a result, intra-cell interference is substantially reduced and the system throughput is enhanced.

In [57] the performance of key interference management techniques across the 802.16m and 3GPP-LTE standards (in particular RRM schemes which include FFR and power control) are considered, but they refer to standard cellular network deployments.

There are enough works in literature dealing with interference control in OFDMA networks ([18],[58],[59],[60]), but they mainly refer to non-hierarchical scenarios and so they do not consider system-specific issues related to femtocells. For example in [58] the problem of inter-cell interference reduction is first addressed using a graphic approach, where no precise SINR information is required (so limiting the feedback signaling), and then the channel assignment is made by taking instantaneous channel conditions into account. In [59] an approach to the frequency assignment problem tailored to OFDMA networks, called *Dynamic Frequency Planning* (DFP), is presented. DFP can decrease the network interference and increase significantly the network capacity by dynamically adapting the radio frequency parameters to the environment. In [50] authors extend DFP approach to WIMAX femtocell scenarios to avoid macrocell to femtocell interference and also femtocell to femtocell interference, improving the network capacity. The main drawback in [50] is the supposition of a centralized network architecture, where a centralized entity should collect the data, take the decisions and distribute the informations. This, due to the possible large number of femtocells, might significantly complicate the centralized optimization process. Moreover some femtocells could be also installed by end users, without a cell-planning. As a consequence, the number and the locations of active femtocells are not known to the operators. Therefore, interference caused by femtocells can not

be managed using a centralized approach. Instead distributed architectures, where each femtocell is able to select its own sub-channels, would be preferred. Femto Forum [61] presents work done to address interference management in the context of OFDMA (particularly LTE-FDD) femtocell systems.

Some studies focus on how to control the interferences between femtocells and macrocells, exploiting power control strategies: ([48],[62],[63]) show the power control method of a femto-BS and its performance when the femtocell operates in the same spectrum as the macrocell. However, even though the power control of the femto-BS is properly executed, the macrocell users who are very close to the femto-BS may suffer a high interference, which makes it impossible for them to communicate with their anchor macro-BS.

In [64] authors propose a simple solution for power loading and resource allocation in femtocell networks to maximize the femtocell throughput, limit the interference to the macrocell, and maintain the fairness among femto users. In the proposal each femtocell carries out power loading and resource allocation independently. Taking the interference constraints into account, they propose an *iterative water filling* algorithm to improve the system performance and a proportional fair scheduling algorithm to maintain the fairness among the femto users.

In [65] a game theory approach is used: the objective function is defined as a capacity maximization with pricing as a monotonically increasing function with user power. Thus this algorithm optimizes both power and rate for all the users in the system.

4.5 Admission control techniques: state of art

An effective management of radio resources, due to their limited availability, plays a crucial role in wireless communication systems as a mean to ensure QoS to users. *Radio Resource Management* (RRM) includes aspects such as the study of efficient resource allocation strategies and transmission power control techniques, the choice of adaptive modulation and coding schemes and not least the development of appropriate admission control policies. The need for admission control stems from the fact that there is a maximum limit of users that can be adequately served within a network in general or more specifically within a cell, depending on the network design and the type of traffic sources. In other words, with reference to a multimedia OFDMA

context, an admission control policy must evaluate if an OFDMA cell can support a given set of transmission requests (characterized by different QoS requirements) with a given amount of available resources (subcarriers, power, modulation and coding schemes), also considering the quality of channels (the average channel gains) between the Base Station and the requesting users. In addition to this, in heterogeneous networks, in presence of CSG femtocells, admission control must be functional to prevent unauthorized users from associating.

There are many works on admission control in the literature, most of which relate to classical cellular contexts. A first classification for the existing proposals can be made considering *reactive* and *proactive* strategies. The approach followed by the first class consists simply in accepting or not a new service request based on the availability of resources and the specific requirements of the request. The other class of schemes instead exploit measurements in order to accept or not a new request based on some kind of prediction of future arrivals and requirements.

Along with the ability to accept new users in the system, handoff events must be opportunely managed too: indeed a common feature of admission control approaches is to ensure the continuity of ongoing services at the expense of new requests. It is usual to distinguish two types of handoff: *inter-cell handoff* and *intra-cell handoff*. *Inter-cell handoff* is the process to maintain service continuity when a mobile user moves from its initial serving Base Station to an adjacent one. *Intra-cell handoff* is a process of resource reassignment which occurs when the movement of a user within a cell causes the degradation of its service level. The typical case is an user who moves to the cell edge: at first it experiences good radio conditions (close to the base station), then, as it moves away from the base station, it will require more resources in order to keep its bit rate constant. In the first handoff situation the cell that receives the user must allocate sufficient resources to accommodate its request, while in the second case additional resources within the same cell are necessary to maintain the QoS requirements. In both cases outage can happen due to resource insufficiency.

Some proposed schemes reserve a fixed number of resources exclusively for the handoff management ([66],[67],[68]). However these schemes are not efficient in OFDMA systems. The reason is that OFDMA systems let high spectrum utilizations through dynamic and flexible

channel and power allocations and so fixing a-priori (without following the changes in the traffic pattern) the set of subchannels reserved for handoff can result in a low use of spectrum. So from this point of view it seems better to use the total available bandwidth by minimizing on the other hand the transmit power of Base Stations. Proposals based on this assumption consider the transmit power of the Base Stations, rather than the number of channels used in the cell, as an indicator of the traffic load. In [69] authors propose an admission control scheme based on power reservation for handoff calls and specifically they separately calculate the power levels to be reserved respectively for *intra-* and *inter-cell handoff* events. In [70] a density-based admission control is presented. New users are accepted or not, depending on the area in which they appear: in particular a lower number of new users are admitted in areas with high user density in order to guarantee more availability to those in migration. A higher priority is assigned to calls migrating from one region to an adjacent one over new calls arriving to the system. This priority is obtained considering an acceptation ratio value (depending on the number of users already present in the considered area) for new calls, instead not considered for migrating calls.

Authors in ([71],[72]) propose admission control strategies for WiMax networks, characterized by different traffic classes. In [71] authors distinguish between new users and new connections or old connections with updated QoS requirements (generated by subscribers already admitted to the network). So when a new request arrives in the system the Base Station determines if it is a new user or not. In the first case, if there are not enough resources to support all users, the new user is rejected, while the QoS of registered users is maintained. Instead, if the user is already registered and the request is only a new connection, the resources are redistributed among the different connections of the same user according to a greedy approach that tries to favor traffic classes with higher priority. The resources for BE of registered connections are borrowed by the new connection with higher priority; if there are not sufficient resources to support all connections, it is supposed to support the UGS and RTPS connections already existing in the system, possibly rejecting the new connection. In [72] admission control problem is decomposed into two independent uplink and downlink subproblems. Admission tests on UL and DL are made and only the connection requests that pass both admission tests

can be eventually accepted. Each single subproblem is independently studied as an optimization problem under a certain objective function, which should maximize the revenue of service providers or the satisfaction of subscribers. From a service provider's point of view, the objective of a good admission control strategy is to admit as many users as possible, while ensuring the feasibility of the resource allocation; on the other hand users would prefer admission control policies that can achieve maximal utility or, equivalently, the maximum access bandwidth. The optimal revenue strategy, which only considers the profit of service providers, is also known as the *stochastic knapsack problem* ([73],[74]). The problem can be posed in these terms: given a set of requests with associated different priorities, a generic service provider evaluates the "average revenues" generated by accepting them and he admits the connections which guarantee higher "revenues". Authors in [72] combine a revenue strategy with a fairness approach, in order to reach a satisfactory tradeoff between service providers' and subscribers' needs. In the first part the proposed algorithm allocates a certain amount of bandwidth to each traffic class in order to guarantee fairness constraint, while in the second phase, to meet the utility constraint, only the traffic classes that can produce an utility higher than a fixed threshold are chosen as possible candidates for bandwidth allocation.

The loading-based admission control, in which the number of users already admitted in the system or the total resource utilization factor are considered to make the admission choices, has an advantage due to its simplicity and easy implementation, but it can be less efficient than other measurement based schemes. Authors in ([75],[76]) consider admission control policies which optimize objective function such as the blocking rate or probability subject to signal quality constraint. In [77] a scheme based on the direct monitoring of the QoS metrics is presented. Specifically the QoS parameter taken into account is the delay, defined as the total time during which a packet resides in the wireless system including scheduling and transmission times. An arriving packet is efficiently rejected if its estimated delay is larger than the pre-defined threshold. In [78] authors develop a queueing model based on discrete-time Markov chain (DTMC) to analyze packet-level QoS performances (specifically the average packet delay) in an OFDMA context. The peculiarity is that they use a fuzzy logic approach arguing that the system parameters, such as channel quality measurements and traffic source parameters, are often very

imprecise and so it is difficult to provide accurate estimates. Based on this consideration, rather than relying on these imprecise input informations, they use the number of allocated subchannels and the 'fuzzified' amount of load in the cell for deciding if an incoming request can be accepted or not. In [79] an optimization stategy to minimize a "weighted sum of blocking" is definied: each traffic class is modeled through a blocking probability and a weight; depending on the values of weights, the "minimum weighted sum of blocking strategy" can give different priorities to different traffic classes.

Generally, the feasibility of the resource allocation and admission control strategies depends on the number of high-priority (HP) users in the network. In fact a large number of HP users would render their management infeasible. HP users are in general variable in their data rate requirements and so a HP user is admissible only if the network has enough resources to satisfy its QoS requirement. Authors in [80] follow an approach that aims to maximize the total utility of the BE users after satisfying the HP users' demand. They identify bit-rate and bit-error rate (BER) as QoS metrics.

Parameter	Value
Carrier Frequency	2500 MHz
K_{FFT}	1024
K	864
K_{PBU}	18
U	48
T_{sym}	102 μs
B	10 MHz
d_{site}	1000 m
v_{MS}	3 km/h
$Scenario\ Macro$	Urban Macro 15° AS
$Scenario\ Femto$	Urban Micro

Table 8: Main system parameters.

2Macro-0Femto		**2Macro-4Femto**		**2Macro-8Femto**		**2Macro-16Femto**	
To Macro	*To Femto*	*To Macro*	*To Femto*	*To Macro*	*To Femto*	*To Macro*	*To Femto*
200	0	166	34	138	62	104	96

Table 9: User associations in the different scenarios.

5 A simulation analysis of hierarchical network performance

Simulations were run for the macro-femto context (with an open access configuration for the femto-BSs), considering four different scenarios and varying the number of femtocells, the percentage of resources usage and the power budget for macro and femto-BSs. A random allocator performing, respectively, a uniform distribution of power on the allocated resources and an optimized power distribution (i.e. according to a *water filling* approach) was implemented in each cell.

Table 8 summarizes the numerical settings adopted in simulation, where d_{site} is now the distance between two macro-BSs. Macro and femto environments are respectively approximated with the Urban Macro and the Urban Micro models (described in the Appendix). All the simulated scenarios are characterized by constant numbers of macroBSs (2) and users (100 per macro-site, for a total number of 200 users randomly spread across the entire network). The macro-BSs and the MSs positions are the same in all the scenarios, while the femto-BSs (which number varies in each context) are located among the macro-BSs, according to a predefined position grid. Fig. 24 plots the four considered layouts and Table 9 summarizes how the users are distributed among the macro-cells and the femto ones in the different contexts.

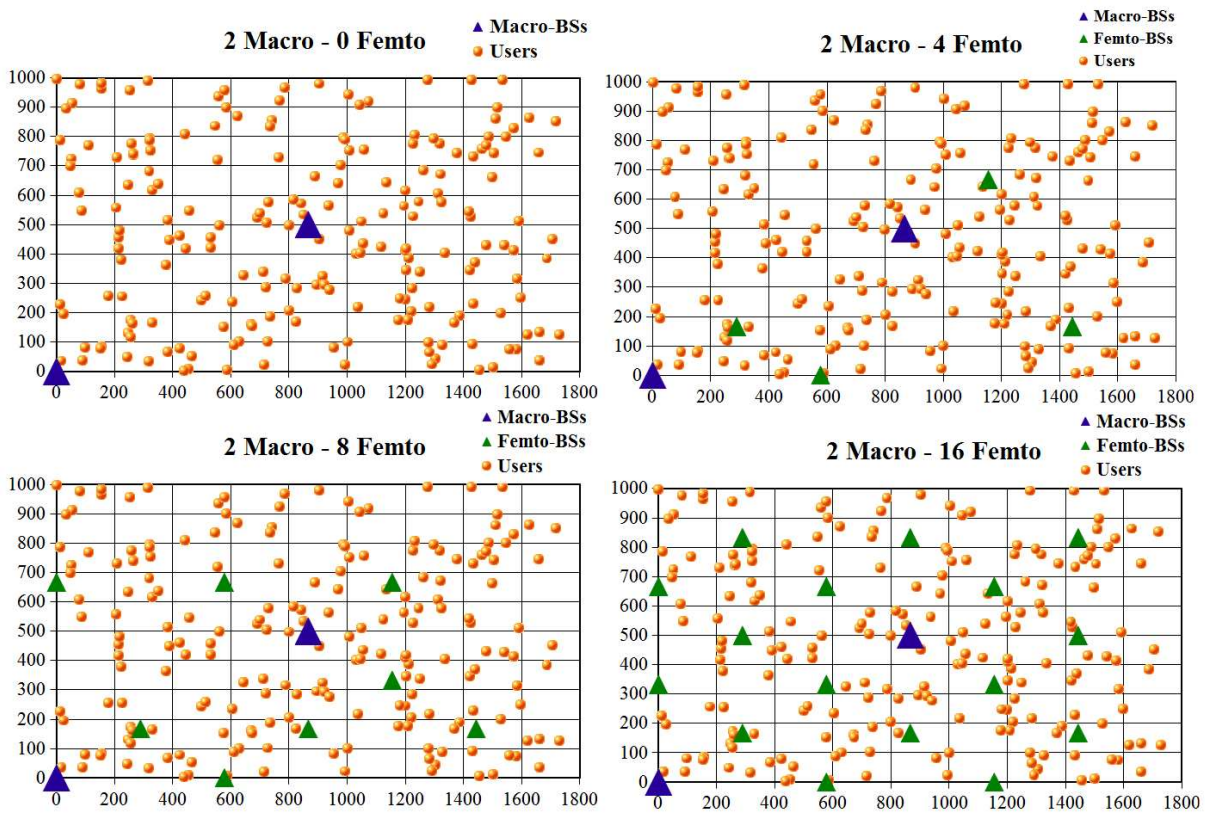

Figure 24: Layouts (dimension in meters) associated to the simulated scenarios.

Just as an example, Fig. 25 plots a snapshot of the associations for the scenario with 2 macrocells and 4 femtocells. Different colors show how the 200 users are distributed among the serving-BSs in this particular context. Remember (see the Appendix for more details) that, due to the toroidal implementation of the layout, femto- or macro-BSs located on an outer edge of the grid are replicated on the opposite side.

Different from the simulations run for the homogeneous context and described in section 3.4, now the focus is on a single allocation step. In each scenario, each MS is associated to a fixed BS, from which the received signal strength is the strongest. Each BS (macro or femto one) independently assigns resources to the associated users in a random way: one hundred different random resource allocations are performed and results are averaged. Simulations aim to evaluate how the presence of femtocells can affect the network performance under different conditions, mentioned at the beginning of paragraph.

The results are discussed in the following sections: per-MS and aggregated capacity values were taken out in order to highlight respectively per-user and macroscopic effects due to

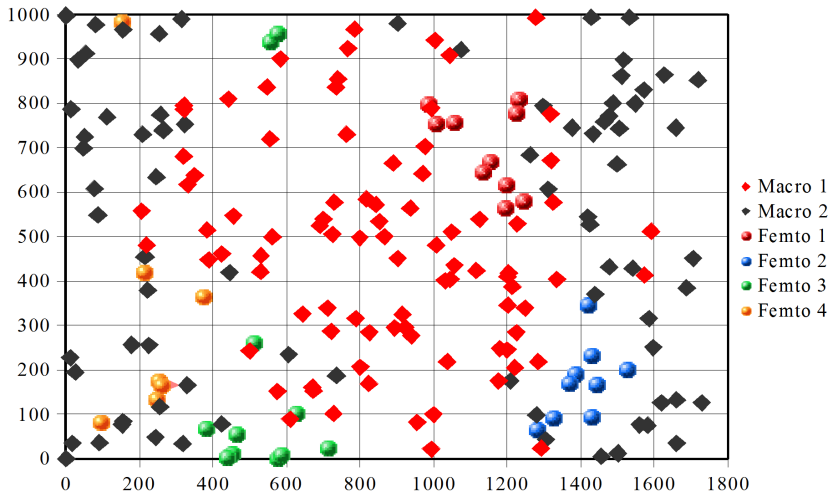

Figure 25: Distribution of users among the serving-BSs in the 2Macro-4Femto scenario (grid in meters).

the introduction of a varying number of femto-cells in the network.

A brief introduction merits the last section of the chapter, where energy considerations are taken into account. Nowadays the trend is to develop green networks, with a low energetic impact. So energy considerations play an increasingly dominant role in the planning of next-generation networks. Our simulations confirm that femto-BSs provide a consistent improvement in the system capacity maintaining, at the same time, a very low energy consumption, compared to the macro-BSs. For this reason the use of femtocells represents a suitable solution for the deployment of green technologies. We made energy considerations about the radio base stations comparing, through simulations, the energy wasted to transmit a bit respectively by macro and femto stations. In order to make a complete analysis, we also evaluated the energetic impact at the user-side. In this case we referred to the 802.11 technology, for evaluating experimental measurements, and specifically to a common USB dongle, under different operation conditions (different PHY transmit rates and transmit powers). The rationale of this study was to understand the impact of transmit power tunings on the overall card consumption, under the assumption that 3G USB cards (over which we do not have full configuration control) will exhibit a similar behavior. Furthermore, the accurate measurements performed in the 802.11 environment have allowed the identification of the consumption quota of different card sub-systems, including the power amplifier, the RF-front end, the baseband and the host interface.

5.1 User Capacity Distributions

In this section the cumulative distributions of per-user capacity values (averaged on 100 iterations) are compared. Specifically, for each scenario and for a fixed power allocation strategy (uniform or according to the *water filling* approach), three distinct cumulative functions (respectively for all the users in the network, for the users associated to the macro-BSs and for the users associated to the femto-BS) are taken into account. This evaluation has been carried out in order to characterize the average behaviour of all users on one side, while maintaining separate statisticts for users associated to macro-BSs (hereafter labeled as macro users) and users associated to femto ones (labeled as femto-users).

Fig. 26 plots these functions in the different scenarios under examination. When femtocells are present in the network, femto users get capacity values significantly higher than those experienced by macro users. The curves associated to the femto users in fact overlap with the top of the cumulative functions of all the users, vice versa the curves associated to the macro users lie down on the bottom of these curves. The greater is the number of femtocells, the more the curves shift to the right, which means higher capacity values for the users. This phenomenon is more evident in the next section where the aggregated capacity values are considered. Another aspect that emerges from the figure is that the curves associated to the *water filling* are better than those ones associated to the uniform power allocation scheme from a certain point. In this regard, for a fixed scenario, by comparing the vectors of per-MS capacity values of the uniform and the *water filling* case, we noted the presence of zero values only in the latter case. This is due to the principle on which the *water filling* algorithm is based on: it prefers to assign zero power when a resource is too bad, preserving it for the best resources. Consequently users to which the allocator has assigned scarce resources can get zero values of capacity. From a global point of view however the *water filling* improves the system performance, as shown in the following sections. On the other hand, when an uniform power allocation is considered, a constant quota of power is always assigned, regardless of the resource quality. Consequently even the worst users get values of capacity different from zero.

Table 10 resumes the main statistics of the curves plotted in Fig. 26. Average and standard deviation values are associated to the cumulative distributions of all the users, while,

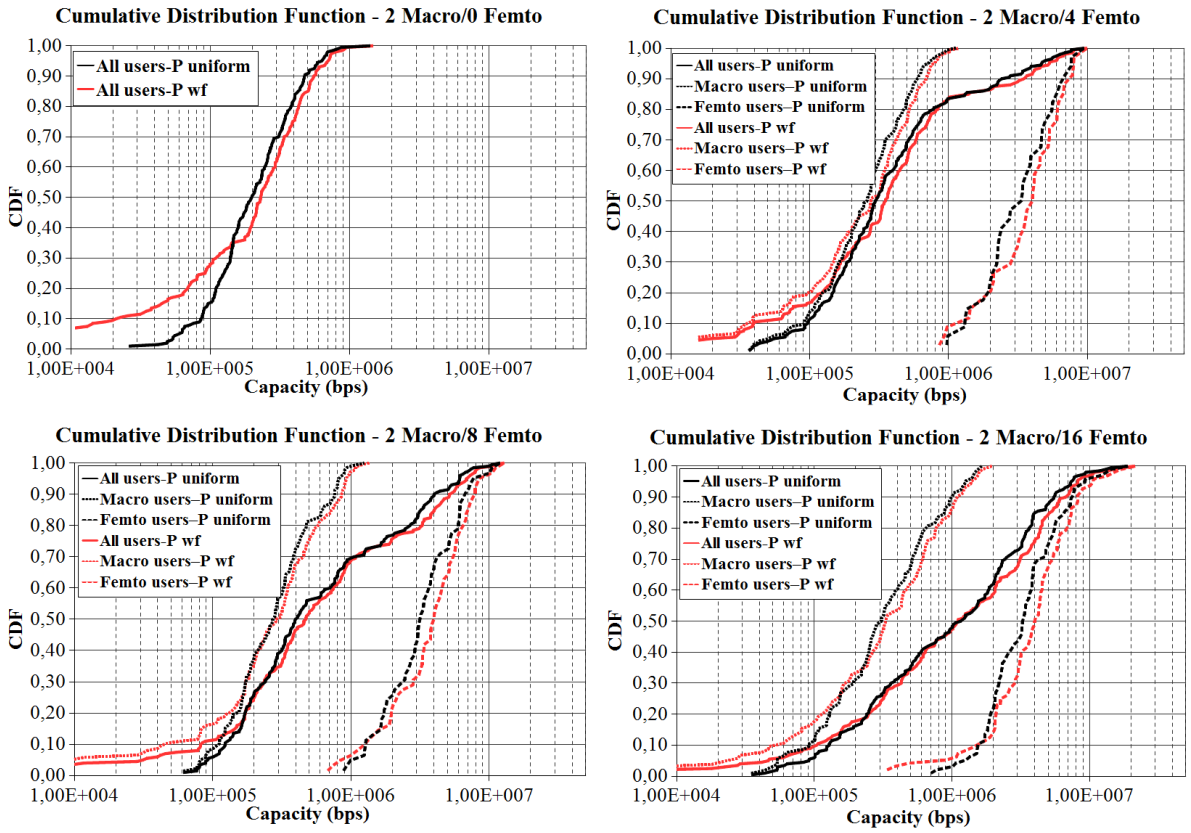

Figure 26: Cumulative Distribution Functions in comparison.

together with the average, we chose to characterize macro and femto cumulative distributions through the data rate fairness index, defined in section 3.3.

The analysis of the average values shows that the increment in the number of femtocells has beneficial effects in all the cases, even for the macro users. This may seem counterintuitive because as the number of femtocells grows, we could expect more interference to macro users. We analyzed this aspect with a specific set of simulations: we considered as reference just a macro-user associated to the same macro-BS in all the scenarios. For each scenario we considered 100 iterations forcing the allocator of this BS to assign all the resources to the selected user, continuing the other BSs to allocate resources to their users randomly. For each iteration we estimated an average value of per-resource capacity experienced by the selected user. Then we averaged all these values, obtaining a single estimation for each scenario. We compared these values and we noted that they decreased by increasing the number of femtocells, due to the interference introduced by them. Nevertheless, for a fixed number of users in the network (in this

	CDF All users				**CDF Macro users**				**CDF Femto users**			
	avg		st dev		avg		FI		avg		FI	
	un	*wf*	*un*	*wf*	*un*	*wf*	*un*	*wf*	*un*	*wf*	*un*	*wf*
2M-0F	0.25	0.27	1.87E+05	2.25E+05	0.25	0.27	0.65	0.59	/	/	/	/
2M-4F	0.89	0.98	15.74E+05	17.59E+05	0.31	0.32	0.67	0.63	3.73	4.22	0.75	0.77
2M-8F	1.43	1.63	21.14E+05	24.01E+05	0.34	0.37	0.66	0.61	3.85	4.43	0.72	0.74
2M-16F	2.18	2.53	27.80E+05	32.30E+05	0.44	0.49	0.57	0.56	4.07	4.73	0.65	0.65

Table 10: CDF statistics (average values in Mbps).

case 200), when the number of femtocells increases, users, previously associated to macro-BSs, migrate to femto-BSs. Consequently macro-BSs are less loaded and residual macro users obtain on average more resources (although scarce), resulting in an improvement of their capacities.

Standard deviation values show an increasing dispersion of the capacity values when the number of femtocells increases. The comparison of fairness indices also shows that the repartition of the capacity among the users is less fair when the number of active femtocells is high. Moreover the distribution of power according to the *water filling* approach, compared to the uniform distribution, improves the fairness among the femto users (they experience similar good channel conditions), and degrades the fairness among the macro users (occurring in this case a higher variability in the channel conditions).

5.2 Benefits of partial resource usage

A partial usage of resources was tested by forcing only the macro-BSs to use a fraction of the available resources (respectively 10, 50, 70 and 100 percent, for consistency with the simulations run in the homogeneous case). Different from the previous context, however, the choice made by BSs about the resources to use is now random (i.e. it is not based on the best SINR values experienced at the previous step). Results are shown in Fig. 27 in which the aggregated capacities (total, macro and femto) are plotted, by varying the scenarios (the number of femocells) and the percentage of resource usage.

Apart from the scenario with only macro-BSs, in all cases in which femtocells are active a partial usage of the resources is beneficial in terms of aggregated network capacity. It increases more and more by reducing the percentage of allocated resources in macro cells, due to the increment of femto users capacities. Their growth is predominant on the decrease of macro

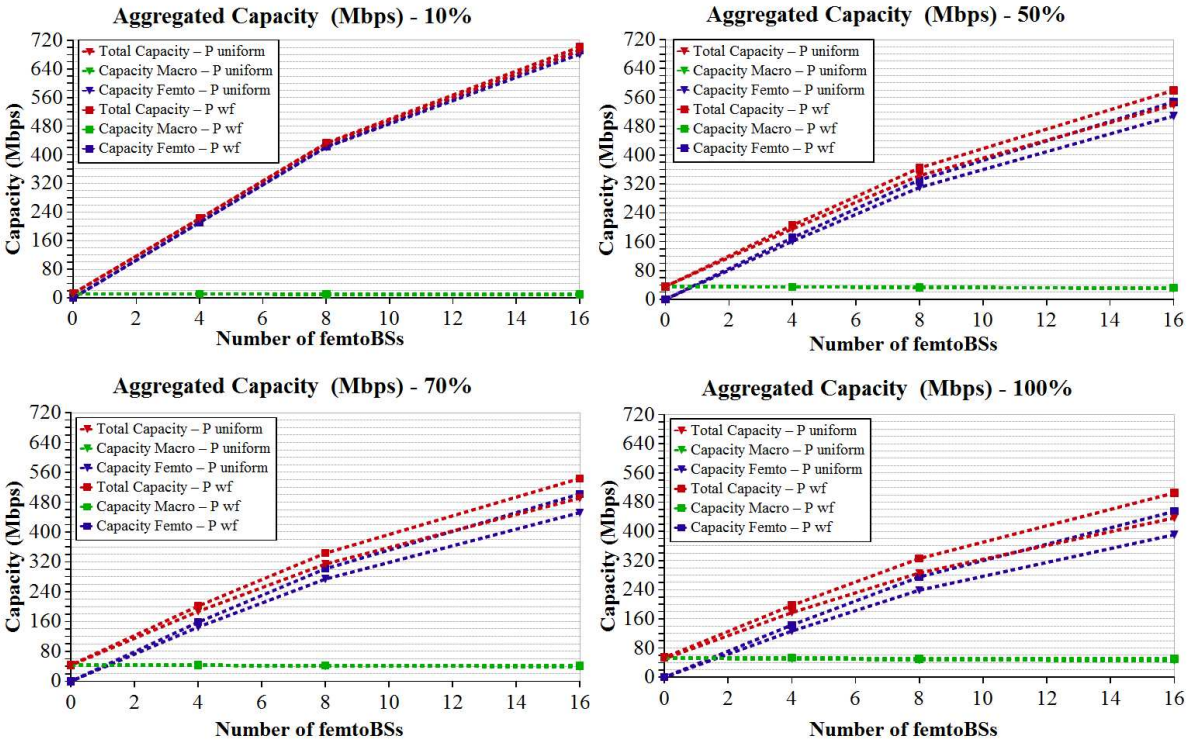

Figure 27: Impact of partial resource usage in macrocells.

users capacities and so even a 10 percent of resource usage in macrocells would seem to be justified. However it is worth recalling that usually a minimum data rate must be guaranteed to macro users too, so a solution with a very low percentage of allocated resources in macrocells can not be practical in the reality, although it leads to an increment of the overall capacity.

Because of the different scales of values, Fig. 28 plots apart the aggregated capacities of macrocells, in order to emphasize the difference between the uniform distribution of power on the assigned resources and the application of the *water filling* scheme. Figures show the aggregated *gross* capacity, without considering the resource consumption due to the signaling overhead. It is possible to note that the simple uniform allocation scheme, requiring no feedback from the MSs, provides results comparable with the *water filling* scheme when the number of active femtocells and the percentage of resource usage are low. In fact in contexts where the number of BSs (macro and femto ones) is high, the interference levels in general are higher too, consequently the difference between good and bad resources is more relevant and the *water filling* has a greater impact. Moreover, if the number of samples (resources) on which the power

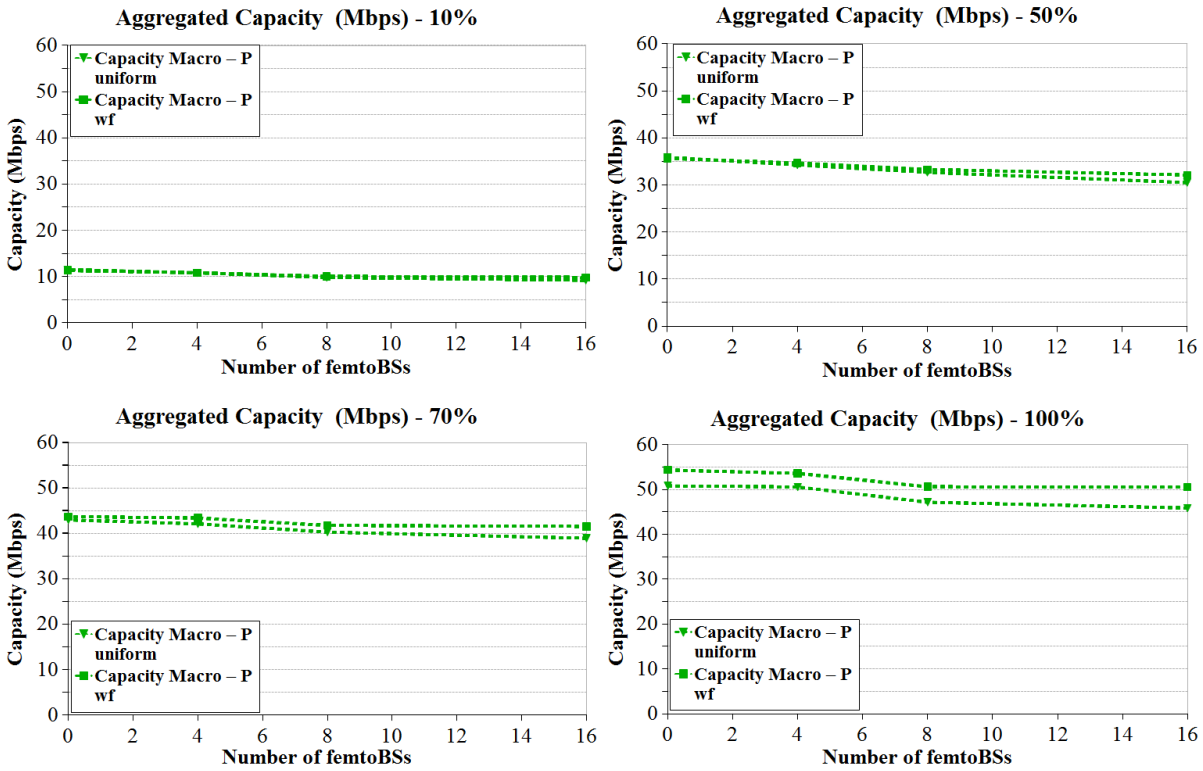

Figure 28: Impact of partial resource usage in macrocells (Macro curves).

optimization must be done is low, uniform and *water filling* approaches lead to similar results, while, if the number of resources (depending on the percentage of resource usage) is high, the difference between the optimized allocation of power and the uniform one is more marked.

Finally, in order to make more general considerations, we also considered the case in which all the BSs in the network (i.e. including the femto-BSs) have to perform a partial use of available resources. We ran simulations under this assumption, the results are plotted in Fig. 29. In order to make an immediate comparison with Fig. 27, we chose to adopt the same scale for the graphs of the two series. Fig. 29 shows that forcing femtoBSs to not use all the available resources too causes slight beneficial effects to macro users but, on the other hand, penalizes femto users. The result is no benefit from the network perspective.

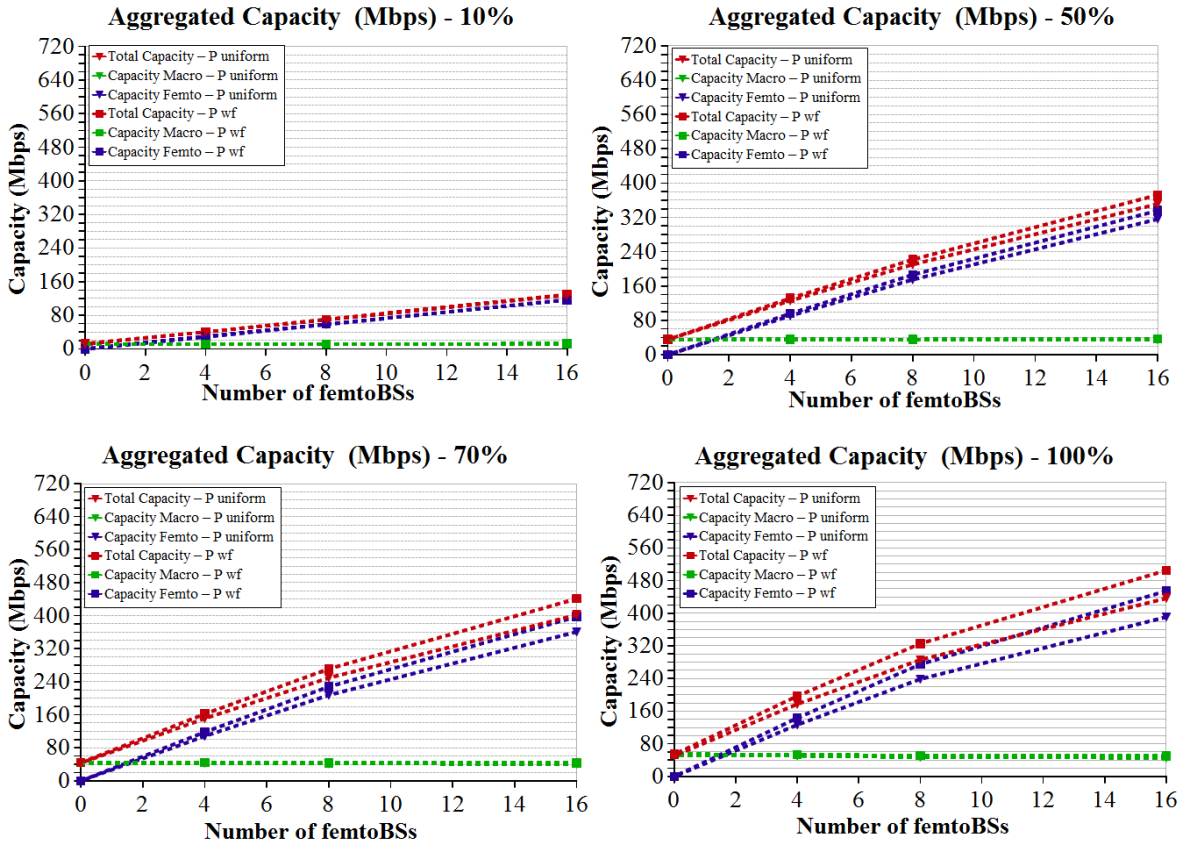

Figure 29: Impact of partial resource usage both in macrocells and in femtocells.

5.3 BS-side energy considerations

In order to evaluate the impact of BS power setting on the network performance, simulations were repeated varying the transmission power levels associated to macro- and femto-BSs. We considered as a reference case a power budget of 20 Watt and 0.01 Watt respectively for macro- and femto-BSs, that is also the configuration considered in all the simulations considered so far in this chapter. We ran a first set of simulations raising the power level of macro-BSs to 30 Watt, maintaining the femto power level to 0.01 Watt. Then we repeated the simulations by increasing the femto-BS power level by a factor of 10 (from 0.01 Watt to 0.1 Watt), maintaining the macro level constant to 20 Watt. All the results, averaged over 100 iterations, refer to a total usage of resources in each cell. Figures 30 and 31 respectively plot the aggregated capacities (total, macro and femto) for the configurations of power described above. The first graph in both the figures is relative to the reference case 20 Watt-0.01 Watt.

An increment of the power levels used in macro-cells leads to a lower network aggre-

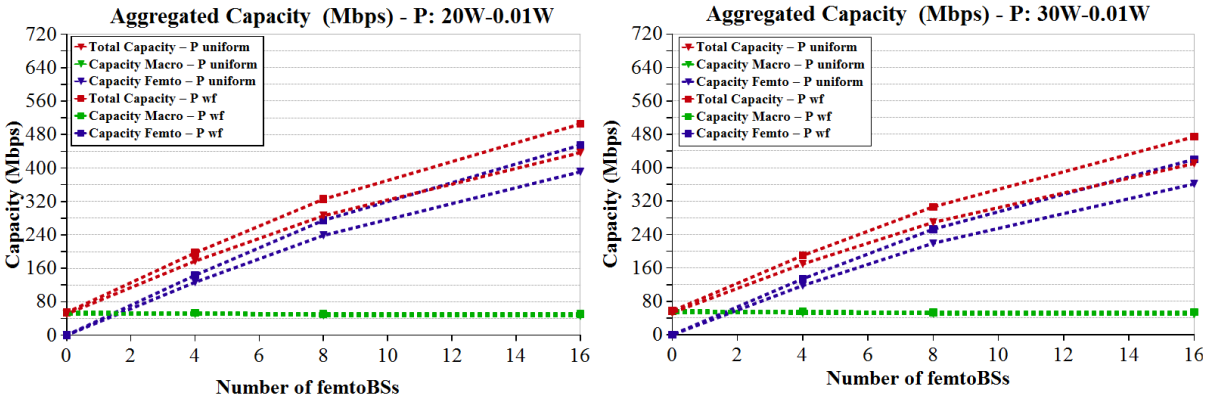

Figure 30: Effect of the increment of macro-BSs power levels.

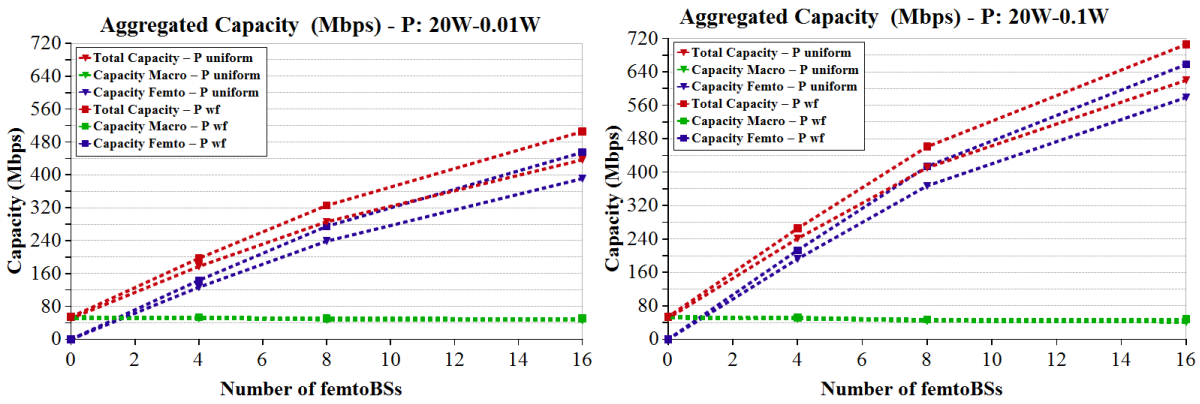

Figure 31: Effect of the increment of femto-BSs power levels.

gated capacity in all scenarios in which femtocells are present: in fact it has a marginal positive effect on macro users compared to the devastating effect on femto users, whose interference level becomes unacceptable. On the other hand, an increment in the power levels used in femto-cells leaves almost unchanged the situation of macro users (being almost irrelevant for them a change in the range considered for femto-cells) but it greatly enhances the service level of femto users (who already experience privileged channel conditions). This is an important result because it shows that, acting opportunely on the configuration parameters of femto-BSs (in this case setting an appropriate level of power), throughput performance of femto-users can be furtherly optimized. Moreover unlike the macro-BSs, the configuration of these femto-BSs can be performed directly by the end users.

Finally, Figures 32 and 33 show the BSs energy efficiencies, in terms of per-bit energy consumption. Graphs at the top of each series plot macro and femto energy consumption to-

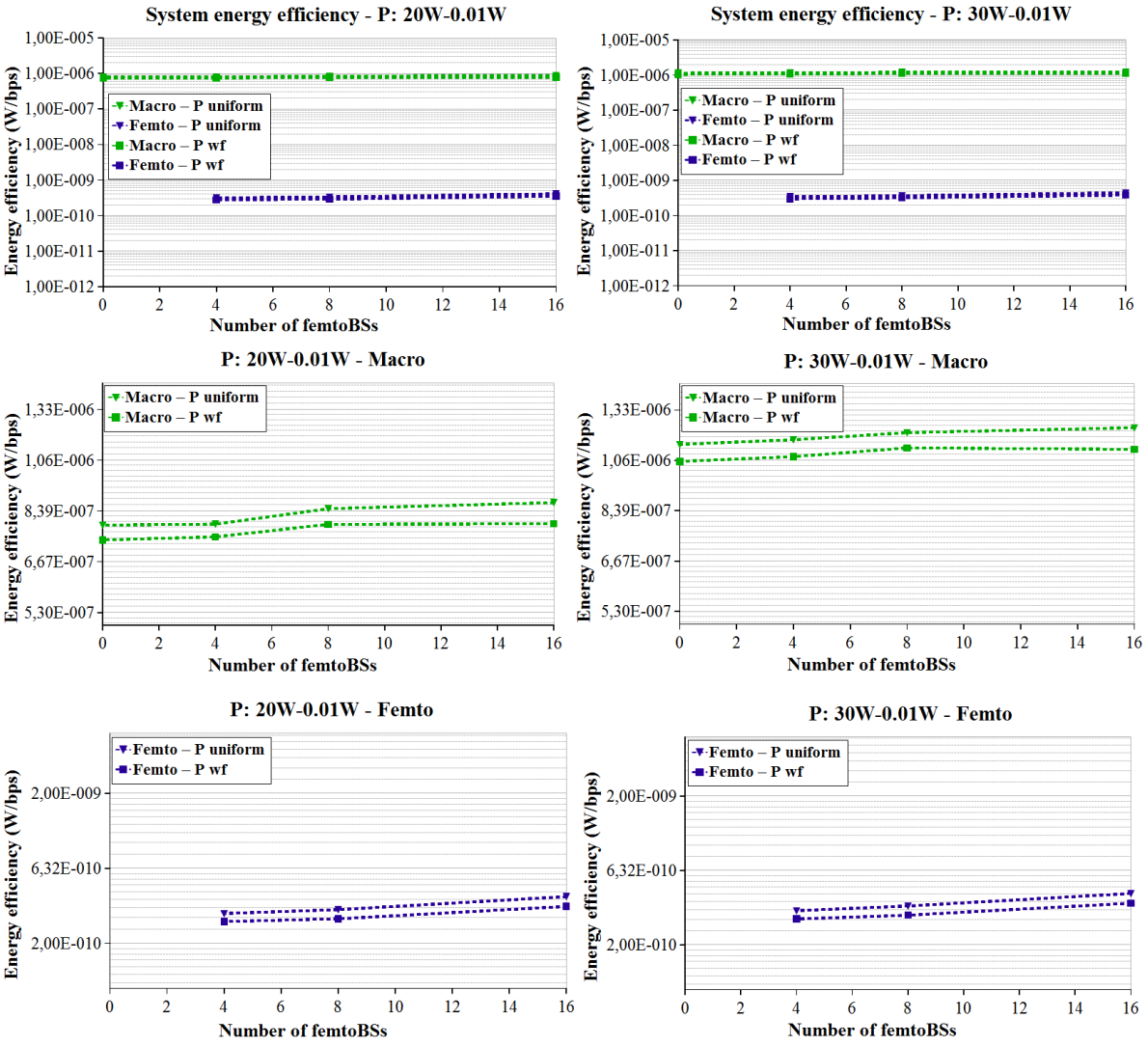

Figure 32: Changes in the system energy efficiency due to the increase of macro-BSs power levels.

gether, in order to make an immediate visual comparison of the two contributions. Graphs below instead separately show the individual curves (respectively macro and femto), in order to emphasize the impact of *water filling* on the energy consumption of BSs. Both in Fig. 32 and 33 the first column refers to the configuration 20 Watt-0.01 Watt, taken as a reference. In the previous sections it was showed that femto-BSs enables a consistent system improvement in the system capacity. In addition to this, now figures demonstrate that femto-BSs maintain, at the same time, the energy consumption significantly lower than macro-BSs, even three order of magnitude lower. Overall, you tend to have higher energy consumption in crowded scenarios, i.e. scenarios with a high number of BSs. In any case, the application of *water filling* always guarantees a lower energy consumption, because the optimization of the power distribu-

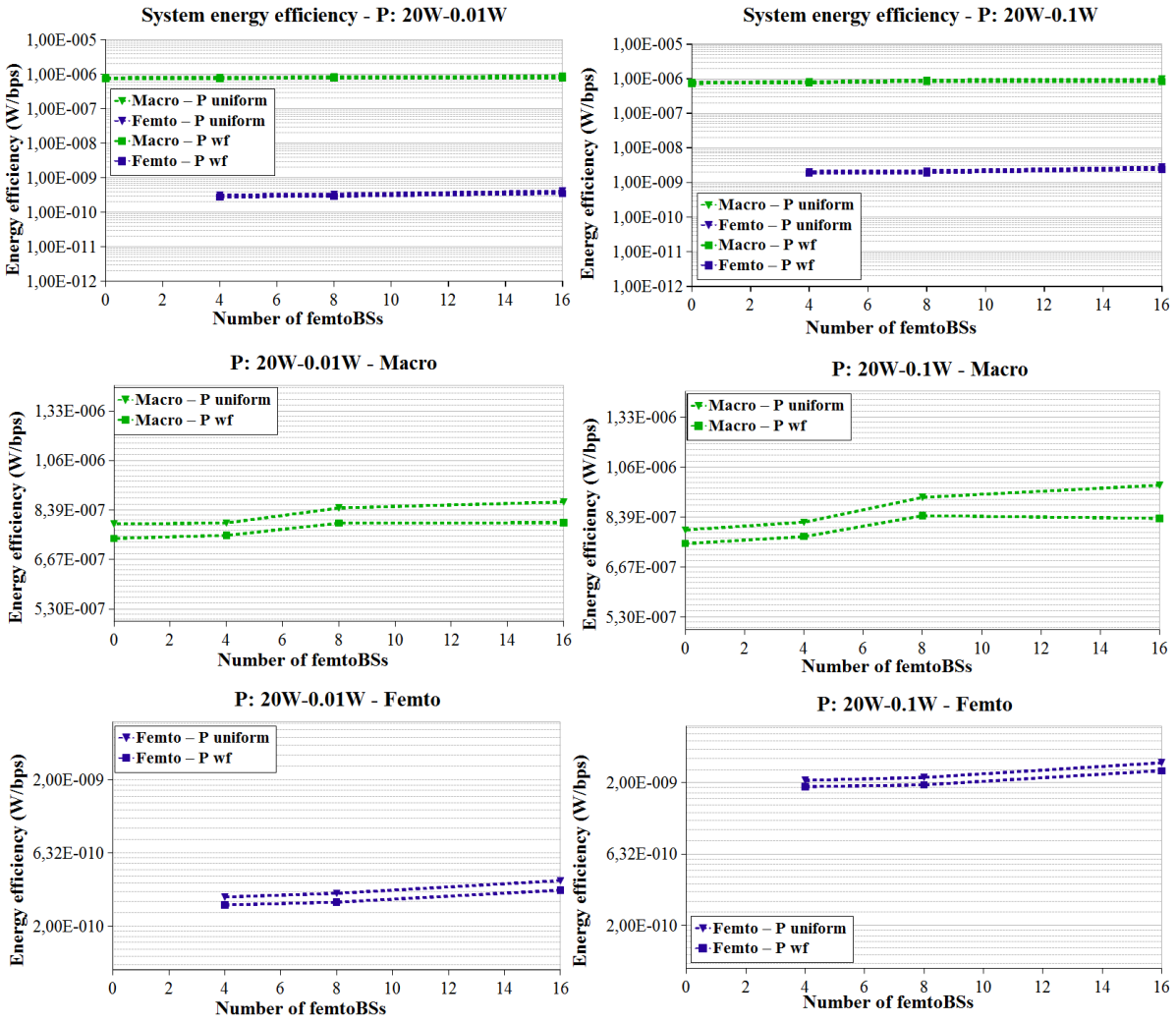

Figure 33: Changes in the system energy efficiency due to the increase of femto-BSs power levels.

tion leads to a careful management of it, thus avoiding unnecessary wastage of energy. A final consideration is that when the power level increases, there is a major energy consumption: if the power is set higher in macro-BSs, the macro energy consumption grows up, vice versa if the power is increased in femto-BSs, the femto consumption rises up, reducing the gap with the macro level (even if it is still substantial).

5.4 User-side energy considerations

As mentioned in the chapter introduction, this section is devoted to the analysis of the energy consumption at user-side, with reference to the WiFi technology for the reasons described above.

Due to the impressive proliferation in next generation networks of mobile devices, equipped with wireless interfaces and to the limited battery power they rely on, reducing the energy consumption of WLAN interfaces has become increasingly a very important research issue. Indeed, several energy saving mechanisms, more or less technology-dependent, have been explored in literature.

Transmit power control (TPC) has been largely proposed as a solution to improve the performance of packet radio systems in terms of increased throughput, spatial reuse and battery lifetime for mobile terminals. However, the benefits of transmit power control schemes on these different performance figures may strongly depend on the employed PHY technology and channel access mechanism. Most of the existing proposals quantify the energy saving provided by TPC in WiFi networks via simulation. These results are based on power consumption models of WiFi interfaces, which are summarized into a set of power consumption values referring to different node states (namely, transmitting, receiving, idle and doze). Obviously, the performance evaluation of these schemes strongly depends on the setting of these values.

We dealt with the problem of quantifying the energy saving that can be provided in WiFi networks by means of TPC [81]. To this purpose, the power consumption of some commercial WiFi cards under different transmit power levels was experimentally characterized. We carried out several experimental tests under different operation conditions and modulation schemes. Our methodology, similarly to the methodology described in ([82],[83]) has been able to provide: i) a direct measurement of instantaneous card consumptions, and ii) an indirect measurement of average (or per-packet) energy consumptions. Differently from previous results, the approach here reported aim to rigorously control the transmit power and to compare the OFDM and DSSS modulations. The results, described in the following sections, show that little space should be left to TPC for effectively reducing energy consumption of WiFi cards, due to the power consumed in idle states.

The rest of the chapter is organized into three further sections. In the first one the 802.11 standard is briefly reviewed in order to define different card states corresponding to different power consumptions. Then a description of the experiments is made, by illustrating the used methodological approach and the measurement elaborations. Final section is dedicated to pro-

vide a card sub-system decomposition, enlightening the fixed power consumption overheads.

5.4.1 Energy consumption in WiFi cards

Regardless of the specific card implementation, we can expect that the energy consumption of WiFi cards depends both on physical layer (PHY) and medium access control layer (MAC) operations. As far as concerns the PHY layer, in current 802.11a/b/g standards different modulations (e.g. DSSS and OFDM) and coding schemes are available for frame transmissions. Each scheme corresponds to a different activity interval required for transmitting or receiving a frame, which leads to different energy consumptions. Moreover, each scheme also exhibits a different processing complexity, which may cause further differences in the instantaneous power absorption. As far as concerns the MAC layer, the WiFi standard is based on a *Carrier Sense Multiple Access with Collision Avoidance* (CSMA/CA) protocol, called *Distributed Coordination Function* (DCF). DCF has been designed for optimizing wireless medium utilization while maintaining the protocol simplicity. Therefore, it is based on some design choices which do not take into account energy consumption problems. For example, the use of an asynchronous access protocol is intrinsically inefficient for the reasons discussed in this section.

DCF operations can be summarized as follows. A station with a new frame to transmit has to monitor the channel state, until it is sensed idle for a period of time equal to a *Distributed InterFrame Space* (DIFS). If the channel is sensed busy before the DIFS expiration, the station has to add a further backoff delay before transmitting, in order to avoid a synchronization with the transmissions of other stations. The backoff interval is slotted for efficiency reasons and is doubled (up to a maximum value) at each consecutive failed transmission. Frame transmissions have to be explicitly acknowledged with ACK frames, because the CSMA/CA does not rely on the capability of the stations to detect a collision by hearing the channel. The ACK frames are immediately transmitted at the end of a frame reception, after a period of time called *Short InterFrame Space* (SIFS) shorter than a DIFS. If the transmitting station does not receive the ACK within a specified ACK_Timeout, it reschedules the packet transmission, according to the given backoff rules.

These access operations imply that a new frame transmission can start at any time in-

stants on the channel and active stations have to continuously monitor the wireless medium in order to intercept incoming frames. As a consequence, a station spends a significant amount of time in monitoring the channel, regardless of the presence of incoming or outcoming traffic. Summarizing, during the activity intervals, a WiFi card can be in various operational states, which include:

- transmission, when the card is involved in the physical irradiation of an ongoing frame;
- reception/overhear, when the card is involved in demodulating a frame destinated to itself or to another station;
- idle, when the card is monitoring the channel, ready to reveal channel busy signals, but no signal is present;
- doze, when the card radio transceiver is turned off.

Different operational states correspond to different power absorptions. Let W_{tx}, W_{rx}, W_{idle} and W_{doze} be the generic power absorbed, respectively, in transmission, reception, idle and doze state. Regardless of the card implementation, we can expect that $W_{tx} \geq W_{rx} \geq W_{idle} \geq W_{doze}$.

Assuming that no power saving mechanism is employed (i.e. the card never switches to the doze state), the minimum energy $E_{min}(T)$ consumed in a given activity interval T is:

$$E_{min}(T) = W_{idle} \cdot T \tag{33}$$

This minimum consumption is experienced when the card does not transmit and receive any frames during the whole activity time. Conversely, the energy consumption is maximized when the card spends the maximum possible time in the transmission state. Since the standard limits the maximum frame size, this condition is verified when i) the card transmission buffer is never empty (i.e. the card works in saturation conditions); ii) the frames are transmitted at the minimum PHY rate; iii) no other station accesses the channel. The ratio tx of the time spent in transmission for a card working in saturation conditions, in absence of contending stations, can be easily evaluated by considering the beginning of a new transmission as a regeneration instant. Specifically, being $\overline{b}$, T_{DATA}, and T_{ACK}, respectively, the average time spent in backoff,

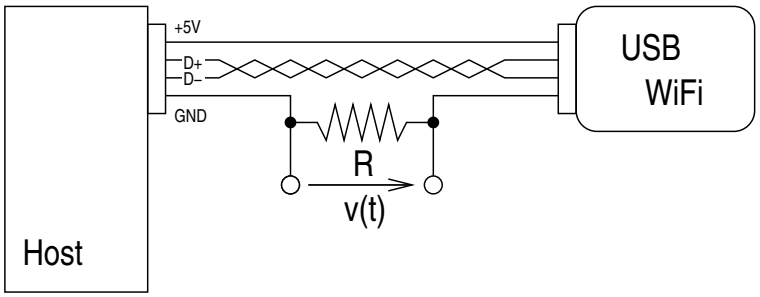

Figure 34: Power measurement setup.

in transmitting a data frame and in receiving an ACK frame, it results:

$$tx = \frac{T_{DATA}}{T_{DATA} + SIFS + T_{ACK} + DIFS + \overline{b}} \tag{34}$$

For example, for the maximum admittable payload size of 2304 byte and the 802.11g PHY, it results $tx = 0.95\%$ at 6 Mbps and $tx = 0.70\%$ at 54 Mbps. The ratio rx of the time spent in reception corresponds to the ACK duration ratio within a transmission cycle, i.e.:

$$rx = \frac{T_{ACK}}{T_{DATA} + SIFS + T_{ACK} + DIFS + \overline{b}} \tag{35}$$

For example, for the previous case of 802.11g PHY with a payload length of 2304 byte and a data and acknowledgment rate of 6 Mbps, it results $rx = 1.2\%$. Given the tx ratio and rx ratio, the average power consumption $\overline{W}$ can be evaluated as:

$$\overline{W} = tx \cdot W_{tx} + rx \cdot W_{rx} + (1 - tx - rx) \cdot W_{idle} \tag{36}$$

Therefore, the energy $E(T)$ consumed during T results:

$$E(T) = \overline{W} \cdot T \leq [txW_{tx} + (1 - tx)W_{idle}] \cdot T = E_{min} + tx \cdot (W_{tx} - W_{idle}) \cdot T \tag{37}$$

5.4.2 Energy consumption measurements

Methodology To the best of our knowledge, in literature there are a few detailed measurement studies of the energy consumption of WiFi Cards. These studies can be divided into two general approaches: i) indirect measurements, obtained by monitoring the total energy consumed

by laptops whose WiFi interface is enabled or disabled, ii) direct measurements, obtained by monitoring the input current drawn by the network card. We followed this second approach, for the case of USB WiFi cards. In fact, for these cards, it is immediate to probe the input current, by accessing the ground wire of the USB cable. Specifically, as shown in Fig. 34, we inserted a test resistor along the ground wire, in series with the card, and we measured the voltage at the resistor. Measurements were obtained using a 500 MHz Agilent digital oscilloscope, devised to acquire a complete voltage trace during an acquisition interval T. By opportunistically tuning the temporal granularity of the oscilloscope traces, we are able to monitor the current values drawn during frame transmissions, frame receptions, channel monitoring and backoff. The instantaneous power consumptions are then evaluated, in the hypothesis of fixed input voltage $V_{in} = 5V$ and resistive input impedance of the card, as:

$$P(t) = V_{in}\frac{v(t)}{R} \tag{38}$$

where $v(t)$ is the direct measurement of the test resistor voltage, and $v(t)/R$ is the indirect measurement of the current drawn by the card. Elaborating the oscilloscpe traces, we also averaged the instantaneous values for characterizing the W_{tx}, W_{rx} and W_{idle} values and the overall average consumption $\overline{W}$. In order to cross-validate our results, we performed some additional measurements by means of a digital multimeter. This instrument allows tracking the average power consumption at time scales much longer than a frame transmission time (e.g. 1 second). Thus, we compared these average values with the elaborations of the oscilloscope traces.

Although the results presented in this thesis mainly refer to the D-Link DWL G-122 card, based on the Ralink chipset RT2500USB, we repeated our measurement campaign for other test cards (namely, Netgear WG111v2, Asus WL-167G and Linksys WUSB 300N), and for different operating systems (Windows and Linux). The four WiFi cards are depicted in Fig.35.

The host laptop was an Acer Extensa 5220, connected in ad-hoc mode with another identical laptop. As a traffic generator, we used the Iperf [84] tool with a CBR source over UDP. Unless otherwise specified, the source rate has been set to 100Mbps (in order to guarantee

Figure 35: WiFi cards used in the experimental tests.

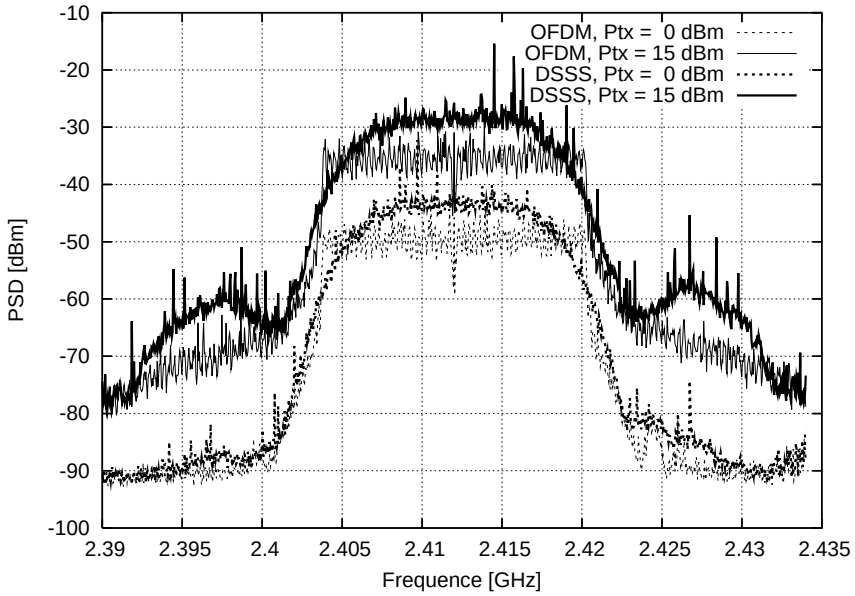

Figure 36: Power Spectral Density of OFDM and DSSS signals, for Ptx = 15 dBm and Ptx = 0 dBm.

saturation of the transmission buffer) with a frame length equal to 1470 bytes. We ran different experiments, changing the PHY transmit rate r and the PHY transmit power Ptx employed by the cards. These parameters have been changed by means of the card configuration interface at the driver level. In some cases (e.g. the very recent Linksys card), some configuration options were not available. Therefore, we used the D-Link card as a reference card thanks to the availability of a full featured driver.

We carefully checked that the values specified at the driver level were conform to the actual values adopted by the cards. About the PHY transmit rate, we considered a very simple validation test, by comparing the actual frame transmission times with the expected ones. The actual frame transmission times have been measured at the oscilloscope, by identifying time

intervals during which the card drew the maximum current value. About the PHY transmit power, we monitored the RSSI values sampled at the receiver for different configuration of the transmit power, while maintaining the transmitter and the receiver node at the same position. We noticed that the RSSI values experienced increments or decrements corresponding exactly to the changes applied at the transmitter side. Some exceptions have been found when we set transmit power values higher than 15 dBm. In fact, despite the regulatory limit is higher, some cards do not allow settings higher than 15 dBm. Finally, we also checked that the *Power Spectral Density* (PSD) revealed by means of a spectrum analyzer changed in agreement with the PHY transmit power. Fig. 36 plots some traces of our spectrum analyzer, obtained for Ptx=15 dBm and Ptx=0 dBm, in the case of r=6 Mbps (OFDM modulation) and r=11 Mbps (DSSS modulation).

Impact of transmit power Figures 37 and 38 plot the power absorption traces collected during some experiments lasting T=5 ms. The figures refer to the D-Link DWL G-122 card and have been obtained for Ptx=15 dBm (Fig. 37) and Ptx=0 dBm (Fig. 38) at different transmit rates (namely, 1 Mbps, 6 Mbps, 11 Mbps and 54 Mbps). Unless otherwise specified, we always refer to this test card.

Focusing on Fig. 37, we can easily recognize the different working states of the card under test. The higher power levels correspond to the transmission states, whose duration depends on the employed rate. The time intervals between two consecutive transmissions correspond to the reception of the ACK frames and to the subsequent random backoff process. The figure visualizes that the power consumption experienced during these two phases, i.e. in reception and idle mode, is substantially the same. In order to better visualize the ACK reception times, we set the network basic rate at 2 Mbps. In each trace, we can recognize a narrow spike over the lower level at the end of each frame transmission, which corresponds to the ACK reception. For the 54 Mbps trace, we can observe two small spikes between the transmission of the sixth and seventh frame. We verified, by means of a traffic sniffer, that this spike is due to the reception of a beacon frame transmitted by the receiver[1].

[1]We recall that in ad-hoc networks, all the nodes schedule the beacon transmission at regular time instants. When a given node succeeds in transmitting the beacon, all the other pending ones are suspended.

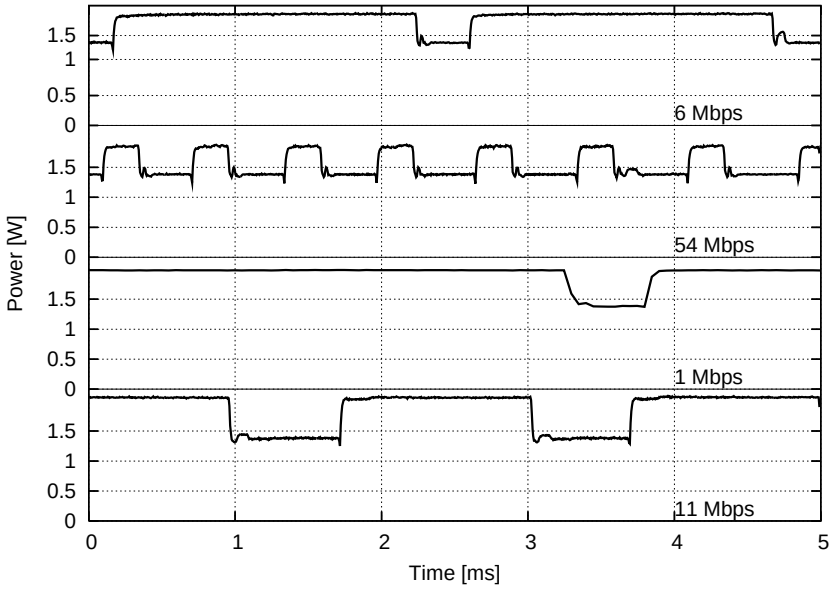

Figure 37: Instantaneous power consumption in saturation conditions for different transmit rates - Ptx = 15 dBm.

By comparing Fig. 37 and Fig. 38, it is qualitatively evident that for Ptx=0 dBm the power W_{tx} consumed in the transmission state is reduced. However, such a reduction is marginal for the OFDM modulated frames (i.e. for the 6 Mbps and 54 Mbps cases), while is appreciable for the DSSS ones. The power consumption experienced in reception and idle state is approximately the same in both the figures.

Table 11 quantifies our previous considerations. We estimated the W_{tx}, W_{rx} and W_{idle} values, by quantizing the traces plotted in Figures 37 and 38 into three different levels (an high level for the transmission state, an intermediate level for the reception state, and a low level for the idle state), and by averaging the instantaneous values collected for each level. By using these estimates, we evaluated the average power consumption according to eq. (36) and we compared such an evaluation with the trace average values and with the multimeter measurements. The average values have been summarized under the $\overline{W}$ column and identified, respectively, by the Eqn, Osc and Mul label. The results obtained with the three different methodologies are in good agreement. Since equation (36) is based on the computation of the frame transmission times, the agreement of these results also proves that the actual transmission rate is equal to the nominal one, set at the driver level.

From the table, we can observe that the power consumed in reception (W_{rx}) and idle

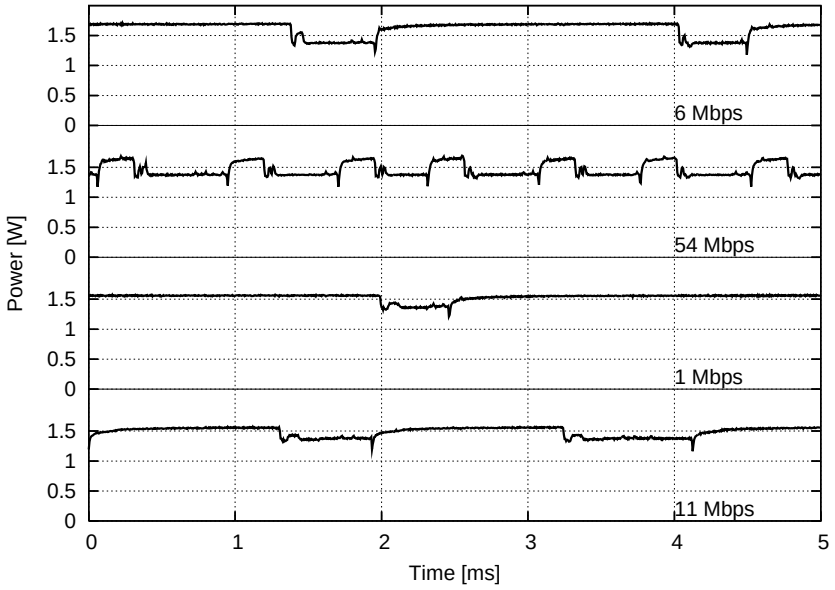

Figure 38: Instantaneous power consumption in saturation conditions for different transmit rates - Ptx = 0 dBm.

	W_{tx}		W_{rx}		W_{idle}		$\overline{W}_{15dBm}$			$\overline{W}_{0dBm}$		
r	15 dBm	0 dBm	15 dBm	0 dBm	15 dBm	0 dBm	Eqn	Osc	Mul	Eqn	Osc	Mul
1 Mbps	1.98	1.54	1.40	1.40	1.38	1.38	1.94	1.94	1.96	1.52	1.49	1.53
11 Mbps	2.06	1.56	1.40	1.40	1.38	1.38	1.84	1.86	1.79	1.50	1.54	1.49
6 Mbps	1.85	1.64	1.44	1.44	1.38	1.38	1.77	1.77	1.74	1.60	1.62	1.59
54 Mbps	1.85	1.64	1.44	1.44	1.38	1.38	1.57	1.55	1.51	1.49	1.46	1.44

Table 11: Per-state and average power consumption values [W].

(W_{idle}) state are comparable in all the cases. By reducing the transmit power Ptx from 15 dBm to 0 dBm, the W_{tx} values are reduced of about 20% for r=1 Mbps and r=11 Mbps (DSSS case), and about 10% for r=6 Mbps and r=54 Mbps (OFDM case). These reductions are reflected in lower percentual reduction of the average power consumption $\overline{W}$. Note that the table refers to a card working in saturation conditions. Since in most cases the transmission time is a small fraction of the whole activity time, the reduction of the W_{tx} values by means of TPC has a marginal effect on the overall energy consumption of the cards.

Finally, Table 12 summarizes the results of similar measurements carried out with different cards. From the table we note that, for each card, the W_{idle} and W_{rx} values are comparable. For the cards transmitting at 15 dBm, we also note that the power W_{tx} consumed in the transmission state may vary from 1.85 W up to 2.69 W because of different card designs and implementations.

Card	Ptx	W_{tx}	W_{rx}	W_{idle}
Linksys	15	2.69	1.65	1.61
Netgear	15	2.01	1.58	1.39
Asus	12	1.40	1.01	0.97
D-Link	15	1.85	1.44	1.38

Table 12: Power consumption values for different cards for $r = 6$ Mbps [W].

r	$\overline{W}$	Thr	E(T)/bit
1 Mbps	1.94	0.915	2.12e-6
11 Mbps	1.86	6.192	3.00e-7
6 Mbps	1.77	4.458	3.97e-7
54 Mbps	1.55	13.706	1.13e-7

Table 13: Average power [W], average throughput [Mbps], and energy per-bit [J/b] at different rates.

Impact of transmit rate The most evident effect of the PHY transmit rate on energy consumption is obviously related to the duration of frame transmissions. As the transmit rate increases, the ratio tx spent by the card in transmission state is reduced, thus resulting in a lower average $\overline{W}$ value. Moreover, the reduction of the transmission times allows to deliver an higher number of frames during T. Therefore, the per-bit energy consumption is further improved. Table 13 quantifies these considerations by summarizing the $\overline{W}$ (which is proportional to the energy consumption $E(T)$), the average throughput, and the per-bit energy consumption observed in saturation conditions at different rates. From the table, we can conclude that the PHY transmit rate strongly affects the per-bit energy consumption of the cards.

In section 5.4.1, we have implicitly assumed that each card is characterized by a fixed W_{tx} value, which does not depend on the transmit rate, and that such a value is constant during the whole transmission interval T_{DATA}. However, these assumptions are not rigorous. In Table 11 we can see a clear difference between the OFDM and DSSS modulations (W_{tx} is about 1.8 W for the OFDM case and about 2 W for the DSSS one). While in OFDM mode the W_{tx} is about the same for the 6 Mbps and 54 Mbps case, some differences appear in DSSS mode, as the transmit rate changes from 1 to 11 Mbps. In order to better visualize this phenomenon, Fig. 39 plots the instantaneous power consumption observed for the DSSS modulations. The traces collected at different rates have not been labeled, since we can easily recognize the 1, 2, 5.5 and 11 Mbps traces according to frame transmission duration.

From the figure it is evident that the instantaneous W_{tx} values slightly grow as the trans-

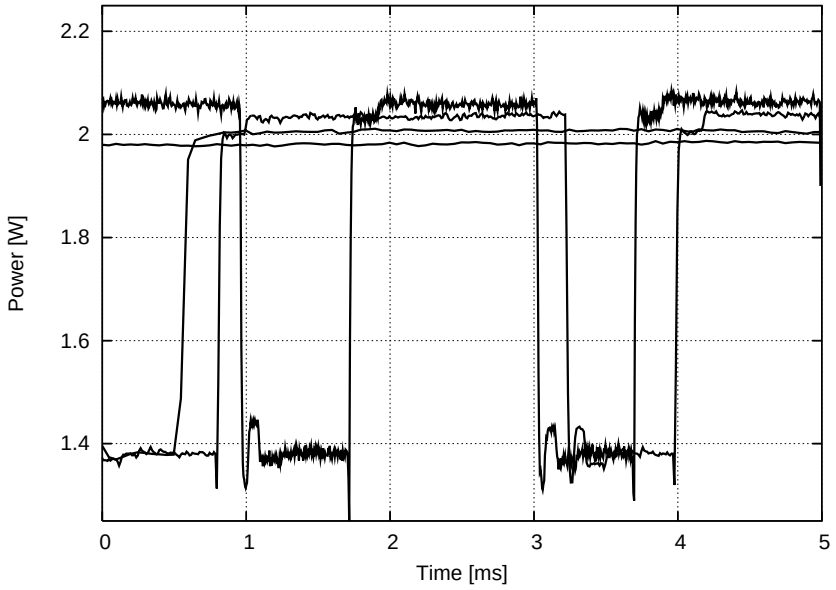

Figure 39: Instantaneous power consumption at 1, 2, 5.5. and 11 Mbps.

mit rate increases. We suspect that this increment is due to the additional processing complexity introduced by the higher rate modulations. At the beginning of the frame transmissions, for the 5.5 Mbps and 11 Mbps traces, we can also recognize that the preamble transmission is characterized by a power consumption lower than during the rest of the frame.

5.4.3 Energy consumption components

The power consumption measurements described in the previous section have been obtained by considering the card under test (i.e. a D-Link DWL G-122 card) as a black box. In other words, we characterized the instantaneous power consumption without identifying the different hardware components responsible of partial absorptions. Indeed, the decomposition of the overall consumption into independent sub-systems performance can be very enlightening for the design of effective power saving schemes.

Fig. 40 shows a card block diagram, analogous to the one depicted in [85]. The card has been decomposed into: a Power Amplifier (PA), an RF subsystem (RF), a MAC/BaseBand processor, and a USB host interface (USB).

Each of these sub-blocks gives a different and easily recognizable contribution to power consumption. The Power Amplifier is relevant only during transmission bursts. Most WiFi implementations feature an external power amplifier. The reason for choosing an external power

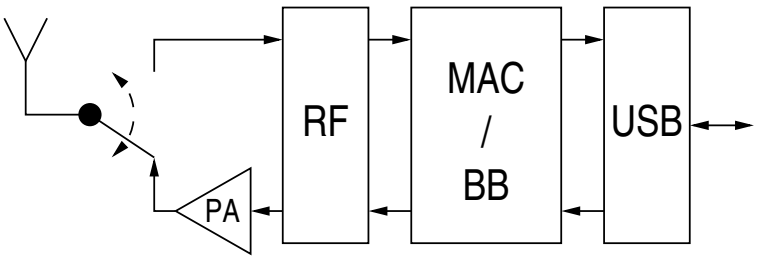

Figure 40: System blocks of a USB WiFi card.

amplifier is that the realization of low-voltage CMOS linear power amplifiers for OFDM signals is an extremely challenging task. In fact, the OFDM signal has a very high *Peak-to-Average Power Ratio* (PAPR) which makes difficult designing efficient linear power amplifiers[2]. The RF subsystem, which is responsible for frequency synthesis, synchronization, up and down conversion and low-noise amplification, absorbs power while the card is not dozen. The power consumption due to baseband processing is very different depending on if the station is transmitting or receiving. When the card is in transmission state, the baseband processor just encodes and modulates the frames, thus resulting in a very lower power consumption. Conversely, when the card is in reception state, several actions are needed, such as timing and fine frequency synchronization, channel estimation and equalization and, in the case of OFDM signals, channel decoding. All these operations make the baseband processing more power-eager during reception than during transmission. Since the MAC processing has an event-based low-rate schedule, its power consumption is very low. Finally, a component which turnes out to have a significant contribution to the overall power consumption is the *Universal Serial Bus* interface to the host. In the following, we try to dissect separately the contribution of each component.

Power amplifier We can identify the power consumption W_{PA} due to the power amplifier by considering $W_{PA} = W_{tx} - W_{idle}$. From Table 11, for a nominal Ptx value of 15 dBm, it results $W_{PA} \simeq$ 600 mW in the case of DSSS modulations, and $W_{PA} \simeq 470$ mW in the case of OFDM modulations. Such values are compatible to a power amplifier efficiency of about 5%.

Note that the lower W_{PA} value experienced under the OFDM mode is not due to an higher efficiency in amplifying OFDM signals. In fact, by integrating the PSD traces collected by the spectrum analyzer, we found that, despite of the same nominal transmit power, the power

[2]The most efficient power amplifiers found in the literature have an efficiency which may approximately vary from 40% [86] down to less than 10% [87] as the amplifier gain increases.

radiated in OFDM mode is 4.4 dB lower that the power radiated in DSSS mode. This phenomenon can be explained as a side-effect of the non-linearity of the power amplifier. When operating in DSSS mode (i.e. with low PAPR), the power amplifier can be fed with high level signals, without triggering spectral spurs. Conversely, when operating on OFDM signals (i.e. with high PAPR), the signal levels have to be attenuated in order to avoid spur signals impairing the spectral mask requirements.

RF front-end and baseband processing We assume that the baseband power consumed when the card is in transmission state is neglegible. As far as concern the reception state, we identify the power consumption W_{BB} due to the baseband processing as $W_{BB} = W_{rx} - W_{idle}$. From Table 11, it results $W_{BB} \simeq 20$ mW in the case of DSSS modulations, and $W_{BB} \simeq 60$ mW in the case of OFDM modulation. As expected, the W_{BB} computation leads to the same results in case of Ptx = 15 dBm and Ptx = 0 dBm.

In order to compute the RF front-end power consumption W_{RF}, we also measured the instantaneous power W_{doze} absorbed by our card while in doze state. The measurement has been carried out by switching the card transceiver off. By processing the oscilloscope traces, we obtained an average W_{doze} value of 760 mW. Assuming that W_{RF} is independent from the transmission or reception state, we consider $W_{RF} = W_{idle} - W_{doze} \simeq 620$ mW.

Universal Serial Bus / host interface We assume that the power consumption resulting in the doze state is mainly due to the USB interface. Therefore, $W_{USB} \simeq W_{doze} = 760$ mW. Our measurements are compatible to the power consumption of a common USB / Host interface [85], which is about 600/700 mW. Note that this contribution represents an high fraction of the whole card consumption, being comparable to the W_{PA} value measured at full transmit power. This high value may be explained with the high speed of the PHY featured in the Universal Serial Bus specification [88].

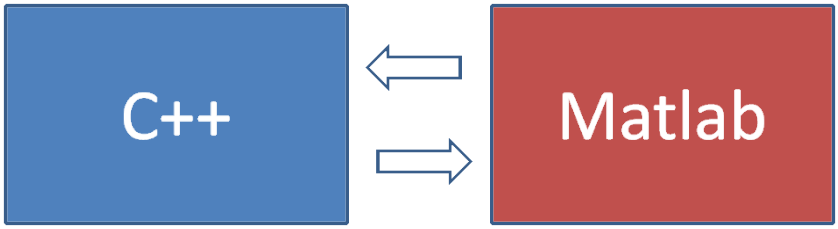

Figure 41: Semplified block diagram of the simulator.

6 Appendix

6.1 Part A: High level description of the simulator and interference model

The simulation results disseminated throughout the thesis were obtained by using an interacting MATLAB/C++ custom-made simulator (Fig. 41). It is based on a mixed geometrical-stochastic model that can simulate a cellular layout including an accurate interference model.

Specifically, the network topologies considered in all the simulations and the channel evolutions have been implemented in C++, while the allocation policies and the capacity computation have been implemented in MATLAB. The choice to use an independent C++ simulator for simulating the channels stems from the fact that this task is the most critical one from a computation point of view. Moreover, since the channel coefficients depend on the physical and propagation environment and evolve independently from the allocation policies, the channel simulation can be carried out independently from the allocations, without affecting the overall simulation accuracy.

The simulator has a clock-driven architecture, whose time unit is given by the symbol time. The C++ routine is executed at the beginning of the simulation and provides the BS grid, the MS positions, the channel gain coefficients at each simulation symbol $t \in [0, T]$. For each simulation step t, the allocation module is run sequentially at each BS, in order to determine the allocated PBUs and the power allocations on them. Such a sequential allocation is only a simulation feature and does not affect the system performance. In fact, whenever the allocation module requires a channel state feedback, the feedback is assumed to be signaled in the previous frame. Therefore, the interference is evaluated by considering all the allocations performed at time $t - 1$.

An example of a network layout is shown in Fig. 42 on the following page: it refers to a

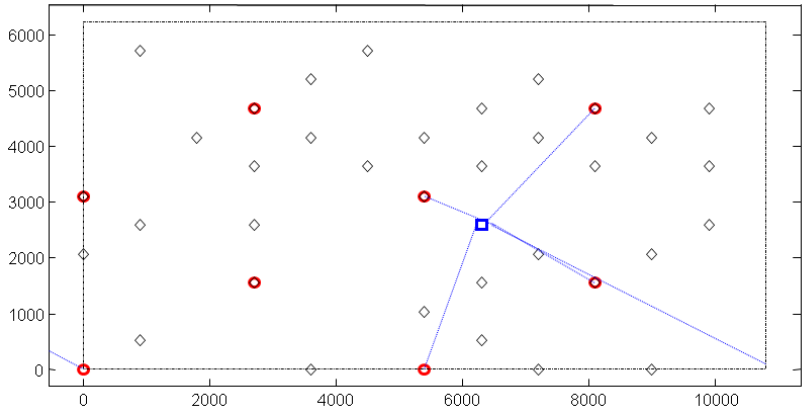

Figure 42: Example of a homogeneous network layout (grid in meters).

context with a single layer of BSs (macro-BSs) which serve users disseminated throughout the network.

The BSs (identified by red spots) are deployed on a regular grid (according to an hexagonal cell geometry), while the MSs (represented by diamonds) are distributed on the whole topology in a random way. All the stations are arranged on a toroidal surface: thanks to this implementation of the grid, the stations (BSs and MSs) located on the rightmost part of the grid are adjacent those ones placed on the leftmost part of it, similarly the BSs located at the top of the grid are adjacent those ones arranged on the underside of the grid. In this way a correct signal/interference model is obtained, also for the stations located on the edge of the grid.

The signal received by a generic MS consists of N time-delayed multipath replicas of the transmitted signal. These N paths are defined by powers and delays and are chosen randomly according to the channel generation procedure explained in [3]. Each path consists of M subpaths. Each MS in the grid senses the presence of multiple BSs and it associates itself to the BS from which the signal strength is perceived as stronger; consequently the remaining BSs are marked as interfering ones. With reference to the layout depicted in Fig. 42, for the selected MS, the links towards the sensed BSs are marked with dashed blue lines: the example just shows as a BS, apparently far from the MS (because located on the opposite side of the grid), is actually sensed by it, due to the toroidal implementation of the grid.

Fig. 43 on the following page shows another example of layout, which instead refers to a mixed macro-femto context. Two layers of BSs, the macro ones, identified by blue full spots and the femto ones, identified by blue empty spots, are superimposed on the same network,

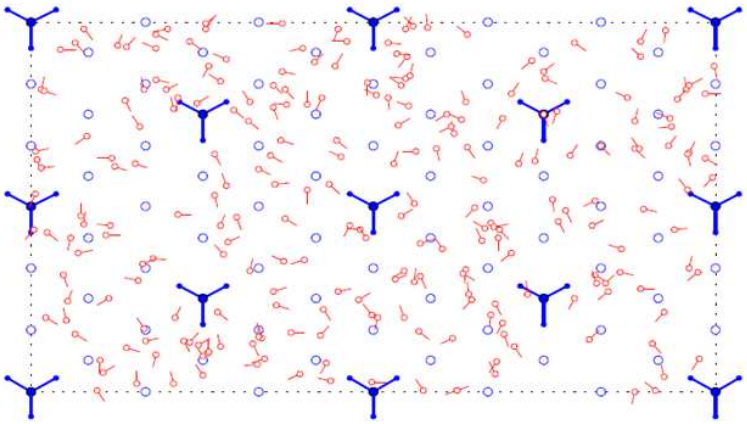

Figure 43: Example of a mixed macro-femto layout.

while the MSs, identified by red empty spots, are still arranged randomly.

The figure also shows some additional details with respect to the previous layout depicted in Fig. 42 on the previous page. The three segments which depart from the spots identifying the macro-BSs indicate that the macro-cells are three-sectored, while the segments departing from the red spots indicate the motion direction of the MSs. Three types of sectoring are possible for the macro-cells, each one corresponding to a different implemented antenna configuration: you may have non-sectored (which corresponds to an omnidirectional radiation pattern), 3-sector and 6-sector cells. The last two configurations will be analyzed in detail in the next section.

The number of BSs sensed by each MS depends on the channel gain values between the MS and the BSs: depending on these gains, for a selected MS, a BS can appear *under noise* (if the signal coming from it is below the noise threshold), *masked* (by nearby BSs) or *active*. In the first two cases the BS will not be detectable, viceversa it will be sensed as serving-BS or interfering one.

Fig. 44 on the following page shows, for a fixed context and a generic MS, the *Power Spectral Density* (PSD) associated to the channels between the selected MS and the BSs in the grid: as shown in the figure, only a few BSs are on average above the fixed threshold, marked by a dashed line, the other ones are undetectable for the MS.

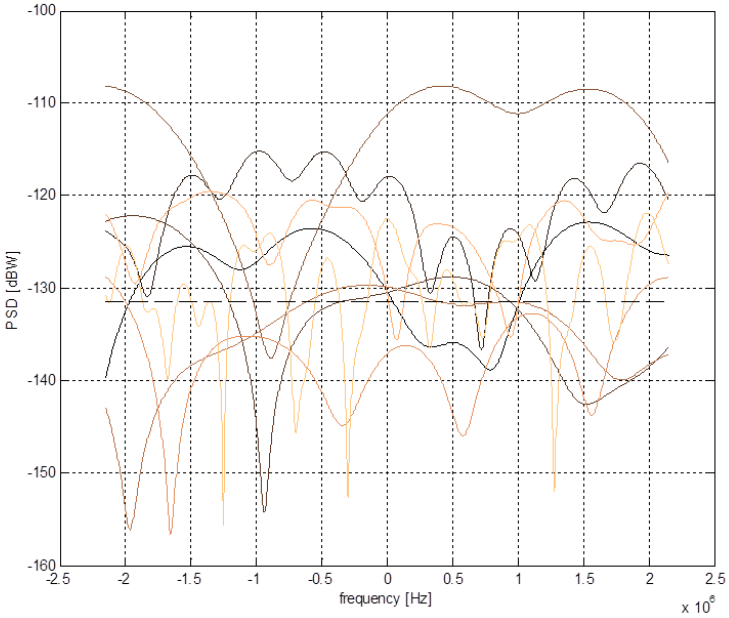

Figure 44: Example of PSD associated to MS-BSs channels.

6.2 Part B: BS antenna configurations

Different configurations and antenna patterns for the BSs are implemented in the simulator, in a consistent way with the specifications reported in [3].

Fig. 45 on the next page shows the angular parameters, considering a generic BS-MS link:

- Ω_{BS} is the BS antenna array orientation, defined as the difference between the broadside of the BS array and the absolute North (N) reference direction;
- θ_{BS} is the LOS (*Line of Sight*) AoD (*Angle of Departure*) direction between the BS and the MS, with respect to the broadside of the BS array;
- $\delta_{n,AoD}$ is the AoD for the n_{th} path with respect to the LOS AoD θ_0;
- $\Delta_{n,m,AoD}$ is the offset for the m_{th} subpath of the n_{th} path with respect to $\delta_{n,AoD}$;
- $\theta_{n,m,AoD}$ is the absolute AoD for the m_{th} subpath of the n_{th} path at the BS with respect to the BS broadside;

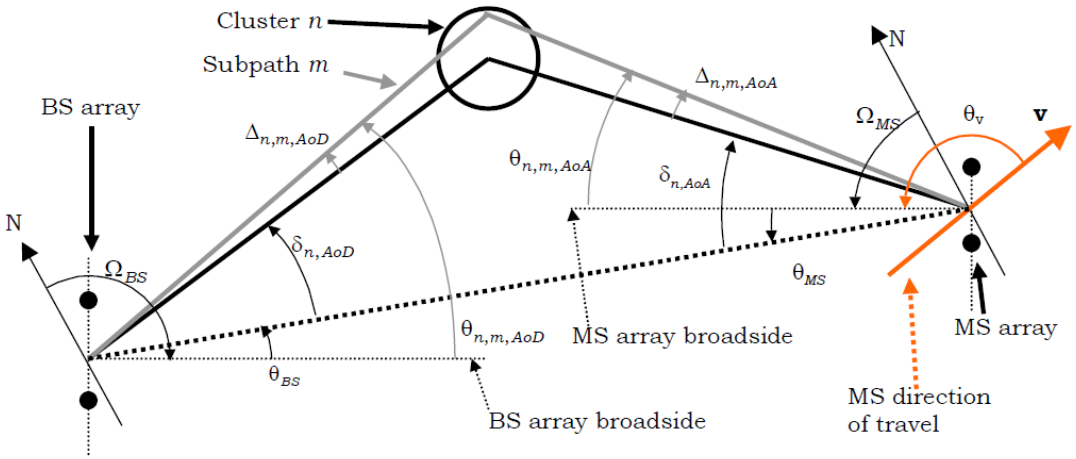

Figure 45: Definition of BS-MS angular parameters [3].

- Ω_{MS} is the MS antenna array orientation, defined as the difference between the broadside of the MS array and the absolute North reference direction;
- θ_{MS} is the angle between the BS-MS LOS and the MS broadside;
- $\delta_{n,AoA}$ is the AoA (*Angle of Arrival*) for the n_{th} path with respect to the LOS AoA $\theta_{0,MS}$;
- $\Delta_{n,m,AoA}$ is the offset for the m_{th} subpath of the n_{th} path with respect to $\delta_{n,AoA}$;
- $\theta_{n,m,AoA}$ is the absolute AoA for the m_{th} subpath of the n_{th} path at the MS with respect to the MS array broadside;
- ***v*** is the MS velocity vector;
- θ_v is the angle of the velocity vector with respect to the MS broadside $\theta_v = arg(v)$.

As mentioned in the previous section, besides the omnidirectional antenna configuration, two additional BS antenna patterns were implemented in the simulator, in order to support 3-sector and 6-sector macro-cell scenarios. These antenna patterns are designed for diversity-oriented applications (i.e. large inter-element spacing). For beamforming applications that require small spacings, alternative antenna designs should be considered leading to different antenna patterns.

The expression which describes the radiation pattern of a generic BS is:

$$A(\theta) = -min[12(\frac{\theta}{\theta_{3dB}})^2, A_m] \tag{39}$$

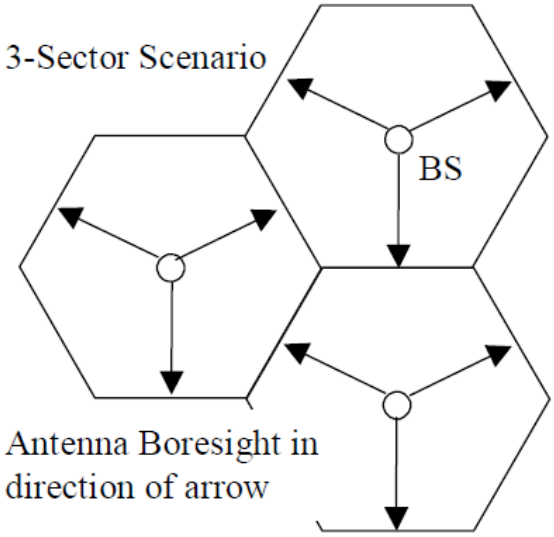

Figure 46: Boresight pointing direction for 3-sector cells [3].

where: θ ($-180° \leq \theta \leq 180°$) is defined as the angle between the direction of interest and the boresight of the antenna, θ_{3dB} is the 3dB beamwidth in degrees, and A_m is the maximum attenuation.

For a 3-sector scenario, θ_{3dB} is 70 degrees, A_m is 20dB, and the antenna boresight pointing direction is shown in Fig. 46. Remember that the boresight is defined as the direction to which the antenna shows the maximum gain. The correspondent antenna pattern, for forward and reverse links, is plotted in Fig. 47 on the next page: the antenna gain is 14dBi.

For a 6-sector scenario, θ_{3dB} is 35 degrees and A_m is 23dB, which results in the pattern shown in Fig. 48 on page 89; the boresight pointing direction is plotted in Fig. 49 on page 90. So, compared with the 3-sector antenna pattern, the beamwidth is reduced by half to 35 degrees, consequently the corresponding gain is 3dB higher (17dBi).

6.3 Part C: Implemented environments and correspondent Path Loss models

The 3GPP and 3GPP2 industry alliances jointly developed channel models that can be used for the evaluation of cellular systems with multiple antenna elements. The models are defined for three environments, which are also the environments implemented in the simulator and cited in the thesis, namely:

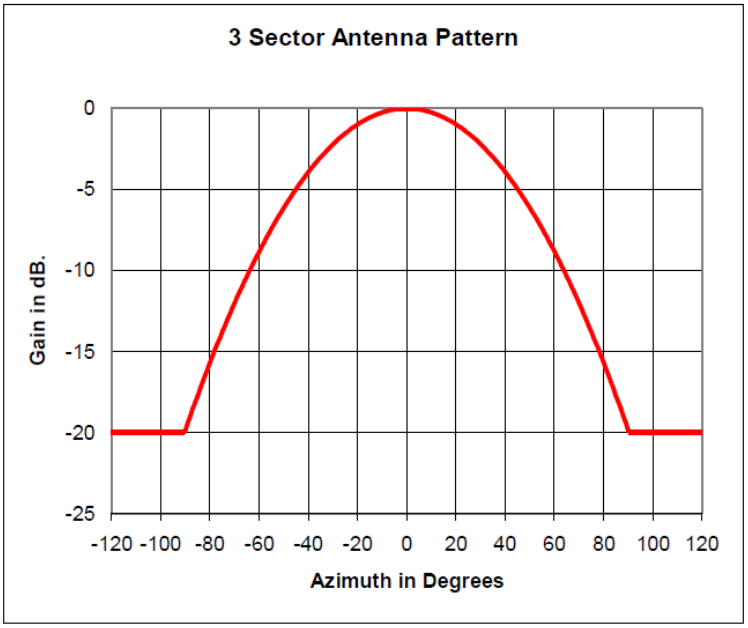

Figure 47: Antenna pattern for 3-sector cells [3].

- *Suburban Macrocell* (valid for BS to BS distances of approximately 3Km);
- *Urban Macrocell* (same assumption for the inter-site distance);
- *Urban Microcell* (BS to BS distance less than 1Km).

Macro cell environments assume that BS antennas are above rooftop heigth, while for the urban microcell scenario BS antennas are assumed to be at rooftop heigth.

Table 14 on page 91 describes the parameters used in each environment, where:

- σ_{AS}: is the *Angle Spread*, defined as the root mean square (RMS) of angles with which an arriving path is received by the BS array;
- σ_{DS}: is the root mean square of delays associated to the reflections. Remember that the maximum delay time spread is defined as the difference between the time of arrival of the earliest significant multipath component (typically the *line of sight* component) and the time of arrival of the latest multipath component;
- σ_{AoD}: is the mean angle with which an arriving or departing path is received or transmitted by the BS with respect to the boresite; ipotizing the uplink-downlink reciprocity, the AoD/AoA angles are identical;

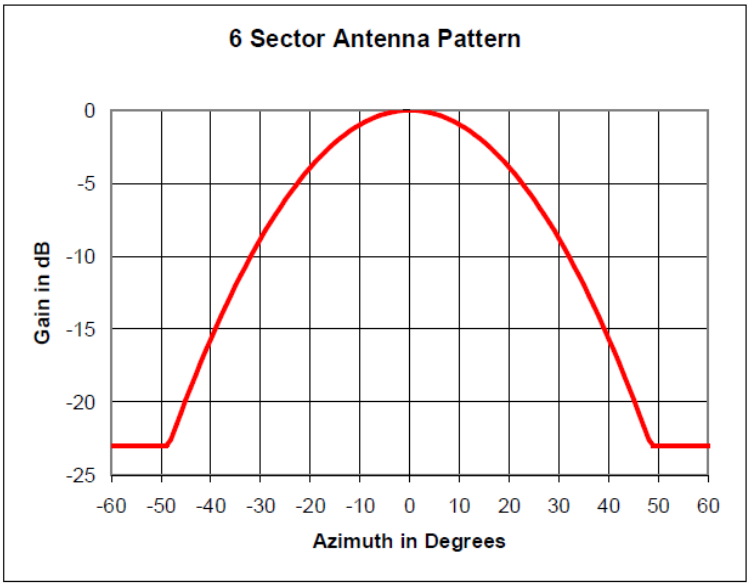

Figure 48: Antenna pattern for 6-sector cells [3].

- σ_{SF}: is the lognormal shadow fading random variable. Remember that lognormal shadowing describes the random shadowing effects for a large number of different locations with the same distance but with different environmental clutter on the propagation path;
- $\eta(a, b)$: is a random variable (Gaussian) distribution with mean a and variance b;
- $U(a, b)$: is the uniform distribution, whose support is defined by two parameters, a and b, which are its minimum and maximum values;

With reference to the *Path Loss models*, cited in the last row of Table 14 on page 91, those ones implemented in the simulator are:

- *Free Space*: it is the simplest model which describes the loss in signal strength of an electromagnetic wave that would result from a *line of sight* path through free-space (usually air), with no obstacles nearby to cause reflection or diffraction. *Free Space Path Loss* is proportional to the square of the distance d (in meters) between the transmitter and the receiver and to the square of the frequency f (in hertz) of the radio signal. By neglecting the system losses, the equation for the $PL_{free-space}$ is:

$$PL_{free-space} = (\frac{4\pi d}{\lambda})^2 = (\frac{4\pi df}{c})^2 \tag{40}$$

where λ is the signal wavelength (in meters) and c is the speed of light in a vacuum

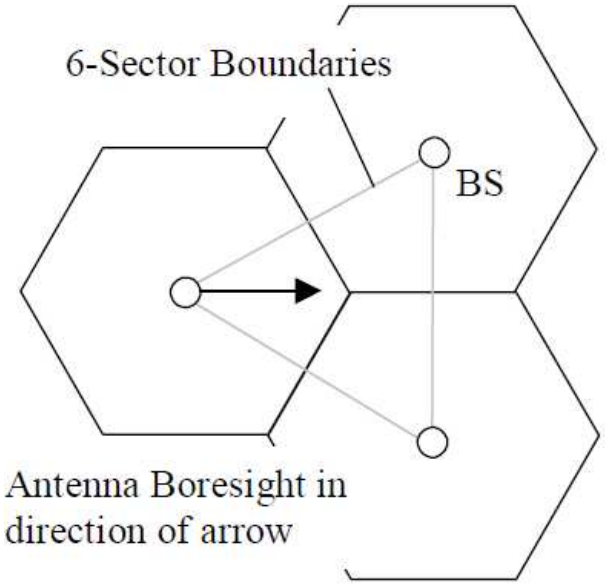

Figure 49: Boresight pointing direction for 6-sector cells [3].

2.99792458 x 10^8 m/s. For typical radio applications, it is common to find f measured in units of MHz, d in km and the $PL_{free-space}$ expressed in dB. Manipulating appropriately equation (40), the following expression in dB can be obtained:

$$PL_{free-space}[dB] = 20log_{10}(d) + 20log_{10}(f) + 32.45 \tag{41}$$

- *Power exponent*: as the previous model, with an exponent η major than 2, tipically in the range of 2 to 4:

$$PL_{exponent} = (\frac{4\pi d}{\lambda})^{\eta} = (\frac{4\pi df}{c})^{\eta} \tag{42}$$

The exponent 2 is for propagation in free space (the previous case), 4 is for relatively lossy environments and for the case of full specular reflection from the earth surface (the so-called *flat earth model*). In some environments however, especially in presence of buildings and obstacles in general, the path loss exponent can reach values in the range of 4 to 6. The models analyzed so far are very simple and not much realistic, they have been implemented primarily for educational purposes. The models which follow, on the other hand, are classical empirical models adaptable to real contexts, actually used in the simulations reported throughout the thesis. For a complete treatment of them, you can refer to ([89],[90]).

Channel Scenario	Suburban Macro	Urban Macro	Urban Micro
Number of paths (*N*)	6	6	6
Number of sub-paths (*M*) per-path	20	20	20
Mean AS at BS AS at BS as a lognormal RV $\sigma_{AS} = 10\wedge(\varepsilon_{AS}x + \mu_{AS}),\ x \sim \eta(0,1)$	E(σ_{AS})=5^0 μ_{AS} = 0.69 ε_{AS} = 0.13	E(σ_{AS})=8^0, 15^0 8^0 μ_{AS} = 0.810 ε_{AS} = 0.34 15^0 μ_{AS} = 1.18 ε_{AS} = 0.210	NLOS: E(σ_{AS})=19^0 N/A
$r_{AS} = \sigma_{AoD} / \sigma_{AS}$	1.2	1.3	N/A
Per-path AS at BS (Fixed)	2 deg	2 deg	5 deg (LOS and NLOS)
BS per-path AoD Distribution standard distribution	$\eta(0, \sigma^2_{AoD})$ where $\sigma_{AoD} = r_{AS}\sigma_{AS}$	$\eta(0, \sigma^2_{AoD})$ where $\sigma_{AoD} = r_{AS}\sigma_{AS}$	U(-40deg, 40deg)
Mean AS at MS	E($\sigma_{AS, MS}$)=68^0	E($\sigma_{AS, MS}$)=68^0	E($\sigma_{AS, MS}$)=68^0
Per-path AS at MS (fixed)	35^0	35^0	35^0
MS Per-path AoA Distribution	$\eta(0, \sigma^2_{AoA}(\mathrm{Pr}))$	$\eta(0, \sigma^2_{AoA}(\mathrm{Pr}))$	$\eta(0, \sigma^2_{AoA}(\mathrm{Pr}))$
Delay spread as a lognormal RV $\sigma_{DS} = 10\wedge(\varepsilon_{DS}x + \mu_{DS}),\ x \sim \eta(0,1)$	μ_{DS} = - 6.80 ε_{DS} = 0.288	μ_{DS} = -6.18 ε_{DS} = 0.18	N/A
Mean total RMS Delay Spread	E(σ_{DS})=0.17 μs	E(σ_{DS})=0.65 μs	E(σ_{DS})=0.251μs (output)
$r_{DS} = \sigma_{delays} / \sigma_{DS}$	1.4	1.7	N/A
Distribution for path delays			*U*(0, 1.2μs)
Lognormal shadowing standard deviation, σ_{SF}	8dB	8dB	NLOS: 10dB LOS: 4dB
Pathloss model (dB), *d* is in meters	31.5 + 35log$_{10}$(*d*)	34.5 + 35log$_{10}$(*d*)	NLOS: 34.53 + 38log$_{10}$(*d*) LOS: 30.18 + 26*log$_{10}$(*d*)

Table 14: Environment parameters [3].

- *Hata*: it is the *Path Loss model* on which macrocell environments are based on. It provides formulas to evaluate path loss versus distance for various scenarios: large sites, small and medium cities or rural areas. The expression which describes the model is:

$$PL_{Hata}[dB] = (44.9 - 6.55\log_{10}(h_{BS}))log_{10}(\frac{d}{1000}) + 45.5 + \\ + (35.46 - 1.1h_{MS})log_{10}(f_c) - 13.82log_{10}(h_{BS}) + 0.7h_{MS} + C \tag{43}$$

  where h_{BS} and h_{MS} are respectively the BS and the MS antenna heights (in meters), f_c is the carrier frequency (in MHz), d the distance (in meters) between the BS and the MS and C a constant factor ($C = 0dB$ for suburban macro and $C = 3dB$ for urban macro). The expressions reported in the last row of Table 14, respectively for suburban macro and urban macro, $PL = 31.5 + 35log_{10}(d)$ and $PL = 34.5 + 35log_{10}(d)$, are obtained evaluating the equation (43) for $h_{BS} = 32m$, $h_{MS} = 1.5m$ and $f_c = 1900MHz$. The distance d is required to be at least $35m$.

- *Walfish-Ikegami*: considering the assumptions set in the simulator, i.e. a BS antenna

height of $12.5m$, a building height of $12m$, a building to building distance of $50m$, a street width of $25m$, a MS antenna height of $1.5m$, an orientation of $30deg$ for all paths, the selection of metropolitan center, the following semplified expressions can be derived, respectively for the NLOS (44) and LOS (45) case:

$$PL_{Walfish-Ikegami-NLOS}[dB] = -55.9 + 38\log_{10}(d) + (24.5 + \frac{1.5f_c}{925})log_{10}(f_c) \quad (44)$$

$$PL_{Walfish-Ikegami-LOS}[dB] = -35.4 + 26\log_{10}(d) + 20log_{10}(f_c) \quad (45)$$

The expressions of the table are obtained evaluating the previous ones for a f_c value of 1900 MHz.

7 Conclusions

Along with a technological evolution of networks, with new emerging technologies – specifically 3GPP *Long Term Evolution* (LTE) and IEEE 802.16 (WiMAX) – designed to provide applications and services characterized by high data rate and stringent requirements of QoS, in recent years there has also been an evolution of networks from an architectural point of view, migrating from traditional cellular networks (with macro Base Stations located on the territory to provide connectivity to users) to heterogeneous network scenarios where different devices coexist in the same layout. A modeling study of these emerging network scenarios, together with a simulative approach devoted to provide important design guidelines, has been the subject of this thesis.

With reference to a classical OFDMA network with a reuse factor equal to 1 and characterized by only macro-BSs (possibly with different transmit power levels), some preliminary considerations, supported by simulations, have been carried out in order to emphasize scenarios in which network planning and mobile station feedbacks are (or are not) advantageous.

Simulations run under different propagation models have shown that, overall, *water filling* approach, independently performed in each cell, performs better than uniform distribution of power on subchannels, not only on cell-basis but also from a network perspective, in terms of aggregated network capacity. Simple uniform allocation scheme, requiring no feedback from the MSs, provides results comparable with the *water filling* scheme only in case of micro-propagation model (where, with a very high probability, a LOS component between each BS and the MSs exists), while it under-performs *water filling* in case of macro-propagation model. The LOS component leads to high channel gains (which are also comparable from a *Resource Block* (RB) to another) and to a limited inter-cell interference. Therefore, selective power allocations and frequency planning are useless or even harmful in micro-propagation environments. On the other hand, when the LOS component is absent and the channel gains vary significantly from a RB to another, as in macro-propagation environments, power allocations based on *water filling* provide significantly better performance than uniform power allocations. Furthermore higher capacity values are perceived under a *fractional water filling* scheme (i.e. a scheme which applies the *water filling* algorithm only on a pre-defined sub-set of the available carriers),

showing that a resource repartition among the cells (i.e. a control on the inter-cell interference) is advantageous for this propagation scenario. Such a difference is even higher considering that the *fractional water filling* requires a signaling overhead lower that *water filling*. The rational of considering both *water filling* and *fractional water filling* is that utilizing or non utilizing all the resources available in each cell can lead to different interference levels among the cells. Since *water filling* intrinsically discards the carriers experiencing the worst channel and interfering conditions, the *fractional water filling* can be regarded as a kind of dynamic and distributed scheme for resource repartition among the cells.

Fractional use of resources, under certain assumptions, is also beneficial in heterogeneous macro-femto environments, where femto-BSs, i.e. devices from the same functionality of the macro-BSs but at low power (and therefore low coverage) and low cost, are deployed in the same layout of macro-BSs. Due to their capability to ensure coverage and service to users experiencing bad channel conditions, such as users on cell-edge or users in indoor environments, femto-BSs provide a consistent improvement in the system capacity maintaining, at the same time, a very low energy consumption, compared to the macro-BSs. For this reason the use of femtocells also represents a good solution for the deployment of green networks. When femto-cells are present in the network, femto users get capacity values significantly higher than those experienced by macro users. The drawback is the repartition of the capacity among the users, which is less fair when the number of active femtocells is high, although the overall network capacity is increased. Moreover a distribution of power according to the *water filling* approach, compared to the uniform distribution, causes more fairness among the femto users (they experience similar good channel conditions), and less fairness among the macro users (occurring in this case a higher variability in the channel conditions). A simple uniform allocation scheme, requiring no feedback from the MSs, provides results comparable with the *water filling* scheme when the number of active femtocells and the percentage of resource usage are low.

Fractional use of resources in such heterogeneous contexts is tested by forcing respectively only the macro-BSs or all the BSs (macro plus femto) to use a fraction of the available resources. In all cases where femtocells are switched on, a partial usage of the resources is beneficial in terms of aggregated network capacity if only macro-BSs partly use the resources

(due to the reduction of interference experienced by femto users and their consequent increment in capacity); vice versa forcing also femto-BSs to limit the use of resources leads to no benefit from the network perspective (due to the heavy penalties for femto users compared to the slight beneficial effects perceived by macro users).

With reference to energy implications, which increasingly play a dominant role considering the recent trend to design green networks, the major energy efficiency of femto-BSs, compared to macro-BSs, has already been mentioned. By varying the transmit power levels respectively in macro- and femto-BSs, it has been noted that an increment of macro power level leads to a minor network aggregated capacity in all scenarios in which femtocells are present. In fact it has a marginal positive effect on macro users compared to the devastating effect on femto users, whose interference level becomes unacceptable. On the other hand an increment in the femto power level leaves almost unchanged the situation of macro users (being almost irrelevant for them a change in the values of power at those orders of magnitude) but it greatly enhances the service level of femto users (who already experience privileged channel conditions). When the power level increases, there is a major energy consumption: if the power is set higher in macro-BSs, the macro energy consumption grows up, vice versa if the power is increased in femto-BSs, the femto consumption rises up, reducing the gap with the macro level, even if still substantial. The highest consumption of energy occurs in crowded scenarios, i.e. scenarios with a high number of BSs. In any case, the application of *water filling* always guarantees a lower expenditure of energy, because the optimization of the power distribution leads to a careful management of it, thus avoiding unnecessary wastage of energy.

Due to the impressive proliferation in next generation networks of mobile devices, equipped with wireless interfaces and to the limited battery power they rely on, reducing their energy consumption has become increasingly a very important research issue. So, in order to make a complete analysis, the energetic impact at the user-side has also been evaluated. The results of a measurement campaign have been discussed. We referred to the 802.11 technology, for evaluating experimental measurements, and specifically to a common USB dongle. The rationale of this study was to understand the impact of transmit power tunings on the overall card consumption, under the assumption that 3G USB cards (over which we do not have full con-

figuration control) will exhibit a similar behavior. The accurate measurements have allowed to evaluate the energy consumption of these cards under different operating conditions (different PHY transmit rates and transmit powers), isolate the consumption quota of different card sub-systems, including the power amplifier, the RF-front end, the baseband and the host interface, and study the effects of power control on their energy saving (which has led to support the low efficiency of this technique aimed at saving energy).

Measurements in fact have shown that the reduction of the transmission power has a marginal effect on the overall energy consumption of WiFi cards, due to the power consumed in idle states. The power consumption experienced in reception and idle state is approximately the same in all the cases and it is independent from the transmit power level chosen. On the other hand, depending on the specific card, the power consumed in the transmission state can vary in an appreciable way, due to the different card designs and implementation. *Transmission Power Control* (TPC) could help to save some energies when cards spend the maximum possible time in the transmission state (i.e. saturation conditions, minimum PHY rate, absence of contending stations), which represents a non-typical situation. However this technique has a lower impact when the cards work in OFDM mode rather than in DSSS mode. PHY transmit rate strongly affects the per-bit energy consumption of the cards: in fact when the transmit rate increases, the per-bit energy consumption improves.

Finally identifying the consumption quota of different card sub-systems, in order to design effective power saving schemes, is always very important: for the USB cards, the investigated case, an high fraction of the whole card consumption is due to the USB interface, which represents a high fixed overhead.

References

[1] Z. Cao, U. Tureli and Y. D. Yao, "Deterministic Multiuser Carrier Frequency Offset Estimation for Interleaved OFDMA Uplink," *IEEE Transactions on Communications*, vol. 52, pp. 1585 – 1594, September 2004.

[2] G. de la Roche, A. Valcarce, D. Lopez-Perez and J. Zhang, "Access control mechanisms for femtocells," *IEEE Communications Magazine*, July 2009.

[3] "3GPP TR25.996 v8.0.0 (2008-12), 3rd Generation Partnership Project; Technical Specification Group Radio Access Network; Spatial channel model for Multiple Input Multiple Output (MIMO) simulations (Release 8)."

[4] J. G. Andrews, A. Ghosh and R. Muhamed, "Fundamentals of WIMAX: Understanding Broadband wireless Networking," *Prentice Hall*, 2007.

[5] S. Sesia, I. Toufik and M. Baker, "LTE - The UMTS Long Term Evolution: From theory to practice," *Wiley*, 2009.

[6] "Part 16: Air Interface for Fixed and Mobile Broadband Wireless Access Systems," *IEEE Std. 802.16e-2005*.

[7] H. Sari, "A review of OFDMA and SC-FDMA and some recent results," *WICAT SC-FDMA Workshop*, March 2009.

[8] C. R. Stevenson, G. Chouinard, Z. Lei, W. Hu, S. J. Shellhammer and W. Caldwell, "IEEE 802.22: The First Cognitive Radio Wireless Regional Area Network Standard," *IEEE Communications Magazine*, January 2009.

[9] J. Li, G. Liu and G. B. Giannakis, "Carrier frequency offset estimation for OFDM-based WLANs," *IEEE Signal Process. Lett.*, vol. 8, no. 3, pp. 80–82, March 2001.

[10] P. H. Moose, "A technique for orthogonal frequency division multiplexing frequency offset correction," *IEEE Transactions on Communications*, vol. 42, no. 10, pp. 2908–2914, October 1994.

[11] J. J. Beek, P. O. Borjesson, M. L. Boucheret, D. Landstrom, J. Arenas, P. Odling, C. Ostberg, M. Mahlqvist and S. K. Wilson, "A time and frequency synchronization scheme for multiuser OFDM," *IEEE J. Select. Areas Commun.*, vol. 17, no. 11, pp. 1900–1914, November 1999.

[12] S. Barbarossa, M. Pompili and G. B. Giannakis, "Channel-independent synchronization of orthogonal frequency division multiple access systems," *IEEE J. Select. Areas Commun.*, vol. 20, no. 2, pp. 474–486, February 2002.

[13] I.E. Telatar, "Capacity of multi-antenna gaussian channels," *European Transactions on Telecommunications*, vol. 10, no. 6, pp. 585–595, Nov./Dec. 1999.

[14] A. Goldsmith, S.A. Jafar, N. Jindal and S. Vishwanath, "Capacity limits of MIMO channels," *IEEE Journal on Selected Area in Communications*, vol. 21, no. 5, pp. 684–702, Jun. 2003.

[15] F.I. Di Piazza, S. Mangione and I. Tinnirello, "Maximizing network capacity in an heterogeneous macro-micro cellular scenario," *16th IEEE Symposium on Computers and Communications (ISCC) - Kerkyra, Corfu, Greece*, pp. 365–370, August 2011.

[16] M. Ebrahimi, M.A. Maddah-Ali and A.K. Khandani, "Power allocation and asymptotic achievable sum-rates in single-hop wireless networks," *CISS, Princeton, NJ*, March 2006.

[17] G. Li and H. Liu, "Downlink Radio Resource Allocation for Multi-Cell OFDMA System," *IEEE Transactions on Wireless Communications*, vol. 5, no. 12, pp. 3451–3459, December 2006.

[18] H. Kim, Y. Han and J. Koo, "Optimal subchannel allocation scheme in multicell OFDMA systems," *in Proc. IEEE VTC*, May 2004.

[19] S.H. Paik, S. Kim and H.B. Park, "A resource allocation using game theory adopting AMC scheme in multi-cell OFDMA systems," *2010 2nd International Conference on Future Computer and Communication (ICFCC)*, vol. 2, pp. V2–344, May 2010.

[20] I.G. Fraimis, V.D. Papoutsis and S.A. Kotsopoulos, "A Distributed Radio Resource Allocation Algorithm with Interference Coordination for Multi-cell OFDMA Systems," *2010 IEEE 21st International Symposium on Personal Indoor and Mobile Radio Communications (PIMRC)* , pp. 1354–1359, December 2010.

[21] A.G. Gotsis and P. Constantinou, "Adaptive single-cell OFDMA resource allocation for heterogeneous data traffic," *Networking and Communications*, pp. 96–103, 2008.

[22] I.C. Wong and B.L. Evans, "Optimal Downlink OFDMA Resource Allocation With Linear Complexity to Maximize Ergodic Rates," *IEEE Transactions on Wireless Communications*, vol. 7, no. 2, February 2008.

[23] V. Tralli, R. Veronesi and M.Zorzi, "Power-shaped advanced resource assignment for fixed broadband wireless access systems," *IEEE Trans. Wireless Commun.*, vol. 3, pp. 2207–2220, Nov. 2004.

[24] R. Veronesi, V. Tralli, J. Zander and M. Zorzi, "Distributed dynamic resource allocation for multicell SDMA packet access networks," *IEEE Trans. Wireless Commun.*, vol. 5, pp. 1–12, 2006.

[25] C.Y. Wong, R.S. Cheng, K.B. Letaief and R.D. Murch, "Multiuser OFDM with Adaptive Subcarrier, Bit, and Power Allocation," *IEEE Journal on Selected Areas in Communications*, vol. 17, no. 10, pp. 1747–1758, October 1999.

[26] J. Jang and K.B. Lee, "Transmit Power Adaptation for Multiuser OFDM Systems," *IEEE Journal on Selected Areas in Communications*, vol. 21, no. 2, pp. 171–178, February 2003.

[27] W. Rhee and J.M. Cioffi, "Increase in Capacity of Multiuser OFDM System Using Dynamic Subchannel Allocation," *VTC 2000*, pp. 1085–1089, 2000.

[28] Z. Shen, J.G. Andrews and B.L. Evans, "Adaptive Resource Allocation in Multiuser OFDM Systems with Proportional Rate Constraints," *IEEE Trans. on Wireless Communications*, July 2005.

[29] I. de Bruin, G. Heijenk, M. El Zarki and L. Zan, "Fair channel-dependent scheduling in CDMA Systems," *Proc. IST Mobile and Wireless Communications Summit 2003*, pp. 737–741, June 2003.

[30] M.H. Ahmed, H. Yanikomeroglu and S. Mahmoud, "Fairness enhancement of link adaptation techniques in wireless access networks," *Proc. IEEE VTC2003-Fall*, vol. 3, pp. 1554–1557, October 2003.

[31] S. Pietrzyk and G.J.M. Janssen, "Subcarrier Allocation and Power Control for QoS Provision in the Presence of CCI for the Downlink of Cellular OFDMA Systems," *Vehicular Technology Conference, 2003. VTC 2003-Spring. The 57th IEEE Semiannual*, vol. 4, pp. 2221–2225, July 2003.

[32] S.Pietrzyk and G.J.M. Janssen, "Radio Resource Allocation for Cellular Networks Based on OFDMA with QoS Guarantees," *Global Telecommunications Conference, 2004 - GLOBECOM '04. IEEE*, vol. 4, pp. 2694–2699, Jan. 2005.

[33] G. Fodor, C. Koutsimanis, A. Racz and N. Reider, "Intercell Interference Coordination in OFDMA Networks and in the 3GPP Long Term Evolution System," *Journal of Communications*, vol. 4, no. 7, pp. 445–453, August 2009.

[34] Y. Akaiwa, "An Adaptive Base Station Cooperated Cellular System and Its Theoretical Performance Analysis," *2011 IEEE 73rd Vehicular Technology Conference (VTC Spring)*, pp. 1–5, July 2011.

[35] H. Zhang, N. Mehta, A. Molisch, J. Zhang and H. Dai, "On the Fundamentally Asynchronous Nature of Interference in Cooperative Base Station Systems," *Mitsubishi Electric Research Laboratories*, pp. 6073 – 6078 , June 2007.

[36] D. Goodman and N. Mandayam, "Power Control for Wireless Data," *Personal Communications, IEEE* , vol. 7, pp. 48–54, August 2002.

[37] T.K. Chee, C-C. Lee and J. Choi, "A Cooperative Game Theoretic Framework for Resource Allocation in OFDMA Systems," *10th IEEE Singapore International Conference on Communication Systems (ICCS), 2006*, pp. 1–5, Feb. 2007.

[38] A. Muthoo, "Bargaining Theory with Applications," *Cambridge University Press*, 1999.

[39] S. Yeh, S. Talwar, S. Lee and H. Kim, "WIMAX Femtocells: A Perspective on Network Architecture, Capacity and Coverage," *IEEE Communication Magazine*, vol. 46, no. 10, pp. 58–65, October 2008.

[40] Socrates project, "Use cases for self-organizing networks," *IEEE Global Telecommunications Conference (GLOBECOM 2007), Washington, DC*, 2008.

[41] D. Lopez-Perez, A. Ladanyi, A. Juttner, and J. Zhang, "OFDMA femtocells: a self-organizing approach for frequency assignment," *International Symposium on Personal, Indoor and Mobile Radio Communications*, pp. 2202–2207, September 2009.

[42] V. Chandrasekhar and J.G. Andrews, "Spectrum Allocation in Two-tier Networks," *IEEE Trans. on Wireless Communications*, 2009.

[43] L.Xu, C.Sun, X.Li, C.Lim and H.He, "The methods to implementate self optimization in LTE system," *International Conference on Computer Theory and Applications - ICCTA 2009*, October 2009.

[44] H.Claussen, L.T.W.Ho and L.G.Samuel, "An overview of the femtocell concept," *Bell Labs Technical Journal*, vol. 13, no. 1, pp. 221–245, May 2008.

[45] H. Claussen, L.T.W. Ho and L.G. Samuel, "Self-optimization coverage for femtocell deployments," *Wireless Telecommunications Symposium*, pp. 278–285, April 2008.

[46] V.Chandrasekhar and J.G.Andrews, "Uplink capacity and interference avoidance for two-tier femtocell networks," *IEEE Global Telecommunications Conference (GLOBECOM 2007), Washington, DC*, pp. 3322–3326, November 2007.

[47] D. Lopez-Perez, G. de la Roche, A. Valcarce, E. Liu and J. Zhang , "Access Methods to WIMAX Femtocells: A downlink system-level case study," *IEEE International Conference on Communication Systems*, November 2008.

[48] H. Claussen, "Performance of Macro- and Co-channel Femtocells in a Hierarchical Cell Structure," *IEEE 18th International Symposium on Personal, Indoor and Mobile Radio Communications - PIMRC 2007*, vol. 1, pp. 1–5, September 2007.

[49] A. Valcarce, G. De La Roche, A. Juttner, D. Lopez-Perez and J. Zhang, "Applying FDTD to the coverage prediction of WiMax femtocells," *EURASIP Journal on Wireless Communications and Networking*, Feb. 2009.

[50] D. Lopez-Perez, G. de la Roche, A. Valcarce, A. Juttner and J. Zhang , "Interference avoidance and dynamic frequency planning for WIMAX femtocells networks," *IEEE International Conference on Communication Systems*, pp. 1579–1584, November 2008.

[51] H. Zheng, C. Zhu and W. Chen, "System performance of self-organizing network algorithm in WiMax femtocells," *ACM International Conference on Wireless Internet (WICON)*, November 2008.

[52] B.-G. Kim, J.-A. Kwon and J.-W. Lee, "Utility-based subchannel allocation for OFDMA femtocell networks," *2011 Proceedings of 20th International Conference on Computer Communications and Networks (ICCCN)*, August 2011.

[53] I. Guvenc, M.R. Jeong, F. Watanabe and H. Inamura, "A hybrid frequency assignment for femtocells and coverage area analysis for co-channel operation," *IEEE Comm. Letters*, vol. 12, no. 12, pp. 880–882, Dec. 2008.

[54] B. Li, Y. Zhang, G. Cui, W. Wang, J. Duan and W. Chen, "Interference coordination based on hybrid resource allocation for overlaying LTE macrocell and femtocell," *IEEE 22nd International Symposium on Personal, Indoor and Mobile Radio Communications*, 2011.

[55] H. Lei, L. Zhang, X. Zhang and D.Yang, "A novel multi-cell OFDMA system structure using Fractional Frequency Reuse," *IEEE International Symposium on Personal, Indoor and Mobile Radio Communications (PIMRC)*, Sept. 2007.

[56] M. Assaad, "Optimal Fractional Frequency Reuse (FFR) in multicellular OFDMA system," *IEEE Vehicular Technology Conference (VTC)*, Sept. 2008.

[57] N. Himayat, S. Talwar, A. Rao and R. Soni, "Interference Management for 4G Cellular Standards," *IEEE Communications Magazine*, August 2010.

[58] Y. Chang, Z. Tao, J. Zhang and J. Kuo, "A graph-based approach to multi-cell OFDMA downlink resource allocation," *IEEE GLOBECOM '08*, Nov. 2008.

[59] D. Lopez-Perez, A. Juttner and J. Zhang, "Optimization methods for dynamic frequency planning in OFDMA networks," *Network 2008, Budapest, Hungary*, Sept. 2008.

[60] S.Y. Tu, K.C. Chen and R. Prasad, "Spectrum sensing of OFDMA systems for cognitive radios," *IEEE Int. Symp. Personal Indoor and Mobile Radio Commun. (PIMRC), Athens, Greece*, pp. 1–5, Sept. 2007.

[61] Femto Forum, www.femtoforum.org, "Interference Management in OFDMA femtocells," March 2010.

[62] T.W. Lester and H. Claussen, "Effects of User-Deployed, Co-Channel Femtocells on the Call Drop Probability in a Residential Scenario," *IEEE 18th International Symposium on Personal, Indoor and Mobile Radio Communications (PIMRC 2007), Athens, Greece*, vol. 1, pp. 1–5, Sept. 2007.

[63] T.W. Lester, H. Claussen and L.G. Samuel, "Self-optimization of Coverage for Femtocell Deployments," *Wireless Telecommunication Symposium 2008 (WTS 2008), Ponoma, CA, U.S.A.*, vol. 1, pp. 278–285, April 2008.

[64] F. Cao and Z. Fan, "Power loading and resource allocation for femtocells," *2011 IEEE 73rd Vehicular Technology Conference (VTC Spring)*, pp. 1–5, 2011.

[65] I. Sugathapala and N. Rajatheva, "Game theory based capacity and power optimization in OFDMA femtocell networks," *6th International Conference on Industrial and Information Systems, ICIIS, Sri Lanka*, Aug. 2011.

[66] M.Fang, I.Chlamtac and Y.B.Lin, "Channel occupancy times and handoff rate for mobile computing and PCS networks," *IEEE Trans. Comp.*, vol. 47, pp. 679–692, June 1998.

[67] R.Ramjee, R.Nagarajan and D.Towsley, "On optimal call admission control in cellular networks," *IEEE Infocom'96*, pp. 43–50, 1996.

[68] B.Epstein and M.Schwartz, "Reservation strategies for multimedia traffic in a wireless environment," *IEEE VTC'95*, pp. 165–169, 1995.

[69] C.Qin, G.Yu, Z.Zhang, H.Jia and A.Huang, "Power Reservation-based Admission Control Scheme for IEEE 802.16e OFDMA Systems," *WCNC 2007*.

[70] C.Tarhini and T.Chahed, "Density based admission control in IEEE 802.16e Mobile WiMax," *Wireless Days, 2008. WD '08. 1st IFIP, project WINEM (Wimax Networking Engineering and Multihoming)*.

[71] J.Zeng, B.Xie, F.Ma and Y.Li, "A dynamic admission control for IEEE 802.16e wireless network," *Third International Conference on Pervasive Computing and Applications, 2008. ICPCA 2008.*, pp. 916–921, 2008.

[72] Bo Rong, Yi Qian, K. Lu, H.-H. Chen and M. Guizani, " Call admission control optimization in WiMax networks," *IEEE Transactions on vehicular technology*, vol. 57, no. 4, 2008.

[73] K.W.Ross and D.H.K.Tsang, "The stochastic knapsack problem," *IEEE Trans. Commun.*, vol. 37, pp. 740–747, 1989.

[74] M.Gravious and Z.Rosberg, "A restricted complete sharing policy for a stochastic knapsack problem in B-ISDN," *IEEE Trans. Commun.*, vol. 42, pp. 2375–2379, 1994.

[75] W.Yang and E.Geraniotis, "Admission policies for integrated voice and data traffic in CDMA packet radio networks," *IEEE JSAC*, vol. 12, no. 4, pp. 654–664, May 1994.

[76] S.Singh, V.Krishnamurthy and H.Poor, "Integrated voice/data call admission for wireless DS-CDMA systems," *IEEE Trans. Signal Processing*, vol. 50, no. 6, pp. 1483–1495, June 2002.

[77] D.-H. Kim, S.-J. Oh, D.Zhang, N.Bhushan and R.Pankaj, "QoS performance based admission control in cellular networks," *2010 IEEE 71st Vehicular Technology Conference (VTC 2010-Spring)*, pp. 1–5, 2010.

[78] D.Niyato and E.Hossain, "Delay-based admission control using fuzzy logic for OFDMA broadband wireless networks," *IEEE International Conference on Communications (ICC), 2006*, vol. 12, pp. 5511–5516, June 2006.

[79] C.C.Beard and V.S.Frost, "Prioritized resource allocation for stressed networks," *IEEE/ACM Trans. Netw.*, vol. 6, no. 5, pp. 618–633, Oct. 2001.

[80] S.Bashar and Z.Ding, "Admission control and resource allocation in a heterogeneous OFDMA wireless network," *IEEE Transactions on wireless communications*, vol. 8, no. 8, August 2009.

[81] F. I. Di Piazza, S. Mangione and I. Tinnirello, "On the effects of transmit power control on the energy consumption of WiFi network cards," *6th International ICST Conference on Heterogeneous Networking for Quality, Reliability, Security and Robustness (ICST QShine 2009), Las Palmas de Grain Canaria (Spain)*, vol. 22, pp. 463–475, Nov. 2009.

[82] L.M. Feeney and M. Nilsson, "Investigating the energy consumption of a wireless network interface in an ad hoc networking environment," *IEEE INFOCOM 2001*, vol. 3, pp. 1548–1557, April 2001.

[83] J.P. Ebert, B. Burns and A. Wolisz, "A trace-based approach for determining the energy consumption of a WLAN network interface," *European Wireless 2002*, pp. 230–236, February 2002.

[84] "http://sourceforge.net/projects/iperf."

[85] K. Fong, D. Tung, M. Lee, S. Lee, B. Wu, P. Cheng, T. Pare, J. Feng, J. Chang, E. Simpson, J. Wong, F. Jann, K. Liao and D. Lo, "A Complete Dual-band Chip-set with USB 2.0 Interface for IEEE 802.11 a/b/g WLAN applications," *Asian Solid-State Circuits Conference 2005*, pp. 257–260, November 2005.

[86] C.-C. Huang, W.-T. Chen and K.-Y. Chen, "High Efficiency Linear Power Amplifier for IEEE 802.11g WLAN Applications," *IEEE Microwave and Wireless Components Letters*, vol. 16, no. 9, pp. 508–510, September 2006.

[87] P.-C. Wang, K.-Y. Huang, Y.-F. Kuo, M.-C. Huang, C.-H. Lu, T.-M. Chen, C.-J. Chang, K.-U. Chan, T.-H. Yeh, W.-S. Wang, Y.-H. Lin and C.-C. Lee, "A 2.4-GHz +25dBm P-1dB linear power amplifier with dynamic bias control in a 65-nm CMOS process," *34th European Solid-State Circuits Conference, 2008*, no. 490-493, September 2008.

[88] "Universal Serial Bus Revision 2.0 specification, http://www.usb.org/developers/."

[89] COST Action 231, “Digital mobile radio towards future generation systems, final report,” *tech. rep., European Communities, EUR 18957*.

[90] http://www.awe-communications.com/Propagation/Urban/COST/index.htm.